Many-body physics meets quantum computation

Kattemölle, J.J.

Publication date
2021
Document Version
Final published version

Many-body physics meets quantum computation

Joris Kattemölle

Many-body physics meets quantum computation

Joris Kattemölle

Many-body physics meets quantum computation

Joris Kattemölle

June 2021

Cover design and font by the author
Cover photograph by Bruce Kelley
Printed by printenbind.nl

The research reported in this thesis was carried out at the Institute for Theoretical Physics, University of Amsterdam, and Centrum Wiskunde & Informatica (CWI), Amsterdam. It was enabled by a grant of the University of Amsterdam, supporting QuSoft and the research priority area 'Quantum Matter & Quantum Information'.

Many-body physics meets quantum computation

ACADEMISCH PROEFSCHRIFT

ter verkrijging van de graad van doctor
aan de Universiteit van Amsterdam
op gezag van de Rector Magnificus
prof. dr. ir. K.I.J. Maex
ten overstaan van een door het College voor Promoties ingestelde commissie,
in het openbaar te verdedigen in de Aula der Universiteit
op woensdag 30 juni 2021, te 11.00 uur

door Joris Johannes Kattemölle
geboren te Oss

Promotiecommissie

Promotor:	prof. dr. C.J.M. Schoutens	Universiteit van Amsterdam
Copromotor:	dr. J. van Wezel	Universiteit van Amsterdam
Overige leden:	prof. dr. H.M. Buhrman	Universiteit van Amsterdam
	prof. dr. F.E. Schreck	Universiteit van Amsterdam
	prof. dr. D. Bouwmeester	Universiteit Leiden
	dr. B.W. Freivogel	Universiteit van Amsterdam
	dr. P.R. Corboz	Universiteit van Amsterdam
	dr. M. Ozols	Universiteit van Amsterdam
	dr. A. Safavi Naini	Universiteit van Amsterdam

Faculteit der Natuurwetenschappen, Wiskunde en Informatica

Publications

This thesis is based on the following publications.

- *Variational quantum eigensolver for the kagome lattice*
  Joris Kattemölle and Jasper van Wezel
  To appear

[80] *Conditions for superdecoherence*
Joris Kattemölle and Jasper van Wezel
Quantum **4**, (2020)

[81] *Dynamical fidelity susceptibility of decoherence-free subspaces*
Joris Kattemölle and Jasper van Wezel
Physical Review A **99**, 6 (2019)

In the course of his PhD, the author has additionally authored the following publication, which is not included in this thesis.

[79] *Entangled wavepackets in the vacuum*
Joris Kattemölle and Ben Freivogel
Journal of High Energy Physics **2017**, 10 (2017)

The introduction of this thesis is partly based on lecture notes and a popular science series on quantum computation that appeared online under the name of the author [78, 77].

Contents

Chapter 1

Introduction

1.1 Popular introduction and summary

A translation of this section into Dutch can be found in Sec. 1.2 on page 10.

1.1.1 Quantum computation

On the 30th of June 2021, the asteroid '2020 AD1' approaches the earth with a relative velocity of approximately 17,000 km/h [52, 54]. Fortunately, it will not hit the earth; on the 4th of July, it will fly by at approximately three lunar distances.

The solar system consist of the sun and the objects orbiting around it. Known objects include the planets, about a million of asteroids and dozens of spacecraft. Computers can simulate the solar system by creating a simplified 'board game' version of it that captures the most important aspects. In case we want to predict if an asteroid is going to hit the earth, these aspects are the velocity (including the direction) and position of the known objects in the solar system. We will henceforth call these positions and velocities, at any given time, the *state* of the solar system at that time. The players of the board game can be thought of as the known objects in the solar system, and the game is designed in such a way that every state of the board game corresponds to a state of the solar system. By playing many rounds of the game, a computer can find future states of the board game, and hence future states of the solar system. In this way, computers can calculate future positions of both the earth and the asteroid '2020 AD1', leading to the prediction that these two celestial bodies will not collide on the 4th of July.[1]

[1] (For experts) Classical computers are not known to be able to efficiently simulate the N-body problem; the only known upper bound on the complexity of this problem is that it is in PSPACE [122]. Note that BPQ$\subseteq$PSPACE [21], also see Sec. 1.5.3. This comes as no surprise since the N-body problem can show chaotic behaviour. Nevertheless, the solar system can be simulated with high accuracy for the next couple of centuries, with error bounds given a posteriori [55, 53, 54].

The players on the board game are bound by the rules of the game. These rules are completely deterministic; there is only one valid move per player per round. This is because the rules of the game have been determined by the laws of *classical mechanics*, which leave no room for an element of choice. The laws of classical mechanics are the natural laws that shape our everyday experiences; if you push a pawn, it starts moving ('$F = ma$'); if you let loose of a apple, it falls (Newton's law of gravitation). These same laws apply to the objects in the solar system.

To enter the world of this thesis, let us leave the solar system behind and zoom in on a tiny patch of the earth, far past the scale of planets, trees, humans, apples, pawns and microorganisms. We now enter the realm of molecules, constituting of electrons, protons and neutrons (Fig. 1.1). Remarkably, different laws of nature reign here; the laws of *quantum mechanics*. Humans are not familiar with these laws because the objects we regularly interact with follow instead the laws of classical mechanics. Quantum mechanics can therefore be counter-intuitive and has a name for being difficult to understand [44].

We would also like to simulate protons, neutrons and electrons. This is because their behaviour determines chemical reactions. Hence, the simulation of protons, neutrons and electrons can help to improve industrial chemical production processes. One example is that of fertilizer [123]. Currently, the production of one of the ingredients of fertilizer consumes about 1% of the world's total energy supply, all in the form of fossil fuels [112]. Yet, bacteria exist that produce that same ingredient without the use of fossil fuels. If we simulated this chemical process, we could learn from the bacteria and potentially produce fertilizer more environmentally friendly [123].

To simulate the behaviour of electrons, protons and neutrons, we need to create a new board game, which we can call the "quantum game", that captures the essential parts of a quantum mechanical system, and let the computer play this game. The pieces of the game now represent protons, neutrons and electrons, which brings with it a change of the rules. The rules are now set by the laws of quantum mechanics. Quantum mechanics is not only difficult to humans, but also to computers; a short calculation[2] shows that just to store the board game version of 37 electrons already requires at least 1 Terabyte of

[2] A classical description of the state of n spin degrees of freedom requires the storage of roughly 2^n complex numbers. Using two floats per complex number, this takes up $2^n \times 2 \times 4$ byte. Solving $2^n \times 2 \times 4$ byte $= 1$ Terabyte for n gives $n \approx 37$. It is possible to simulate n spin degrees of freedom without storing the complete state. This requires poly(n) bytes (i.e. BQP$\subseteq$PSPACE, see [21] and Sec. 1.5.3.) However, the time complexity of this method is believed to still be exponential.

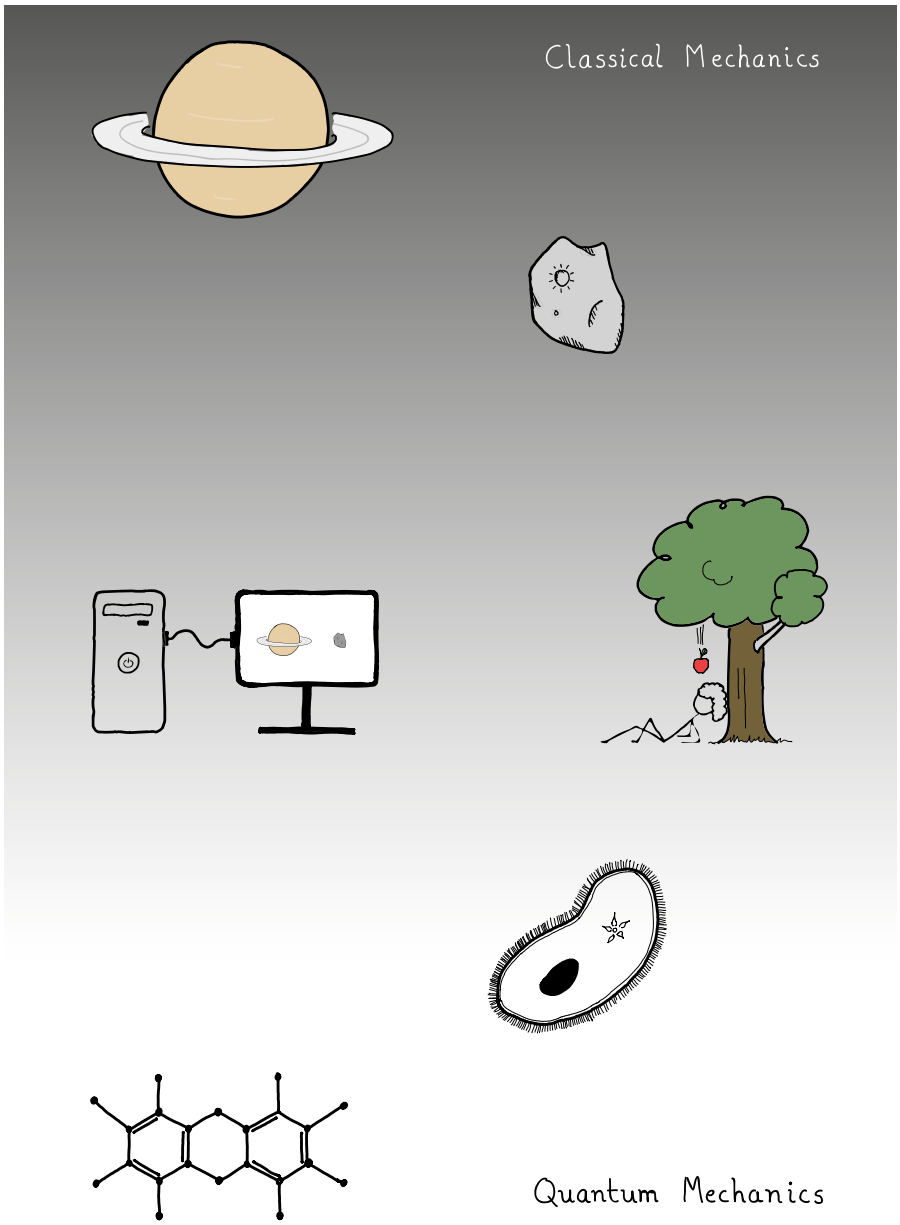

Figure 1.1: The realms of classical and quantum mechanics. The way in which the world of classical mechanics emerges from the world of quantum mechanics is one of the biggest open questions in physics. As far as we can tell there is no sharp delineation between them.

memory. Moreover, this requirement doubles with every electron that is added. This makes it intractable to store the simplified board game version of even a modest number of quantum mechanical particles. For example, it would require much more than all of the worlds' current data storage capacity [126] just to store the board game version of 100 electrons. So, it seems intractable to simulate 100 electrons.

But what if we create a computer out of quantum mechanical particles themselves [19, 45]? Such a computer is called a *quantum computer*. Because the parts of a quantum computer are themselves quantum mechanical, a quantum computer can store the board game version of a quantum mechanical system more naturally than a classical computer. Furthermore, because the parts of a quantum computer follow the rules of quantum mechanics, quantum computers can apply the rules of the quantum game more naturally then a classical computer. Hence, quantum computers have been shown to be able to efficiently simulate quantum mechanical systems [98]. See Fig. 1.2 for a picture of a real quantum computer.

Quantum computers can do much more than playing the quantum game. The extra 'quantum power' of quantum computers can also be used to solve mathematical problems, such as the factorization of whole numbers, as it was shown by Shor [132, 130]. The factorization of a whole number is the task of writing that number as a product of prime numbers. Prime numbers are numbers larger than 1 that can only be divided by 1 and themselves. For example, the factorization of 15 is 3×5. Every whole number can be factored into a unique set of prime numbers. As also noted by Shor, it is widely believed that it is impossible for classical computers to efficiently factor whole numbers; small numbers (such as 15) are still doable, but classical computers quickly reach their limits. Shor was able to prove theoretically that quantum computers, on the other hand, can factorize whole numbers efficiently [132, 130], and could in theory factor numbers with thousands of digits.

The potential of quantum computers to factor large numbers forms a potential threat to online security; if you can factor large numbers (e.g. with a quantum computer), you can decrypt most of the communication over the internet [4]. The ability of a single nation state to factor large numbers before any other could have major (geo)political consequences [144]. The search for security methods that are even unbreakable to quantum computers is an active field of research [4].

Despite their potential in quantum simulation and factorization, quantum computers are still in their infancy. The current state of the art is that a *quantum advantage* has been demonstrated on real

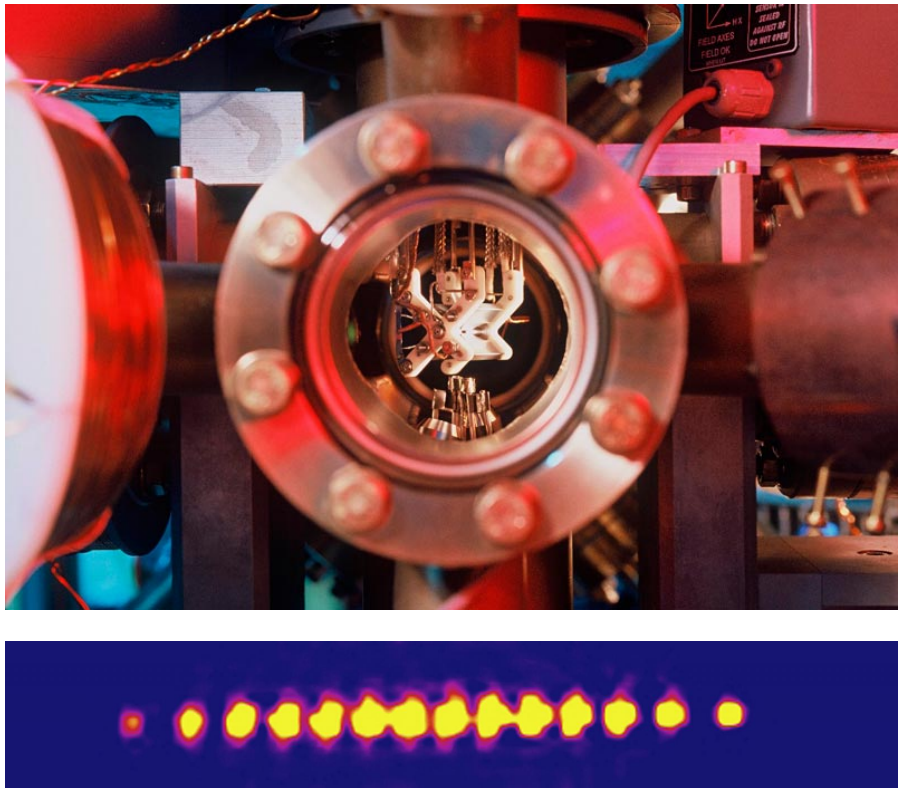

Figure 1.2: (**Top**) A real quantum computer. We are gazing through the window of a container all air was pumped out of (a vacuum chamber). The white contraption in the centre is used to levitate an array of 14 calcium ions ($^{40}Ca^{+}$) in its middle. Each calcium ion is a naturally occurring quantum mechanical system consisting out of 20 protons, 20 neutrons, and 19 electrons. Computations are performed by illuminating the ions with lasers whose rays pass through the windows. The program of the quantum computer determines where and when the lasers shine exactly. The output of the program is obtained by measuring which ions fluoresce and which do not. Image: C. Lackner, University of Innsbruck. (**Bottom**) An array of calcium ions. In reality the width of the array is less than half a millimetre; the whole would fit on the period at the end of this sentence. Nevertheless, the ions are far apart compared to their size (~ 2Å); if the atoms were the size of a person, they would all be roughly 100 Km apart. More information about this specific quantum computer can be found in Ref. [104] and references therein. Image: University of Innsbruck.

quantum computers [11, 153]. This means that there have been quantum computers that performed computational tasks that are believed to be intractable on any classical computer. However, all of these computations were just 'for sports'; the task given to those quantum computers was specifically designed with the goal of showing a quantum advantage, and have no known other applications. There has not been a quantum computer that has shown a *useful quantum advantage*; the ability to perform a *useful* computation that is believed to be intractable on classical computers.

The reason that quantum computers have not yet achieved a useful quantum advantage is that it is really hard to build good quantum computers. This is because, as it turns out, it is much harder to protect quantum computers from unwanted influences from the environment than it is to protect classical computers. These influences could, for example, be magnetic fields or temperature fluctuations. In the quantum game, you can imagine the effect of these influences as a crook that comes in from outside (the environment), making a random illegal move now and then without you noticing. Then, after many rounds, the state of the board game does not faithfully represent the state of the quantum mechanical system being simulated. We call these unwanted influences *noise* even though they may have nothing to do with sound. To reach a useful quantum advantage in the near future, it is indispensable that we gain a thorough understanding of this noise, that we learn how to mitigate it, and that we learn how to deal with any remaining noise.

1.1.2 This thesis

In Chapter 2, we propose a task that is designed to be useful, hard for classical computers, but at the same time well-suited for quantum computers that become available in the near term. The execution of this task could have the potential of showing a useful quantum advantage on a near term quantum computer, which is an important next milestone in the development of quantum computers. The task we propose is the quantum simulation of the kagome lattice (Fig. 1.3). It is a special type of simulation, where we are not so much interested in predicting future states of the kagome lattice, but rather in the task of predicting the state at temperatures close to absolute zero.

Quantum simulation of the kagome lattice can teach us new things about nature. There are materials, such as the mineral Herbertsmithite (discovered in 1972 by - you guessed it - Herbert Smith), of which the magnetic properties are described by electrons on the kagome lat-

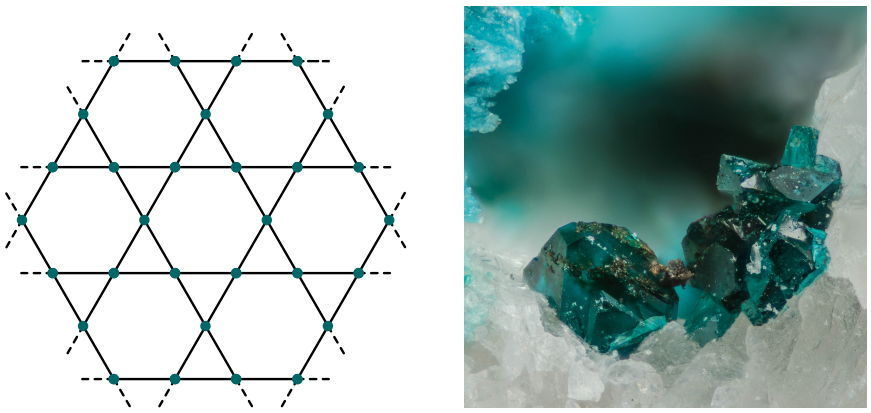

Figure 1.3: (**Left**) The kagome lattice. One electron is situated at every intersection. A line between two intersections depicts a magnetic interaction between the electrons it connects. It is not yet known what the state of this system is at temperatures close to absolute zero. (**Right**) Herbertsmithite, whose magnetic properties are described by electrons on the kagome lattice. Image: Bruce Kelley.

tice [111]. At temperatures close to absolute zero, these properties are not yet understood. This is because the task of simulating the kagome lattice has shown to be difficult for classical computers: despite decades of research effort, the question of the properties of the state of the kagome lattice at temperatures close to absolute zero remains open to this day [89].

We propose a method for the quantum simulation of the kagome lattice that is adapted to the limitations of near term quantum computers. Here, we call that method the kagome quantum game. In this game, one step of one player takes the quantum computer roughly a single step of computation. This is important in near term quantum computers because their computations should take as little time as possible; the longer a computation, the more time noise has had to spoil that computation. Furthermore, the general technique of simulation we use is relatively resilient against noise [102, 117, 113, 125].

To get an idea of how well our method would work on an ideal quantum computer, we run it on a small quantum computer. There is one catch, however: the quantum computer we run it on is not real. It is itself simulated by a classical computer. So there is a double simulation: we programmed a classical computer to simulate a quantum computer that simulates the kagome lattice. This extra step of simulation is nec-

essary because the quantum computer we would need for testing our method does not exist yet. But, as you may ask, if researchers have not succeeded to simulate the kagome lattice on classical computers, how is it possible to simulate a quantum computer that simulates the kagome lattice, on a classical computer? The caveat is that the quantum computer simulates a tiny patch of the kagome lattice, only containing 20 electrons. The simulation of that quantum computer is still doable for classical computers. The 20-electron simulation itself would not be large enough to show a useful quantum advantage. However, if we add a couple of more electrons to the lattice, it soon becomes impossible to do the classical simulation. A quantum computer, however, could still do the simulation.

In Chapter 3, we take a closer look at the noise that hinders quantum computers. Every unit in a quantum computer (called a *qubit*) inevitably interacts with the environment, and hence experiences noise from that environment. We call the amount of noise a unit experiences per second the *noise rate* of that unit. If you add another unit to your quantum computer, the quantum computer as a whole experiences more noise. The total noise rate will be the noise rate of one unit multiplied with the number of units. It was discovered [115, 124, 26] that in some situations, matters might even be worse. There is a special type of noise, called 'super noise' (or rather superdecoherence), with the property that every new unit you add increases the noise rate on every other single unit already in the quantum register. (This means the total noise rate of the total quantum computer now scales as the noise rate per unit times the square of the number of units.) This type of noise could pose a large threat to the feasibility of large scale quantum computers. Therefore, it is important to understand this type of noise thoroughly, and determine exactly when it occurs, and when it does not.

That is exactly what we do in Chapter 3 of this thesis. We give a physical interpretation of the origins of this 'super noise' in the setting of Refs. [115, 124]. Namely, we show that in this setting, an array of units can effectively behave as an antenna. This is undesirable because an antenna is susceptible to electromagnetic radiation, such as radio or Wi-Fi signals. The more units your quantum computer has, the larger this antenna becomes, and hence the more sensitive it becomes. It is this increased sensitivity that leads to 'super noise'. We also show that this type of noise can be easily avoided: the larger the effective antenna becomes, the more its sensitivity concentrates on a single frequency. Thus, a quantum computer with many units only experiences super noise if there is noise on exactly the frequency the antenna tunes in to,

which is something that can be avoided in practical situations. Hence, 'super noise' does not pose a real threat to quantum computers.

In Chapter 4 we study more closely a well-known method for reducing the amount of noise (including regular and super noise). As you might have experienced yourself, in solving a mathematical problem, there are multiple ways of arriving at the same, correct answer. Similarly, a quantum computer may arrive at the same answer to a problem in different ways. Some of these ways might be quicker than others. It was shown that, in theory, there exists 'noiseless ways'; these are ways where the outcome of the computation is as if no noise acted on the quantum computer (that is, the outcome is the correct outcome), even though noise did affect the individual units [83]. A noiseless way might involve a 'detour', and hence may not be the fastest way.

In the theoretical proof of the existence of these noiseless ways [83], perfect knowledge of how the quantum computer reacts to the noise is assumed. In practical situations, however, perfect knowledge of how the quantum computer reacts to noise is arguably impossible. In Chapter 4, we derive a formula with which one can determine how large the effects of the imperfectness of one's knowledge are. Using this formula, one can easily determine how well a noiseless way will work in practice, aiding the design of quantum computers and quantum computational methods.

1.1.3 Conclusion and outlook

Many-body physics is the study of physical systems that are comprised out of many smaller units, or 'bodies'. The solar system is an example of a classical many-body system, and the kagome lattice is an example of a quantum many-body system. The central theme in this thesis is the interplay between many-body physics and quantum computation (hence its title). This interplay knows two directions:

1. We can use quantum computation to better understand many-body quantum physics, such as in Chapter 2.

2. As quantum computers are scaled up, they themselves become many-body quantum systems. Hence, we can use quantum many-body physics to better understand quantum computation, such as in Chapter 3 and Chapter 4.

There is sill a long way to go before quantum computers mature, but once they do, it has the potential to cause a revolution in physics that can match the revolution that was caused by classical computers.

1.2 Introductie en samenvatting in het Nederlands

This is a translation of the previous section into Dutch, omitting footnotes and figure captions. We switch back to English on page 16.

1.2.1 Quantumcomputers

Op 30 juni 2021 komt de planetoïde '2020 AD1' met een relatieve snelheid van ongeveer 17.000 km/h op de aarde af [52, 54]. Gelukkig zal hij de aarde niet raken; op 4 juli schiet de planetoïde voorbij op een afstand van drie keer de afstand tussen de aarde en de maan.

Het zonnestelsel bestaat uit de zon en de objecten in een baan daaromheen. De ons bekende objecten omvatten de planeten, ongeveer een miljoen planetoïden en tientallen ruimteschepen. Met behulp van computers is het mogelijk het zonnestelsel te simuleren. Daartoe wordt er eerst een digitale 'bordspelversie' van het zonnestelsel gemaakt dat enkel de essentiële eigenschappen van het zonnestelsel bevat. In het geval dat we willen voorspellen of een planetoïde de aarde gaat raken, zijn deze eigenschappen de massa, richting, snelheid en positie van de ons bekende objecten in het zonnestelsel. Deze verzameling informatie noemen we vanaf nu de *toestand* van het zonnestelsel. (De toestand verandert met de tijd.) De spelers op het bordspel stellen de ons bekende objecten in het zonnestelsel voor. Het spel is zo ontworpen dat elke toestand van het spel correspondeert met een toestand van het zonnestelsel. Door vele spelronden te spelen kan een computer de toekomstige speltoestanden uitrekenen en daarmee de toekomstige toestanden van het zonnestelsel. Op deze manier heeft een computer onder andere de toekomstige posities van zowel de aarde als de planetoïde '2020 AD1' uitgerekend. Uit deze berekening blijkt dat deze twee hemellichamen elkaar niet zullen raken in de nabije toekomst.

De spelers op het bordspel volgen de spelregels. Deze zijn volkomen deterministisch; voor elke speler is er per beurt één geldige zet. Dit is omdat de spelregels zijn bepaald door de wetten van de *klassieke mechanica*, en die wetten bieden geen keuzevrijheid. De wetten van de klassieke mechanica zijn ook de natuurwetten die onze alledaagse ervaringen bepalen; als je tegen een pion duwt komt er beweging in ('$F = ma$'), en als je een appel loslaat dan valt hij.

Om de wereld van dit proefschrift te betreden laten we het zonnestelsel achter en zoomen we in op een minuscuul stukje aarde. Ver voor-

bij de planeten, bomen, mensen, appels, pionnen en micro-organismen betreden we het rijk van de moleculen. Moleculen bestaan uit protonen, neutronen en elektronen (Fig. 1.1). Verrassend genoeg gelden er op deze schaal andere natuurwetten: die van de *quantummechanica*. Mensen zijn niet gewend aan deze wetten omdat de objecten in ons dagelijks leven de wetten van de klassieke mechanica volgen. Quantummechanica kan daarom tegenintuïtief zijn en staat bekend als ondoorgrondelijk [44].

Het gedrag van protonen, neutronen en elektronen bepaalt het verloop van chemische reacties. Zou het daarom niet mooi zijn als we ook het gedrag van deze deeltjes kunnen simuleren? We zouden dan beter in staat zijn ingewikkelde chemische reacties te begrijpen, wat weer kan leiden tot de verbetering van bepaalde industriële productieprocessen. De productie van kunstmest is daar een voorbeeld van [123]. De productie van een van de ingrediënten van kunstmest is verantwoordelijk voor ongeveer 1% van het wereldwijde energieverbruik, en dat allemaal in de vorm van fossiele brandstoffen [112]. Er bestaan echter bacteriën die datzelfde ingrediënt produceren zonder het gebruik van fossiele brandstoffen. De simulatie van het chemische proces dat deze bacteriën gebruiken zou ons mogelijk in staat stellen van de bacteriën te leren en daarmee kunstmest milieuvriendelijker te produceren [123].

De simulatie van elektronen, protonen en neutronen vraagt om een ander bordspel (het 'quantumspel') dan de simulatie van het zonnestelsel. De spelstukken zijn nu de protonen, neutronen en elektronen. Ook de regels van het nieuwe spel zijn anders. Deze worden nu bepaald door de wetten van de quantummechanica. Quantummechanica is niet alleen ingewikkeld voor mensen, maar ook voor computers. Een korte berekening (voetnoot op pagina 2) laat zien dat er meer dan 1 Terabyte aan geheugen nodig is om de bordspelversie van 37 elektronen op te slaan. Belangrijker nog is dat dit geheugengebruik verdubbelt met elk elektron dat wordt toegevoegd. Het geheugengebruik groeit daarmee exponentieel in het aantal elektronen. Hierdoor is het onmogelijk om van meer dan een klein aantal elektronen de bordspelversie op te slaan. Om bijvoorbeeld de bordspelversie van meer dan 100 elektronen op te slaan is zelfs de huidige wereldwijde data-opslagcapaciteit niet toereikend. Het lijkt dus praktisch onmogelijk om meer dan 100 elektronen te simuleren.

Maar wat nu als we een computer maken die zelf bestaat uit quantummechanische deeltjes [19, 45], zoals elektronen, protonen en neutronen? Dat is precies het idee achter de *quantumcomputer*. Omdat de onderdelen van een quantumcomputer zelf quantummechanische deeltjes zijn, is het voor zo'n computer heel natuurlijk om de bordspelversie

van quantummechanische deeltjes op te slaan. Omdat de onderdelen van een quantumcomputer zelf de wetten van de quantummechanica volgen, is het bovendien voor een quantumcomputer heel natuurlijk om de spelregels van het quantumspel toe te passen. Quantumcomputers kunnen daardoor efficiënt quantummechanische systemen simuleren [98]. Zie Fig. 1.2 voor een afbeelding van een echte quantumcomputer.

Quantumcomputers kunnen zelfs meer dan dat; de extra 'quantumkracht' van quantumcomputers kan ook worden aangewend voor het oplossen van puur wiskundige problemen. Een *priemgetal* is een getal groter dan 1 dat slechts door zichzelf en 1 gedeeld kan worden (zonder rest). De priemgetallen zijn dus $3, 5, 7, 11, \ldots$. Het *ontbinden in priemfactoren* is de taak een gegeven geheel getal te schrijven als product van priemfactoren. Elk getal kan zo ontbonden worden, en deze ontbinding is uniek. Een voorbeeld is $15 \to 3 \times 5$. Voor zover bekend is het voor een gewone, klassieke computer onmogelijk efficiënt getallen te ontbinden. Kleine getallen zoals 15 lukken nog, maar klassieke computers bereiken al snel hun limiet. (Dit is omdat de rekentijd exponentieel groeit in het aantal cijfers van het te ontbinden gehele getal.) Daardoor is het onmogelijk getallen te ontbinden met honderden cijfers. Het blijkt echter [130, 132], dat quantumcomputers in theorie wel efficiënt getallen kunnen ontbinden. (Voor een quantumcomputer groeit de rekentijd niet exponentieel maar als een polynoom in de lengte van het te ontbinden getal.) Ze zouden dus in principe wel in staat kunnen zijn getallen met honderden cijfers te ontbinden.

De veiligheid van de methode die wordt gebruikt voor het versleutelen van berichten die over het internet worden verstuurd, zoals bijvoorbeeld berichten tussen jou en de website van je bank, is gebaseerd op de aanname dat het onmogelijk is getallen met honderden cijfers te ontbinden. Met een quantumcomputer zou je die beveiliging dus kunnen breken. Als slechts enkele landen grote getallen kunnen ontbinden, zou dit onder andere vanwege de spionagepotentie grote gevolgen kunnen hebben voor de wereldwijde machtsbalans [144]. Het onderzoek naar versleutelingsmethoden die zelfs door quantumcomputers niet te breken zijn is daarom ook in volle gang [4].

Ondanks hun potentie staat de ontwikkeling van quantumcomputers nog in de kinderschoenen. De huidige stand van zaken is dat *quantumsuperioriteit* of *een quantumvoordeel* (Engels: 'quantum supremacy' of 'a quantum advantage') is aangetoond op echte quantumcomputers. Dit betekent dat deze quantumcomputers een rekentaak hebben verricht die, voor zover we weten, praktisch onmogelijk is voor klassieke computers. Dit klinkt alsof quantumcomputers nu al volledig

de klassieke computers verslagen hebben, maar dat is niet helemaal zo; de rekentaken waarvoor er een quantumvoordeel is aangetoond op echte quantumcomputers zijn artificieel en hebben geen toepassingen (anders dan het aantonen van een quantumvoordeel). Er is tot op heden geen echte quantumcomputer geweest die een *nuttige* rekentaak heeft uitgevoerd die niet net zo goed op een klassieke computer uitgevoerd had kunnen worden. De mijlpaal van een *nuttig quantumvoordeel* is dus nog niet bereikt.

Quantumcomputers hebben nog geen nuttig quantumvoordeel bereikt omdat het heel moeilijk is om goede quantumcomputers te bouwen. Het blijkt dat quantumcomputers veel moeilijker dan klassieke computers te beschermen zijn tegen ongewilde invloeden uit hun omgeving. Deze invloeden of 'stoorzenders' bestaan bijvoorbeeld uit magnetische velden of temperatuurschommelingen. In termen van het quantumspel (gebruikt voor het simuleren van quantummechanische systemen op een quantumcomputer) kun je de effecten van deze stoorzenders voorstellen als een onverlaat die op onregelmatige tijden stiekem de quantumcomputer binnendringt en een ongeldige zet doet. Na vele spelronden zal de speltoestand van het bordspel niet langer getrouw de toestand van het gesimuleerde quantummechanische systeem representeren. Het effect van de stoorzenders noemen we *ruis*, ook al heeft de ruis, net als bijvoorbeeld witte beeldruis op een ouderwetse beeldbuis, misschien niets met geluid te maken. Om in de nabije toekomst een nuttig quantumvoordeel te bereiken is het essentieel dat we de oorzaken en gevolgen van deze ruis goed begrijpen, dat we begrijpen hoe de ruis verminderd kan worden, en dat we begrijpen hoe er met de overgebleven ruis omgegaan kan worden.

1.2.2 Dit proefschrift

In Hoofdstuk 2 van dit proefschrift stellen we een rekentaak voor die tegelijk nuttig, moeilijk voor klassieke computers, en geschikt voor de quantumcomputers van de nabije toekomst is. Het uitvoeren van deze taak heeft dus de potentie om een nuttig quantumvoordeel aan te tonen. De taak die we voorstellen is de simulatie van het kagomerooster (Fig. 1.3). Het is een speciaal type simulatie waar het niet gaat om het voorspellen van toekomstige toestanden maar om het voorspellen van de toestand bij temperaturen rond het absolute nulpunt ($-273,15\,^{\circ}\mathrm{C} = 0\,\mathrm{K}$).

De simulatie van het kagome-rooster kan ons nieuwe inzichten geven over de natuur. Er zijn materialen, zoals het mineraal Herbertsmithiet (Engels: Herbertsmithite), ontdekt door - u raadt het al - Herbert

Smith, waarvan de magnetische eigenschappen worden beschreven door elektronen op het kagome-rooster [111]. Bij temperaturen rond het absolute nulpunt worden deze eigenschappen nog niet goed begrepen, ondanks decennia aan onderzoek met klassieke computers [89].

In dit proefschrift ontwerpen we een specifieke simulatiemethode speciaal bedoeld voor de kleine, aan ruis onderhevige quantumcomputers van de nabije toekomst. Deze simulatiemethode noemen we hier het *kagome-spel*. Het spel is zo gekozen dat het zetten van een enkele zet een quantumcomputer slechts een enkele rekenstap kost. Deze eigenschap is belangrijk voor de quantumcomputers van de nabije toekomst omdat hun berekeningen zo kort mogelijk moeten duren; hoe langer een berekening duurt, hoe meer tijd de stoorzenders hebben om de berekening in de war te gooien. Bovendien is de algemene simulatiemethode die we gebruiken relatief goed bestand tegen ruis [102, 117, 113, 125].

Om een idee te krijgen van hoe goed onze specifieke simulatiemethode werkt, voeren we deze uit op een kleine quantumcomputer. De quantumcomputer waar we de methode op uitvoeren is echter niet echt; deze wordt zelf gesimuleerd door een klassieke computer. Er is dus sprake van een dubbele simulatie: een klassieke computer simuleert een quantumcomputer die het kagome-rooster simuleert. Deze extra laag simulatie is nodig omdat de quantumcomputer die we nodig hebben om het kagome-spel te testen nog niet bestaat.

Als het onmogelijk is om met klassieke computers het kagome-rooster te simuleren, hoe kan een klassieke computer dan een quantumcomputer simuleren die het kagome-rooster simuleert? Simuleert de klassieke computer dan niet uiteindelijk het kagome-rooster? De kanttekening die hier geplaatst moet worden is dat de quantumcomputer slechts een kleine uitsnede van het kagome-rooster simuleert, met daarop 20 elektronen. De simulatie van die quantumcomputer lukt nog net op een klassieke computer. De simulatie van deze uitsnede op een quantumcomputer is dus niet genoeg voor het aantonen van een quantumvoordeel. Als we echter een wat grotere uitsnede zouden nemen wordt de simulatie al snel onmogelijk voor klassieke computers, terwijl diezelfde simulatie op een echte quantumcomputer in theorie mogelijk blijft.

In Hoofdstuk 3 bestuderen we de ruis die quantumberekeningen stoort. Elke fundamentele eenheid van een quantumcomputer, genaamd *qubit*, interacteert onvermijdelijk met zijn omgeving. Daarom ondervindt elke eenheid apart ruis. Als je een eenheid aan een quantumcomputer toevoegt, ondervindt de quantumcomputer dus als geheel meer ruis. (De totale ruis-intensiteit die een quantumcomputer onder-

vindt is gewoonlijk gelijk aan de ruis-intensiteit die een enkele eenheid ondervindt vermenigvuldigd met het aantal eenheden.)

Er werd echter ontdekt dat deze situatie te rooskleurig zou kunnen zijn. Er is een speciaal type ruis, genaamd *super-ruis* (Engels: 'super noise' of eigenlijk 'superdecoherence'), met de eigenschap dat elke eenheid die je toevoegt de ruis-intensiteit op alle reeds bestaande eenheden doet toenemen [115, 124, 26]. Oftewel, hoe meer eenheden, hoe hoger de ruis-intensiteit van elk van deze eenheden afzonderlijk. (Dit betekent dat de totale ruis-intensiteit die de quantumcomputer ondervindt nu schaalt met het kwadraat van het aantal eenheden.)

Super-ruis zou een grote bedreiging kunnen vormen voor schaalbaarheid van quantumcomputers. Daarom is het essentieel dit type ruis goed te begrijpen en te bepalen wanneer het wel, en wanneer het niet optreedt. Dit doen we in Hoofdstuk 3 van dit proefschrift. Ten eerste geven we een natuurkundige interpretatie van de oorzaak van super-ruis (in de specifieke situatie zoals beschreven in Refs. [115, 124]). We laten zien dat een rij eenheden van een quantumcomputer zich effectief kan gaan gedragen als een antenne. Antennes zijn gevoelig voor elektromagnetische straling, veroorzaakt door bijvoorbeeld wifi- of radiozenders. Hoe meer eenheden een quantumcomputer heeft, hoe gevoeliger deze antenne wordt. In Hoofdstuk 3 laten we zien dat de gevoeligheid dusdanig toeneemt dat er in speciale situaties super-ruis kan ontstaan.

De antenne-analogie laat echter ook zien hoe deze super-ruis in de praktijk gewoonlijk niet voorkomt. We laten namelijk ook zien dat, hoe groter de antenne wordt, hoe meer zijn gevoeligheid zich beperkt tot een enkele frequentie. Het netto-effect van de toenemende gevoeligheid, met tegelijk een afnemende bandbreedte van die gevoeligheid, is dat er gewoonlijk *geen* super-ruis meer optreedt. We concluderen daarom dat super-ruis geen bedreiging vormt voor de schaalbaarheid van quantumcomputers.

In Hoofdstuk 4 bestuderen we een vorm van ruisreductie. Zoals u wellicht zelf ervaren hebt, zijn er voor een gegeven rekenprobleem meerdere manieren om bij hetzelfde, correcte antwoord uit te komen. Ook een quantumcomputer kan op verschillende manieren tot het juiste antwoord op een gegeven rekenprobleem komen. Sommige van deze manieren zijn sneller dan andere. Voor sommige van deze manieren kunnen de effecten van ruis ook minder erg zijn dan voor andere. De snelste manier is misschien niet de manier die het minste last ondervindt van ruis. Onder bepaalde omstandigheden kunnen er zelfs rekenmanieren zijn waarop ruis geen enkel effect heeft, terwijl elk van de eenheden van de quantumcomputer waarop die berekening wordt uitgevoerd wel ruis

ondervindt [83]. Zo'n rekenmanier noemen we *ruisloos*.

In het theoretische bewijs van het bestaan van ruisloze rekenmanieren [83] op quantumcomputers wordt er aangenomen dat het mogelijk is perfecte kennis te hebben over de interactie tussen een quantumcomputer en zijn omgeving. In de praktijk zal deze kennis echter altijd imperfect zijn. In Hoofdstuk 4 leiden we een formule af waarmee men gemakkelijk de effecten van deze imperfectie kan kwantificeren. Met deze formule kan men dus inschatten hoe goed een ruisloze rekenmanier zich in de praktijk zal gedragen zonder deze rekenmanier daadwerkelijk uit te voeren. Dit kan bijdragen aan het verbeteren van quantumcomputers en methoden die gebruikmaken van ruisloze rekenmanieren.

1.2.3 Conclusie en vooruitblik

De veeldeeltjesfysica is de studie naar het collectieve gedrag van systemen die bestaan uit vele deeltjes. Het kagome-rooster vormt een voorbeeld van zo'n veeldeeltjessysteem. Een centraal thema in dit proefschrift is de interactie tussen veeldeeltjesfysica en quantumcomputers. Deze interactie kent twee richtingen:

1. Door het simuleren van quantummechanische systemen kunnen quantumcomputers ons nieuwe inzichten bieden in de veeldeeltjesfysica, zoals in Hoofdstuk 2.

2. Hoe meer eenheden een quantumcomputer heeft, hoe meer deze quantumcomputer zelf een veeldeeltjessysteem wordt. Daarom kunnen we technieken uit de veeldeeltjesfysica gebruiken om quantumcomputers met vele eenheden te beschrijven, zoals in Hoofdstuk 3 en 4.

Er is nog een lange weg te gaan voordat quantumcomputers tot wasdom zijn gekomen. Zodra ze echter zover zijn, zal dit mogelijk een revolutie teweeg brengen in de veeldeeltjesfysica die zich kan meten met de revolutie die klassieke computers teweeg hebben gebracht in de veeldeeltjesfysica.

1.3 Quantum computing

In this section, I give a more technical, yet pedagogical, introduction to quantum computing. All topics covered here can also be found in standard textbooks on algorithms and quantum computation, such as Refs. [32, 108, 34].

1.3.1 Computers

The fundamental unit of information in classical computers is the *bit*; any physical system that, at some level, can be in one of two discrete states. That is, the state space of a bit is $\mathbb{Z}_2 = \{0, 1\}$. Physically, a bit may be implemented as a wire through which there is a current above some threshold ($x = 1$) or below that threshold ($x = 0$). We can visualize the space of possible states of a bit by placing a dot for every state,

$$\begin{matrix} \bullet\ (0) \\ \\ \bullet\ (1) \end{matrix} \quad . \tag{1.1}$$

Going from one bit to two bits, there are now four possible states: 00, 01, 10 and 11. In general, n bits can be in 2^n different states. We denote this state space as $\{0, 1\}^n$. It is customary to denote the value of the jth bit, where we count from right to left, starting with 0, by x_j. That is, we write the state of n bits as the *bitstring* $x = x_{n-1} \dots x_1 x_0$. The bitstrings can be used to represent integers in the following way,

$$\begin{matrix} \dots 000 & (0) \\ \dots 001 & (1) \\ \dots 010 & (2) \\ \dots 011 & (3) \\ \dots 100 & (4) \\ \vdots & \end{matrix}$$

This is called the *binary representation* of the integers. In this representation, a bitstring with a '1' only at place j represents the number 2^j. This can be used to translate between the decimal representation and the binary representation. For example, $15 = 2^3 + 2^2 + 2^1 + 2^0 \mapsto 1111$. This representation is used throughout this thesis. For example, we may write sums of the form $\sum_x f(x)$. If we have n bits, this means $\sum_{x_{n-1},\dots,x_0} f(x_{n-1}, \dots, x_0)$.

Similarly to the mapping between integers, mappings can be made between integers and characters (including spaces, end of line characters, etc.) A well-known mapping is ASCII. Under such a map, a piece of text, such as the source code of a computer program, is essentially a large bitstring.

Computers are machines that implement functions from bitstrings

to bitstrings,

$$f : \{0,1\}^n \to \{0,1\}^m.$$

They take a bitstring as *input*, and provide a (generally) different bitstring as *output*. For example, the input could be the binary representation of a large integer, and the output could be the binary representation of its smallest prime factor.

Now any such implementation of a function can be divided into 'little functions' that only take one or two bits as input. These are like the atoms of the computation of that function. These little functions are called *gates*. A set of gates that can be used to implement an arbitrary computable function, is called a *universal gate set*. A *classical computer* is a computer that uses classical gates. An example is the NAND gate, where $\mathrm{NAND}(x_1, x_2)$ evaluates to 0 if $x = 11$ and to 1 in all other cases. The NAND gate on itself forms a universal gate set for classical computation.

1.3.2 Quantum computers

A *quantum computer* is also a computer, in the sense that it maps bitstrings to bitstrings. The difference with classical computers is in how this map is implemented. During the computation, a quantum computer has access to quantum mechanical bits, or *qubits*, and quantum mechanical gates that act thereon, called *quantum gates*.

1.3.2.1 One qubit

Let us start with a single qubit. This is any quantum system whose state space is the Hilbert space $\mathcal{H}_1 \equiv \mathbb{C}^2$. The vectors in the *computational* or classical basis are denoted as $|0\rangle$ and $|1\rangle$. These vectors are taken to be orthonormal. An arbitrary state can thus be written as

$$|\psi\rangle = \alpha\,|0\rangle + \beta\,|1\rangle\,, \tag{1.2}$$

where the *amplitudes* α and β are complex numbers. An example of a physical system with this state space is a spin-1/2 particle. We may refer to $|0\rangle$ as 'spin up', and to $|1\rangle$ as 'spin down'.

According to the laws of quantum mechanics, when a qubit is measured in the computational basis, the probability of getting the outcome $|0\rangle$ is $|\alpha|^2$, and the probability of outcome $|1\rangle$ is $|\beta|^2$. Since we get an outcome with unit probability, we must require that $|\alpha|^2 + |\beta|^2 = 1$. This is the *normalization condition* on quantum states. Additionally,

in quantum mechanics, states that differ by an overall complex phase cannot be distinguished experimentally. Hence, two states that differ by an overall complex phase are said to be equivalent. It is common to refer to the equivalence classes that can thus be defined as the *states* themselves.[3] A more detailed account of measurement and the redundancy of overall phases is given in Sec. 1.4.1.

Let us incorporate the normalization condition and the phase redundancy in the descriptions of a general qubit state $|\psi\rangle$. Let $\alpha = e^{i\phi_\alpha} r_\alpha$ and $\beta = e^{i\phi_\beta} r_\beta$. Then, $|\psi\rangle = e^{i\phi_\alpha}[r_\alpha + e^{i(\phi_\beta - \phi_\alpha)} r_\beta]$. Disregarding the overall phase, and using the parametrization $\phi_\beta - \phi_\alpha = \phi$, with $\phi \in [0, 2\pi)$, we may write a general state as $|\psi\rangle = r_\alpha |0\rangle + e^{i\phi} r_\beta |1\rangle$. In the current parametrization, the normalization condition reads $r_\alpha^2 + r_\beta^2 = 1$. The $r_\alpha \geq 0$ and $r_\beta \geq 0$ that satisfy this condition form the upper right quadrant of a circle. Hence, we may use the parametrization $r_\alpha = \cos(\theta/2)$, $r_\beta = \sin(\theta/2)$, with $\theta \in [0, \pi]$. We can thus write a general qubit state as

$$|\psi(\theta, \phi)\rangle = \cos\left(\frac{\theta}{2}\right)|0\rangle + e^{i\phi} \sin\left(\frac{\theta}{2}\right)|1\rangle . \tag{1.3}$$

Using this parametrization, any state can be depicted as a point (θ, ϕ) on the unit sphere, called the *Bloch sphere* Fig. 1.4. This sphere is embedded in $\mathbb{R}^3$ by choosing $\hat{\boldsymbol{n}} = (\sin\theta\cos\phi, \sin\theta\sin\phi, \cos\theta)^T$. Both (θ, ϕ) and $\hat{\boldsymbol{n}}$ can be referred to as (representations of) a *Bloch vector*. In Fig. 1.4, also the states $|0\rangle$, $|1\rangle$, and

$$|+\rangle = \frac{1}{\sqrt{2}}(|0\rangle + |1\rangle), \qquad |-\rangle = \frac{1}{\sqrt{2}}(|0\rangle - |1\rangle)$$

are depicted.

Note the difference with the state space of a bit; the qubit has a continuous state space (a sphere), whereas that of the bit is discrete (two points). However, a spherical state space is itself not a quantum mechanical property. For example, the state space of the positional part of a rigid pendulum that can move in two directions is also a sphere. A difference between the qubit and the bi-directional pendulum does arise when we consider measurement; as opposed to the direction of the bi-directional pendulum, it is impossible to measure the direction of the Bloch-vector with a single measurement. Given an axis along which you measure, there are only two possible outcomes of the measurement; 'spin up' in your direction of measurement, or 'spin down' in your direction of measurement. For example, if you measure along

[3] So, formally, the state space of a qubit is $\mathbb{CP}^1 = S^2$.

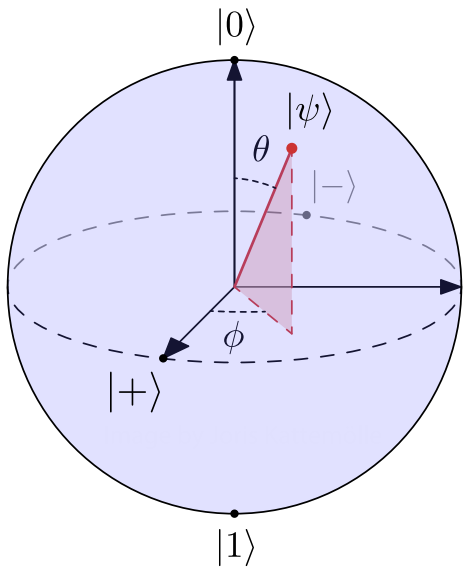

Figure 1.4: The Bloch sphere. The state space of a qubit is a sphere, whereas the state space of a bit consists of just two points [Eq. (1.1)].

the vertical axis, the possible outcomes are $|0\rangle$ and $|1\rangle$. If you measure in the out-of-plane direction, the possible outcomes are $|+\rangle$ and $|-\rangle$. (Also see Sec. 1.4.1.)

1.3.2.2 Single-qubit gates

A *quantum gate* U is a linear operation that generally acts non-trivially only on a couple of qubits. Since quantum states are normalized to unity, such an operation is not allowed to change the norm of state vectors. Therefore, these linear operations must be unitary, $U^\dagger U = \mathbb{1}$.

Let us start with the single-qubit gates. In quantum circuit notation, a single qubit is represented by a single horizontal line. When a gate acts on that qubit, we write that operator in a box that is attached to the line, very much like in classical circuits,

$$|\psi\rangle \longrightarrow \boxed{U} \longrightarrow U|\psi\rangle\,.$$

Here time runs from left to right. In another convention, that is especially used by physicists because of its kinship to space-time diagrams, time runs from bottom to top. This convention is used in Sec. 2 of this thesis.

If we make the identification $|0\rangle \mathrel{\hat{=}} (1,0)^T$ and $|1\rangle \mathrel{\hat{=}} (0,1)^T$, any single-qubit gate can be written as a 2×2 matrix. Common single-qubit

gates include the Pauli-operators

$$X = \begin{pmatrix} 0 & 1 \\ 1 & 0 \end{pmatrix}, \quad Y = \begin{pmatrix} 0 & -\mathrm{i} \\ \mathrm{i} & 0 \end{pmatrix}, \quad Z = \begin{pmatrix} 1 & 0 \\ 0 & -1 \end{pmatrix}, \tag{1.4}$$

the Hadamard gate,

$$H = \frac{1}{\sqrt{2}} \begin{pmatrix} 1 & 1 \\ 1 & -1 \end{pmatrix}, \tag{1.5}$$

and the $RZ(\theta)$ gate,

$$RZ(\theta) = \mathrm{e}^{-\mathrm{i}\theta Z/2}\mathrm{e}^{\mathrm{i}\theta/2} = \begin{pmatrix} 1 & 0 \\ 0 & \mathrm{e}^{\mathrm{i}\theta} \end{pmatrix}. \tag{1.6}$$

The RZ gate is a parametrized gate, and can be implemented for any given θ on many quantum computing platforms. Note how the Z gate is a special case of the RZ gate. Here are some first examples of quantum circuits,

$|0\rangle$ —[X]— $|1\rangle$, $|1\rangle$ —[X]— $|0\rangle$, ('bit flip'),
$|0\rangle$ —[Z]— $|0\rangle$, $|1\rangle$ —[Z]— $-|1\rangle$, ('phase flip'),
$|0\rangle$ —[H]— $|+\rangle$, $|1\rangle$ —[H]— $|-\rangle$.

Since $ZX = Y$, the Y gate can be seen as a bit flip followed by a phase flip. Note that by linearity, the above circuits in itself also define the action of those gates on general states.

We can gain an insightful form of general single-qubit gates U by removing redundancies in its description and introducing an adequate parametrization. This is similar in spirit to the process of obtaining the Bloch-vector. An arbitrary complex 2×2 matrix has 8 real coefficients. The condition that states must remain normalized under U, that is, $U^\dagger U = \mathbb{1}$, provides 4 independent conditions, allowing for the elimination of 4 coefficients. The redundancy of the overall phase of state vectors can be used to eliminate a further coefficient. In this way, it can be shown that a general single-qubit gate can be written as

$$U(\alpha, \tilde{\theta}, \tilde{\phi}) = \mathrm{e}^{-\mathrm{i}\alpha \hat{\boldsymbol{m}} \cdot \boldsymbol{\sigma}/2}, \tag{1.7}$$

with α a real coefficient, $\hat{\boldsymbol{m}}$ a unit vector in $\mathbb{R}^3$, $\hat{\boldsymbol{m}} = (\sin\tilde{\theta}\cos\tilde{\phi}, \sin\tilde{\theta}\sin\tilde{\phi}, \cos\tilde{\theta})^T$ with angles $\tilde{\theta} \in [0, \pi]$, $\phi \in [0, 2\pi)$, and

$\boldsymbol{\sigma} = (X, Y, Z)^T$. Writing out the exponent, and resumming the terms, one can show a formula akin to Euler's formula $\mathrm{e}^{\mathrm{i}\alpha} = \cos\alpha + i\sin\alpha$,

$$U(\alpha, \tilde{\theta}, \tilde{\phi}) = \cos(\alpha/2)\mathbb{1} - \mathrm{i}\sin(\alpha/2)\,\hat{\boldsymbol{m}} \cdot \boldsymbol{\sigma}.$$

Applying this operator to an arbitrary single-qubit state [Eq. (1.3)], it can be given the following interpretation: *the unitary $U(\alpha, \tilde{\theta}, \tilde{\phi})$ rotates the Bloch vector $\hat{\boldsymbol{n}}$ around $\hat{\boldsymbol{m}}$ by an angle α.* From this viewpoint, the gates $X = \mathrm{e}^{-\mathrm{i}\pi X/2}$, $Z = \mathrm{e}^{-\mathrm{i}\pi Z/2}$, and $H = \mathrm{e}^{-\mathrm{i}\pi(1/\sqrt{2},0,1/\sqrt{2})/2}$ are rotations with angle π about the Bloch vectors $(\pi/2, 0)$, $(0, 0)$ and $(\pi/4, 0)$, respectively.

The final single-qubit operation we consider is *measurement*, denoted in circuit notation as

 . (1.8)

This measurement is by convention in the computational basis. The classical outcome of the measurement, that is a single classical bit holding the value 0 or 1, is depicted by the two lines on the right of the meter. As opposed to the other gates in this section, measurement is not a unitary operation.

1.3.2.3 Multiple qubits

The state space of n qubits, $\mathcal{H}_n$, is given by the tensor product space of n single-qubit spaces, $\mathcal{H}_n = (\mathcal{H}_1)^{\otimes n}$. We denote the computational basis vectors of this space by using the binary representation of x, $|x\rangle \equiv |x_{n-1}\rangle \otimes |x_{n-2}\rangle \otimes \ldots \otimes |x_0\rangle$. Note that there thus is a one-to-one mapping between the state of n classical bits and a computational basis vector of n qubits. Therefore, the computational basis is sometimes referred to as the *classical basis*. A general state of n qubits can be expanded over this basis as [cf. Eq. (1.2)]

$$|\psi\rangle = \sum_x c_x\,|x\rangle\,.$$

Note that, again, the c_x are not all independent, for we have the conditions $\sum_x |c_x|^2 = 1$ and the equivalence of $|\psi\rangle$ and $\mathrm{e}^{\mathrm{i}\varphi}\,|\psi\rangle$. Hence, the description of the state of n qubits requires $2 \times 2^n - 2$ real parameters. We can check that, for $n = 1$, we have $C = 2$, e.g. the parameters (θ, ϕ) of the Bloch vector.

Not only is the state space of n qubits much larger than the state space of n bits, it is also much larger than the state space of n static bi-directional pendulums. A state in the latter space is described by

$(\theta_{n-1}, \phi_{n-1}, \theta_{n-2}, \phi_{n-2}, \ldots, \theta_0, \phi_0)$. That is, the description of the position of n static bi-directional pendulums requires $2n \ll 2 \times 2^n - 2$ real parameters.

1.3.2.4 Multiple-qubit gates

For any non-trivial quantum computation, it is essential that the qubits of a quantum computer interact with one another. This is done via multiple-qubit gates. Often, the only multiple-qubit gates a quantum computer can directly implement are 2-qubit gates.

In quantum circuit notation, the state space of two qubits is represented by two parallel horizontal lines. Here we do not assume the qubits are in a product state. When the two qubits are acted upon by a two-qubit operator U, we write that operator in a box like so,

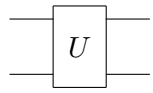

.

A common two-qubit gate is the CNOT gate, defined by

$$\begin{aligned} \text{CNOT}\,|00\rangle &= |00\rangle\,, \\ \text{CNOT}\,|01\rangle &= |01\rangle\,, \\ \text{CNOT}\,|10\rangle &= |11\rangle\,, \\ \text{CNOT}\,|11\rangle &= |10\rangle\,. \end{aligned} \tag{1.9}$$

The CNOT applies a bit flip to the second qubit (the 'target bit') if and only if the first qubit (the 'control bit') is in the state $|1\rangle$. We can, of course, figure out what the CNOT does on arbitrary states by using linearity. The CNOT gate is so common it has its own symbol,

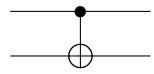

,

where '$\bullet$' is on the control bit, and '$\oplus$' is on the target bit.

As an example that combines single- and two-qubit gates, consider the circuit that generates a singlet state $|s\rangle = (|01\rangle - |10\rangle)/\sqrt{2}$ from an initial state $|00\rangle$,

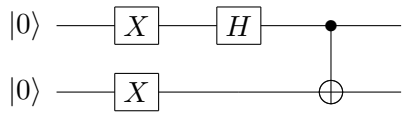

$$\Big\} \; |s\rangle = (|01\rangle - |10\rangle)/\sqrt{2}. \tag{1.10}$$

When the state on the right of the circuit is measured, we get the classical outcomes 01 or 10 with equal probability.

1.3.2.5 Quantum computers

It can be shown that the gate set $\{U(\alpha, \tilde{\theta}, \tilde{\phi}), \text{CNOT}\}$, with U implementable for all parameter values, is *universal*. That is, every unitary on n qubits can be decomposed into a circuit of single qubit gates and CNOT gates only. Up to a constant factor, the total number of gates needed is at most proportional to $n^2 4^n$ [108]. The *depth* of a quantum circuit is the total number of layers of gates in that circuit. For example, the depth of the circuit in Eq. (1.10) is 3.

Like a classical computer, a quantum computer maps bitstrings to bitstrings. It does so as follows. First, the bitstring x is translated to a classical description of a circuit; a list of gates that are to be executed sequentially. For every gate it is specified on which qubit(s) it acts. A quantum computer generally starts with all qubits initialized to some product state, denoted in the computational basis as $|00\ldots0\rangle$ (see the circuit below). After the quantum computer applies all of these gates, some or all of the qubits are measured in the computational basis. This yields a bitstring y, which forms the output of the computation.

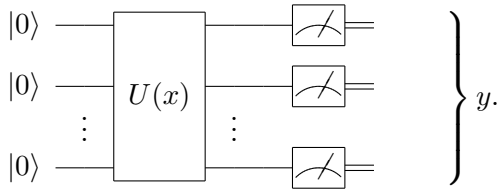

(1.11)

Because of the inherent unpredictability of quantum measurement, the map from bitstrings to bitstring a quantum computer implements is probabilistic, even if the quantum computer is noiseless. This property itself is not unique to quantum computation. There are also classical methods of computation that include the use of a (quasi) random number generator, which are hence (quasi) probabilistic. Even though the output of a quantum computation may be unpredictable, the computation can still be useful. For example, if the input of the computation is an integer x, and the output y is a prime factor of x only with probability 2/3, the computation can be repeated a couple of times until a prime factor is found. Checking if y is a prime factor of x can be done efficiently on a classical computer. Furthermore, the probability of not finding a prime factor after m tries is exponentially small in m.

1.3.3 Asymptotic notation

The field of *complexity theory* is occupied with determining the resources required for computing functions. In this field, statements such as 'on a quantum computer, it takes 1000 hours to factor a 1000-bit integer' (numbers chosen arbitrarily) are not so useful, for it does not tell us anything about the time required for factoring a 1001-bit integer. Also, the statement is highly hardware-dependent. More useful statements are of the form: 'the time required for factoring an n-bit integer scales at most as $f(n)$' (for some given function f).

These kind of statements are made more precise by using *asymptotic notation*. One instance of this kind of notation is the 'big-O' notation $f(n) = O[g(n)]$.

Definition 1.3.1. *If $f(n) = O[g(n)]$, then there exists an n_0 and a $c > 0$ such that*

$$|f(n)| \leq cg(n) \tag{1.12}$$

for all $n > n_0$.

For example, $1000/n^2 = O(1/n)$.

There are many closely related instances of asymptotic notation. If, in the above definition, we demand Eq. (1.12) to hold for *all* $c > 0$, and substitute $O \to o$, we obtain the definition of the 'little-o' notation. If we change the inequality '$\leq$'→'$\geq$', and $O \to \Omega$, we obtain the definition of 'big-Ω' notation. If we change '$\leq$'→'$\geq$', demand the inequality to hold for all $c > 0$, and change $\Omega \to \omega$, we obtain the definition of 'little-ω' notation. Additionally, if $f(n) = \Theta[g(n)]$, then both $f(n) = O[g(n)]$ and $f(n) = \Omega[g(n)]$.

Occasionally one encounters statements as '$f(n) = O[g(\varepsilon)]$ as ε goes to zero'. This means $|f(\varepsilon)|$ is upper bounded by $g(\varepsilon)$ for ε small enough (rather than large enough). Similar statements are encountered for the other forms of asymptotic notation. Additionally, some times the notation $f(n) \in O[g(n)]$ is used instead of $f(n) = O[g(n)]$ (similarly for the other forms of asymptotic notation). This notation is formally more correct.

For some purposes even asymptotic notation is too explicit. For example, we may just be interested in whether or not $f(n)$ is a polynomial in n. In that case we write $f(n) = \operatorname{poly} n$, which, to make the connection to big-O notation, means there is a $m > 0$ such that $f(n) = O(n^m)$. Other variants include $f(n) = \operatorname{polylog} n \equiv \operatorname{poly}(\log n)$.

Statements such as

$$\mathrm{e}^{-\mathrm{i}\theta Z/2} = \mathbb{1} - \mathrm{i}\theta Z/2 + O(\theta^2) \tag{1.13}$$

are encountered. This expression technically incorrect because there should be an operator on the place of '$O(\theta^2)$'. It is to be understood that Eq. (1.13) means $\|e^{-i\theta Z/2} - (\mathbb{1} - i\theta Z/2)\|^2 = O(\theta^2)$, with $\|\cdot\|$ the operator norm.

1.4 Quantum mechanics

We now switch gears, and take a more formal look at quantum mechanics in general. All topics covered fall under those of standard textbook quantum mechanics, such as in [36, 119, 127, 26]. The purpose of this section is to provide definitions, conceptual and technical background for the subsequent chapters. This section may be skipped at first reading.

1.4.1 Measurement

Naively, we might imagine a measurement performed on a quantum mechanical system as follows: there is some quantum mechanical system, possibly in a superposition, that goes into some large, classical measurement device. Upon measurement, the pointer of the device points at some definite outcome ν. Indeed, this is the motivation for the notation of measurement in quantum circuits [Eq. (1.8)]. For example, such a pointer would point at 'spin up' or 'spin down' if the system is a spin-1/2 particle and the device is a Stern-Gerlach apparatus.

In the end, all the atoms of the device follow the laws of quantum mechanics. So, if the quantum state was in a superposition of states, and the measurement device has interacted with the quantum system, why would the pointer not be in a superposition as well? But then again, why do we not see pointers in a superposition in daily life? Actually, nobody knows the answers to these questions, and the problem of unifying quantum mechanics with how we intuitively think measurement devices ought to behave is called the *measurement problem* of quantum mechanics. The problem is closely related to the quantum-classical crossover depicted in Fig. 1.1. Zooming in from the solar system onto a single electron, where does the world of classical pointers stop, and where does that of quantum mechanics begin?

Nevertheless, given that a measurement has occurred with outcome ν, the mathematical description of the effects of that measurement are clear cut. A measurement[4] is described by a set of distinct measure-

[4] More precisely: a *projective measurement*. There are more general mathematical descriptions of measurement in quantum mechanics, but for the current exposition the projective measurement suffices.

ment outcomes ν_i together with set of associated orthogonal projectors, $\{P_i\}_{i=1}^m$. We do not assume $m = \dim \mathcal{H}$. By definition, the projectors satisfy $P_i^2 = P_i$. We furthermore require them to be orthogonal, $P_i P_j = \delta_{ij} \mathbb{1}$, and complete, $\sum_i P_i = \mathbb{1}$. Given these outcomes and projectors, a measurement performed on a state $|\psi\rangle$ yields the outcome ν_i with probability $p_i = \|P_i |\psi\rangle\|^2$. After the measurement the state *collapses* onto the state that will give the measurement outcome ν_i with certainty. This is the state $|\psi'\rangle = P_i |\psi\rangle / \sqrt{p_i}$. The sets $\{\nu_i\}$ and $\{P_i\}$ can be combined into a single linear operator in a meaningful way. Map the outcomes ν_i to distinct real numbers. Then, this linear operator is given by the *observable* $O = \sum_i \nu_i P_i$. This coincides with the spectral decomposition of the Hermitian operator O. Thus, a measurement may also be specified by a single Hermitian operator.

Note that multiplying any $|\psi\rangle$ by an overall complex phase does not change the probability p_i, no matter the observable. Hence, overall phases of vectors in the Hilbert space of any quantum system are unphysical, and can be disregarded. This, together with the normalization condition $\sum_i p_i = \sum_i \|P_i |\psi\rangle\|^2 = \langle\psi| \sum_i P_i |\psi\rangle = \||\psi\rangle\|^2 = 1$, allowed us to obtain the Bloch sphere (Fig. 1.4).

As opposed to measurements in classical physics, the *uncertainty* in the outcome ν_i is *fundamental*. This uncertainty does not stem from a lack of knowledge about the state. For example, if an electron is in the $|+\rangle$ state, we know all about the (spin degree of freedom) of the electron there is to know. Nevertheless, it is impossible to predict the outcome of a measurement of the observable Z. So, we cannot say what the 'value' of spin in the z-direction is. Given an observable $O = \sum_i \nu_i P_i$ and a state $|\psi\rangle$, we can, however, say a priori what the *expectation value* of the measurement outcome is. Consider ν as a random variable (a function from the outcome indexes i to the real numbers ν_i). Then, the expectation value of that random variable, given the state $|\varphi\rangle$, is

$$\begin{aligned}
\mathbb{E}_{|\varphi\rangle}(\nu) &= \sum_i \nu_i p_i \\
&= \sum_i \nu_i \|P_i |\varphi\rangle\|^2 \\
&= \sum_i \nu_i \langle\varphi| P_i |\varphi\rangle \\
&= \langle\varphi| O |\varphi\rangle .
\end{aligned}$$

Given an observable, and a source that repeatedly outputs the same state, the expectation value of an operator can be estimated by repeatedly performing the measurement specified by O and taking the

average of the outcomes. The error in the estimate depends on the number of measurements performed and goes to zero as the number of measurements goes to infinity.

The unpredictability of measurement outcomes relates to the impossibility of of measuring a quantum state in a single measurement. Namely, given a quantum system in an unknown state, any one measurement outcome of any observable O is consistent with many states. For example, if a measurement of the observable Z of a qubit yields the outcome 0, the pre-measurement state of the qubit could have been any point of the Bloch sphere except the point belonging to $|1\rangle$. Hence, is impossible to determine the state of a system with a single measurement.

Given many copies of an unknown state, however, it is possible to measure the expectation value of an operator. Measuring the expectation values of multiple observables allows one to reconstruct the state from the outcomes. Such a process is called *quantum state tomography*. As an example, consider an unknown qubit state $|\varphi\rangle$ with associated Bloch vector $\hat{\boldsymbol{n}}$. It is straightforward to verify that

$$\hat{\boldsymbol{n}} = \left(\langle X\rangle, \langle Y\rangle, \langle Z\rangle\right)^T.$$

Thus, using a source that repeatedly outputs $|\varphi\rangle$, measuring $\langle X\rangle$ and $\langle Y\rangle$, and using $|\hat{\boldsymbol{n}}| = 1 \Rightarrow \langle Z\rangle^2 = 1 - \langle X\rangle^2 - \langle Y\rangle^2$, yields the Bloch vector $\hat{\boldsymbol{n}}$ and hence a classical description of the state $|\varphi\rangle$.

1.4.2 Density operators

When we flip a coin, and it lands behind our back, we do not know whether it landed heads or tails. Before we look at the coin, our knowledge about the state is captured by the probability distribution $p_{\text{heads}} = p_{\text{tails}} = 1/2$. The formalism of *density operators* allows us to incorporate this kind of classical uncertainty into quantum states, on top of the already existing fundamental quantum uncertainty.

Assume again there is some source that repeatedly outputs the same quantum state, but that we are not told which state. We are promised that the source outputs the same state every time, and that in advance this state was chosen from the set $\{|\varphi_i\rangle\}$ according to a specified probability distribution $\tilde{p}_i$. We write $|\varphi_i\rangle = \sum_j c_{ij}\,|j\rangle$. It is not assumed the states are orthogonal.

When we perform many measurements specified by the observable O, each time using a fresh copy of the state, and take the average of the outcomes, we eventually learn $\mathbb{E}_{|\varphi_i\rangle}(\nu)$. But what is the *expected* expectation value? To calculate this, we see $\mathbb{E}_{|\varphi_i\rangle}(\nu)$ as a random variable

over state indices, and calculate its expectation value,

$$\begin{aligned}\mathbb{E}[\mathbb{E}_{|\varphi_i\rangle}(\nu)] &= \sum_i \tilde{p}_i \langle\varphi_i| O |\varphi_i\rangle \\ &= \sum_{ijk} \tilde{p}_i c_{ij}^* c_{ik} \langle j| O |k\rangle \\ &= \sum_{ijk} \tilde{p}_i c_{ij}^* c_{ik} \mathrm{tr}(|k\rangle \langle j| O) \\ &= \mathrm{tr}\left(\rho O\right), \end{aligned} \tag{1.14}$$

where we have defined the *density operator*

$$\rho = \sum_i \tilde{p}_i |\varphi_i\rangle\langle\varphi_i| .$$

We will henceforth use the notation

$$\langle O\rangle_\rho = \mathrm{tr}(\rho O),$$

which is manifestly basis independent. Note that, because $\sum_i \tilde{p}_i = 1$, we have the normalization condition for density operators, $\mathrm{tr}(\rho) = 1$.

The expected expectation value $\langle O\rangle_\rho$ does not change when the source outputs just a single state. Hence, ρ completely captures our knowledge about the output of the source. It is in this way that the density operator forms a generalization of the concept of a quantum state. We will use the term state both for vectors $|\psi\rangle$ and density operators ρ.

Pure classical uncertainty and pure quantum uncertainty are both limiting cases in the density operator formalism. The density operator that describes a purely classical probability distribution over classical product states $|i\rangle$, called a *classical mixture*, is of the form $\rho = \sum_j \tilde{p}_i |i\rangle\langle i|$. Any density operator that is not a purely classical mixture has non-zero off-diagonal matrix elements in the classical basis, called the *coherences* of the density operator. The diagonal matrix elements in the classical basis, on the other hand, are called the *populations*. If we have a source that outputs $|\varphi\rangle$ with certainty, we say the state that the source outputs is a *pure state*, described by $\rho = |\varphi\rangle\langle\varphi|$ (or just $|\varphi\rangle$ if we omit the density operator formalism). We call any state that is not a pure state a *mixed state*.

Because $\rho = \sum_i \tilde{p}_i |\varphi_i\rangle\langle\varphi_i|$, $\sum \tilde{p}_i = 1$, and the fact that the $|\varphi_i\rangle\langle\varphi_i|$ are pure states, ρ is a convex combination of pure states. Therefore, the decomposition of a density operator into pure states is generally

not unique. As an example, consider a qubit that, with equal probability, is in the state $|+\rangle$ or $|-\rangle$. Then $\rho = (|+\rangle\langle+| + |-\rangle\langle-|)/2 = (|0\rangle\langle 0| + |1\rangle\langle 1|)/2$. Thus, we might just as well say that the qubit is in the states $|0\rangle$ and $|1\rangle$ with equal probability.

By applying the definitions of the measurement of pure states, and the interpretation of ρ given in Eq. (1.14), we can generalize the description of measurement to measurement of mixed states ρ. Now, the outcome ν_i is obtained with probability $p_i = \mathrm{tr}(P_i \rho P_i)$. The post-measurement state ρ' is given by $\rho' = P_i \rho P_i / p_i$.

1.4.3 Open quantum systems

Assume we have a quantum system SB that can be divided into a system S and a bath B. The overall Hilbert space is $\mathcal{H} = \mathcal{H}_S \otimes \mathcal{H}_B$, with $\mathcal{H}_S$ the Hilbert space of the system and $\mathcal{H}_B$ that of the bath. Expanded over a basis $\{|i\rangle\}_i^{\dim H_S}$ for S and $\{|j\rangle\}_{j=1}^{\dim H_B}$ for B, a general pure state is of the form $|\Psi\rangle = \sum_{ij} \psi_{ij} |i\rangle \otimes |j\rangle$. Even though we use the same notation for the bases of S and B, these bases need not be physically equal. Operators on $\mathcal{H}_{SB}$ take the form $O = \sum_\alpha O_{ij} S_i \otimes B_j$, with $\{S_i\}$ and $\{B_j\}$ operator bases for S and B respectively.

Consider a general SB density operator $\rho = \sum_{abcd} \rho_{abcd} |a\rangle\langle b| \otimes |c\rangle\langle d|$ and an observable that acts non-trivially on the system only, $O = O_S \otimes \mathbb{1}$. Again, we cannot predict the outcome of a single measurement of O, but we can compute the expectation value of that measurement outcome,

$$\begin{aligned}
\langle O \rangle_\rho &= \mathrm{tr}(\rho O) \\
&= \sum_{ij} \langle i| \otimes \langle j| \left(\sum_{abcd} \rho_{abcd} |a\rangle\langle b| \otimes |c\rangle\langle d| \right) O_s \otimes \mathbb{1} |i\rangle \otimes |j\rangle \\
&= \sum_{ib} \left(\sum_j \rho_{ibjj} \right) \langle b| O_S |i\rangle \\
&= \mathrm{tr}(\rho_S O_S).
\end{aligned}$$

Here, we have introduced the *reduced density operator* $(\rho_S)_{ib} = \sum_j \rho_{ibjj}$. Equivalently, this definition can be written as

$$\rho_S = \mathrm{tr}_B(\rho), \tag{1.15}$$

with $\mathrm{tr}_B(\cdot) = \sum_m \langle m|_B \cdot |m\rangle_B$ the *partial trace* over the bath. Here, we define the operation $\langle m|_B O_S \otimes O_B |m\rangle_B \equiv O_S \langle m| O_B |m\rangle$ for general

system and bath operators O_S and O_B. Note that the latter definition of ρ_S, Eq. (1.15) is manifestly basis independent.

Imagine SB is in a pure state, $\rho_{SB} = |\Psi\rangle\langle\Psi|$, that you are near the location of S and that I am near the location of B, which is light years away from S. Now suppose I measure B in the basis $\{|j\rangle_B\}_j$ on an exact moment that was agreed upon in advance. Suppose I get outcome j. Then, the overall post-measurement state has collapsed to $\rho'_{SB} = (\langle j|_B \rho_{SB} |j\rangle_B) \otimes |j\rangle\langle j| / p_j$ with p_j such that $\mathrm{tr}(\rho'_{SB}) = 1$. Since this is a product state, we can say that the post-measurement state at S, given the outcome j, is $\rho_S^{(j)} = (\langle j|_B \rho_{SB} |j\rangle_B)/p_j$. The effect that the state of S has changed at the instant of measurement, even though S and B are separated by light years and the outcome j could not be predetermined even with complete knowledge of the overall pure state, is called *non-locality*.

However, directly after the measurement, there is no way for you to have learned the outcome. Hence, your knowledge of the state just following my measurement, denoted by $\tilde{\rho}_S$, is

$$\begin{aligned}\tilde{\rho}_S &= \sum_j p_j \rho_S^{(j)} \\ &= \sum_j (\langle j|_B \rho_{SB} |j\rangle_B) \\ &= \rho_S.\end{aligned}$$

So, to the local description of S, and to the outcome of any experiment on S, it does not matter whether B has been measured (without you knowing the outcome) or B has not been measured at all. Hence, the local description of S does not contain all there is to know about part S of SB. We say the local description of S is not *complete*.

1.4.4 Pauli words

The bounded linear operators on a 2^n-dimensional Hilbert space $\mathcal{H}$, $\mathcal{B}(\mathcal{H})$, can be added, and multiplied by complex scalars in the usual sense. Hence, $\mathcal{B}(\mathcal{H})$ forms a complex vector space of dimension 2^4. We may emphasize the vector character of $O \in \mathcal{B}(\mathcal{H})$, by writing $|O\rangle\rangle$. On $\mathcal{B}(\mathcal{H})$, the Hilbert-Schmidt (not to be confused with Herbert Smith) inner product $\langle\langle O|O'\rangle\rangle \equiv \mathrm{tr}(O^\dagger O')$ can be defined. Define the *Pauli words*

$$\mathcal{P}_i = \sigma_{i_1} \otimes \sigma_{i_2} \otimes \ldots \otimes \sigma_{i_{n-1}} \otimes \sigma_{i_n}, \tag{1.16}$$

where $\sigma_0 = \mathbb{1}_{2\times 2}$, $\sigma_1 = X$, $\sigma_2 = Y$, $\sigma_3 = Z$ Pauli-operators [Eq. (1.4)]. The Pauli words have many convenient properties: they are traceless,

except for $\mathcal{P}_{0\ldots0}$, for which $\mathrm{tr}(\mathcal{P}_{0\ldots0}) = 2^n$, they square to the identity, they are Hermitian (and hence unitary), two Pauli words either commute or anti-commute, they have eigenvalues ± 1 (and hence $|\mathcal{P}_i| = 1$ for all i), and they form a group, called the *Pauli group*. The basis of Pauli words can be normalized by introducing the *normalized Pauli words* $\tilde{\mathcal{P}}_i = \mathcal{P}_i/\sqrt{2^n}$.

The property we are most interested in here is that the Pauli words form an orthogonal basis of $\mathcal{B}(\mathcal{H})$. To show this, note that, from the properties of the Pauli operators, it follows directly that $\langle\langle \mathcal{P}_i | \mathcal{P}_j \rangle\rangle = 2^n \delta_{ij}$. Also note there are $4^n = \dim \mathcal{B}(\mathcal{H})$ independent Pauli words. Hence any $O \in \mathcal{B}(\mathcal{H})$ may be written as

$$O = \sum_i c_i \mathcal{P}_i, \tag{1.17}$$

with $c_i = \langle\langle \mathcal{P}_i | O \rangle\rangle / 2^n$. Hence, we could even represent $|O\rangle\rangle$ as a column vector of length 2^4 with entries c_i.

If we restrict O to be Hermitian, the c_i must be real. So, we may write any Hamiltonian on n spins as

$$H = \sum_i h_i \mathcal{P}_i \tag{1.18}$$

with $h_i \in \mathbb{R}$. If we, furthermore, require that H is traceless, which physically we can always do without loss of generality, we have $h_0 = 0$.

The *weight* of a Pauli word is defined as the number of non-trivial single-qubit tensor factors in that word. (The Pauli operator σ_0 is considered trivial.) A Hamiltonian is called *k-local* if all of its terms act non-trivially on at most k qubits. If the Hamiltonian is of the form of Eq. (1.18), this means the weight of any $\mathcal{P}_i$ for which $h_i \neq 0$ is at most k. We stress that k-locality is a weaker requirement than spatial locality of a Hamiltonian. For example, the Hamiltonian $H = \sum_{i,j=1}^{n} Z_i Z_j$ with spins placed randomly in the universe is still called 2-local even though every spin interacts with every other spin and the spins are arbitrarily far apart. Instead of a single Hamiltonian, one often inexplicitly considers a family of Hamiltonians $\{H^{(n)}\}$, where each member $H^{(n)}$ is a Hamiltonian acting on n qubits. This family is called k-local if all $H^{(n)}$ are k-local, with k independent of n. Note that by Eq. (1.18) any k-local Hamiltonian has at most $4^k \begin{pmatrix} n \\ k \end{pmatrix}$ linearly independent terms.

1.4.5 Time evolution

The world is dynamic. An example in classical physics is that of the solar system; the state of the solar system at time $t = 0$ differs from states at $t \neq 0$. Likewise, quantum systems are generally dynamic, and the initial state of a quantum system, $|\psi(0)\rangle$, will differ from the state at earlier or later times, $|\psi(t)\rangle$ ($t \neq 0$). By the linearity of quantum mechanics, $|\psi(t)\rangle$ must be related to $|\psi(0)\rangle$ by some linear operator $U(t)$,

$$|\psi(t)\rangle = U(t)\,|\psi(0)\rangle\,. \tag{1.19}$$

This $U(t)$ is determined by the *Schrödinger equation*. In units where $\hbar = 1$, it reads

$$\partial_t U(t) = -\mathrm{i}H(t)U(t), \tag{1.20}$$

where H is the *Hamiltonian*. By the conservation of probabilities (Sec. 1.4.1), $U(t)$ is unitary, $U(t)U^\dagger(t) = \mathbb{1}$, and hence H is Hermitian, $H(t) = H^\dagger(t)$. By the equivalence of states that differ by a phase, H may be chosen to be traceless, $\mathrm{tr}H = 0$.

If the Hamiltonian is time-independent, $H(t) = H$, the solution of the Schrödinger equation is $U(t) = \mathrm{e}^{-\mathrm{i}tH}$. On the level of states, this means $|\psi(t)\rangle = \mathrm{e}^{-\mathrm{i}tH}\,|\psi(0)\rangle$, or, for density operators, $\rho(t) = \mathrm{e}^{-\mathrm{i}tH}\rho(0)\mathrm{e}^{+\mathrm{i}tH}$. Writing out the exponents, commuting all H to the left of $\rho(0)$, and resuming into an exponent, this can be rewritten as

$$\rho(t) = \mathrm{e}^{-\mathrm{i}t[H,\cdot]}\rho(0), \tag{1.21}$$

with $-\mathrm{i}t[H,\cdot]\rho = -\mathrm{i}t[H,\rho]$.

1.4.5.1 Dyson series

For time-dependent Hamiltonians we have, by the Schrödinger equation,

$$U(t) = \mathbb{1} + \int_0^t \mathrm{d}t'\,\partial_{t'}U(t') = \mathbb{1} - \mathrm{i}\int_0^t \mathrm{d}t' H(t')U(t').$$

This equation is recursive; we can substitute $U(t)$ appearing on the right hand side using the equation itself. Repeating this process, we obtain

$$\begin{aligned} U(t) &= \mathbb{1} - \mathrm{i}\int_0^t \mathrm{d}t' H(t')\big(\mathbb{1} - \mathrm{i}\textstyle\int_0^{t'} \mathrm{d}t'' H(t'')\big(\mathbb{1} - \mathrm{i}\int_0^{t''} \mathrm{d}t''' H(t''')\ldots\big)\big) \\ &= \mathbb{1} - \mathrm{i}\int_0^t \mathrm{d}t'\,H(t') + (-\mathrm{i})^2 \int_0^t \mathrm{d}t' H(t') \int_0^{t'} \mathrm{d}t'' H(t'') + \ldots. \end{aligned} \tag{1.22}$$

This is called the *Dyson series*. It can be written more compactly as

$$U(t) = T\mathrm{e}^{-\mathrm{i}\int_0^t \mathrm{d}t'\, H(t')}, \tag{1.23}$$

with T is the time ordering operator.

1.4.5.2 Schrödinger v.s. Heisenberg picture

Given a state, only the expectation value of an operator is measurable (Sec. 1.4.1). As we shall see, this introduces an ambiguity: are the states evolving in time, or rather the observables themselves? Depending on where one puts the time evolution we obtain different *pictures* of quantum mechanics. Let us assume time-independent Hamiltonians for clarity.

We take the *Schrödinger* picture as the starting point. This is the picture of the last section, where the states evolve in time, but the observables are fixed. In this picture, expectation values are computed as

$$\langle O\rangle(t) = \mathrm{tr}[\underbrace{e^{-\mathrm{i}tH}\rho(0)e^{\mathrm{i}tH}}_{\rho^S(t)}\underbrace{O}_{O^S}],$$

where for later reference we have introduced the Schrödinger picture state $\rho^S(t)$ and the Schrödinger picture observable O.

In the *Heisenberg picture*, on the other hand, the time evolution is absorbed into the observables. Using the cyclic property of the trace, the expectation value may be rewritten as

$$\langle O\rangle(t) = \mathrm{tr}[\underbrace{\rho(0)}_{\rho^H}\underbrace{e^{\mathrm{i}tH}Oe^{-itH}}_{O^H(t)}],$$

where we have defined the time-independent Heisenberg picture state ρ^H and the time-dependent Heisenberg picture observable $O^H(t)$.

1.4.5.3 Interaction picture

The *interaction picture* sits between the Schrödinger and Heisenberg picture; one part of time evolution is absorbed into the states, another part is absorbed into the operators. To obtain this subdivision, we write the Schrödinger Hamiltonian as a sum of two terms,

$$H = H_0 + V.$$

In the interaction picture, we write the expectation value of O as

$$\langle O\rangle(t) = \mathrm{tr}[\underbrace{e^{\mathrm{i}tH_0}e^{-\mathrm{i}tH}\rho(0)e^{\mathrm{i}tH}e^{-\mathrm{i}tH_0}}_{\rho^I(t)}\underbrace{e^{\mathrm{i}tH_0}Oe^{-\mathrm{i}tH_0}}_{O^I(t)}], \tag{1.24}$$

where we have defined the time-dependent interaction picture state $\rho^I(t)$ and time-dependent interaction picture observable $O^I(t)$.

The interaction picture is especially useful when time evolution of states under H_0 is well-understood and the operator norm of V is small, because in that case the Dyson series is a series in the operator norm of V. Define the operators

$$U^I(t) = e^{\mathrm{i}tH_0}e^{-\mathrm{i}tH}, \qquad H^I(t) = e^{\mathrm{i}tH_0}Ve^{-\mathrm{i}tH_0}. \tag{1.25}$$

By taking the derivative of $U^I(t)$, we have

$$\partial_t U^I(t) = -iH^I(t)U_I(t).$$

This is exactly the Schrödinger equation [Eq. (1.20)] if we substitute $U^I \to U$ in and $H^I \to H$. Hence, the Dyson series Eq. (1.22) in the interaction picture, and its solution (Eq. (1.23)), are simply obtained by substituting $U^I \to U$ and $H^I \to H$,

$$U^I(t) = T\mathrm{e}^{-\mathrm{i}\int_0^t \mathrm{d}t' H^I(t')}. \tag{1.26}$$

The Dyson series now becomes a perturbative series in the operator norm of V. Taking into account the first couple of terms of the Dyson series, it can thus be used to treat time evolution perturbatively.

1.4.6 Time evolution of open quantum systems

Consider a system S and a bath B as in Sec. 1.4.3, under the influence of a time evolution operator on SB. The time evolution of the whole induces time evolution on the reduced density operator of S. Assuming for simplicity the initial state of SB is $(\rho_S(0)\otimes|\varphi\rangle\langle\varphi|)$, this is

$$\rho_S(t) = \mathrm{tr}_B[U(t)(\rho_S(0)\otimes|\varphi\rangle\langle\varphi|)U^\dagger(t)]. \tag{1.27}$$

In this section, we study this reduced time evolution.

1.4.6.1 Interaction picture in open quantum systems

For open quantum systems, H_0 is usually taken to be the sum of a term that only acts on the system, the system Hamiltonian $H_S\otimes\mathbb{1}$, and a

term that acts only on the bath, the bath Hamiltonian $\mathbb{1} \otimes H_B$. The interactions between the system and the bath are captured by V.

Let O_S be a system operator. Then,

$$\begin{aligned}\langle O_S \rangle(t) &= \mathrm{tr}_S \left[\rho_S^S(t) O_S^S\right] \\ &= \mathrm{tr}_S \left\{\mathrm{tr}_B[e^{-\mathrm{i}tH_0}\rho^I(t)e^{itH_0}]O_S^S\right\}.\end{aligned}$$

If we assume that V is the only system-bath coupling, then $H_0 = H_S + H_B$, and we obtain

$$\begin{aligned}\langle O_S \rangle_t &= \mathrm{tr}_S\{\mathrm{tr}_B[e^{-\mathrm{i}tH_B}\rho^I(t)e^{itH_B}]e^{itH_S}O_S^S e^{-itH_S}\} \\ &= \mathrm{tr}_S\{\underbrace{\mathrm{tr}_B[\rho^I(t)]}_{\rho_S^I(t)}\underbrace{e^{\mathrm{i}tH_S}O_S^S e^{-itH_S}}_{O_S^I(t)}\}.\end{aligned}$$

In words, the reduced density operator in the interaction picture is the interaction picture density operator with the bath traced out. The system operators transform to the interaction picture system operators as if there were no bath.

1.4.6.2 Quantum channels

The evolution of the reduced system density operator of Eq. (1.27) may be rewritten as

$$\begin{aligned}\rho_S(t) &= \sum_j \langle j|_B U(t)(\rho_S(0) \otimes |\varphi\rangle\langle\varphi|)U^\dagger(t)\,|j\rangle_B \\ &= \sum_j A_j(t)\rho_S(0)A_j^\dagger(t) \\ &= \mathcal{A}(t)[\rho_S(0)].\end{aligned}$$

Here, we have defined the operators

$$A_j(t) = \langle j|_B U(t)\,|\varphi\rangle_B\,, \tag{1.28}$$

and a map from density operators to density operators,

$$\mathcal{A}(t)[\cdot] = \sum_j A_j(t)(\cdot)A_j^\dagger(t). \tag{1.29}$$

Note the operators in Eq. (1.28) are system operators. The notation used there is similar to that used in Eq. (1.15). Also note that, by Eq. (1.28),

$$\sum_j A_j^\dagger(t)A_j(t) = \mathbb{1},$$

as it should, for otherwise $\mathrm{tr}[\rho_S(t)] \neq 1$.

We have taken a physics-inspired approach in arriving at Eq. (1.29). There is, however, another way of arriving at a similar equation. In an axiomatic approach to quantum mechanics, density operators are, by definition, Hermitian Positive Semi-Definite (psd) operators with unit trace. A *quantum channel* $\mathcal{A}$ is defined as map that satisfies the following three axioms. 1) Trace preservation, $\mathrm{tr}(\mathcal{A}[\rho]) = 1$ whenever $\mathrm{tr}(\rho) = 1$. 2) Complete positivity, which means that we not only require $\mathcal{A}$ to be positive, we also require positivity after we add a bath (of any dimension) on which $\mathcal{A}$ acts trivially, that is, we require $\mathcal{A}\otimes\mathbb{1} \geq 0$ for an identity operator $\mathbb{1}$ of any dimension. 3) Convex linearity, which means $\mathcal{A}[\sum_i p_i\rho^{(i)}] = \sum_i p_i\mathcal{A}[\rho^{(i)}]$ for any set of density operators $\{\rho^{(i)}\}_i$.

It can be shown that any map satisfying the axioms above can be written in the *Operator Sum Representation* (OSR) $\mathcal{A}[\cdot] = \sum_i A_i(\cdot)A_i^\dagger$, with $\sum_j A_j^\dagger A_j = \mathbb{1}$, where the A_i are called *Kraus operators* (see e.g. [108]). For fixed t, Eq. (1.29) gives the OSR of the channel on density operators on S that is induced by unitary time evolution on SB with time t. If we let t vary, Eq. (1.29) defines a family of quantum channels. Its members are characterized by different t.

In the construction outlined in the subsection on Pauli words, Sec. 1.4.4, elements of $\mathcal{B}(\mathcal{H})$ may be represented by column vectors of length N^2, with $N = \dim\mathcal{H}$. By the OSR, it is easy to see that quantum channels extend naturally to linear operators from all of $\mathcal{B}(\mathcal{H})$ to $\mathcal{B}(\mathcal{H})$ (instead of only from density operators to density operators). The linear operators on linear operators are also called *super-operators*. Any super-operator $\mathcal{S}$ (including quantum channels) may hence be seen as a $N^2 \times N^2$ matrix with elements $\langle\!\langle\tilde{\mathcal{P}}_i|\mathcal{S}[\tilde{\mathcal{P}}_j]\rangle\!\rangle$, here the $\tilde{\mathcal{P}}_i$ are normalized Pauli words.

Any unitary on SB gives rise to a quantum channel defined on S. The converse is also true: it can be shown that, given any quantum channel $\mathcal{A}$, it is possible to cook up a bath B, a state $|\varphi\rangle$, and a unitary U on SB such that $\mathcal{A}[\rho] = \mathrm{tr}_B(U\rho\otimes|\varphi\rangle\langle\varphi|\,U^\dagger)$ for any ρ. This 'reverse' construction is known as the *Stinespring dilation* (named after W. F. Stinespring).

1.4.6.3 The Lindblad equation

The family of quantum channels arising from reversible, unitary time evolution of a closed system along a given Hamiltonian H, can be written as $\{\mathcal{U}(t)[\cdot] = U(t)(\cdot)U^\dagger(t)\}_t = \{\mathrm{e}^{t\tilde{\mathcal{L}}[\cdot]}\}_t$, with

$$\tilde{\mathcal{L}}[\rho] \equiv -\mathrm{i}[H,\rho] \tag{1.30}$$

the generator of that family. (The super-operator $\tilde{\mathcal{L}}$ can in principle be represented as a $N^2 \times N^2$ matrix, with $N = \dim \mathcal{H}$ (see Sec. 1.4.4). Using the standard matrix exponential, also $\mathrm{e}^{t\tilde{\mathcal{L}}}$ can be thought of as a matrix in the same way.) This family forms a group; $\mathcal{U}(0)$ acts is the identity element, and both closure under composition as the existence of inverses follows from the property

$$\mathcal{U}(t_2) \circ \mathcal{U}(t_1) = \mathcal{U}(t_1 + t_2) \tag{1.31}$$

for all $t_1, t_2 \in \mathbb{R}$.

The theory of quantum channels allows us to generalize the above theory of unitary (and hence reversible) time evolution of quantum systems to a theory that also incorporates irreversible 'non-quantum' dynamics. This theory is commonly referred to as *irreversible quantum dynamics*. We start from the axiomatic approach of quantum channels, and consider a family of quantum channels that satisfies the property

$$\mathcal{A}(t_2) \circ \mathcal{A}(t_1) = \mathcal{A}(t_1 + t_2) \tag{1.32}$$

for all $t_1, t_2 \geq 0$. Such a family is called a *quantum dynamical semigroup*. Note how this requirement is weaker than that of Eq. (1.31). Families satisfying the latter requirement are called a *semi*group because the inverse of $\mathcal{A}(t)$ is not required to exist, reflecting the irreversible nature of the dynamical maps. In analogy with reversible dynamics, suppose the a quantum dynamical semigroup is generated by a super-operator $\mathcal{L}$. That is, suppose $\mathcal{A}(t) = \mathrm{e}^{t\mathcal{L}}$. It follows that

$$\partial_t \mathcal{A}(t) = \mathcal{L}[\mathcal{A}(t)] \tag{1.33}$$

[cf. the Schrödinger equation, Eq. (1.20)]. Defining $\rho(t) = \mathcal{A}(t)[\rho(0)]$, we have, on the level of states,

$$\partial_t \rho(t) = \mathcal{L}[\rho(t)]. \tag{1.34}$$

Such a super-operator $\mathcal{L}$ is called a *Lindbladian*.

We may ask the question: what is the most general form of a Lindbladian? (I.e, what is the most general super-operator $\mathcal{L}$ such that the super-operator $\mathcal{A}(t) = \mathrm{e}^{t\mathcal{L}}$ is trace preserving and completely positive?) To answer this, remember we can ensure $\mathcal{A}(t)$ is a trace preserving and complete positive super-operator by using the OSR of $\mathcal{A}(t)$, $\rho(t) = \sum_i A_i(t)\rho(0)A_i^\dagger(t)$, which is guaranteed to exist. Expand the Kraus operators $A_i(t)$ over a basis F_i that is orthonormal with respect to the Hilbert-Schmidt inner product, with F_0 proportional to the identity. An example of such a basis is formed by the normalized

Pauli words $\tilde{\mathcal{P}}_i$ (Sec. 1.4.4). Then, the *fixed-basis OSR* of that channel becomes

$$\rho(t) = \sum_{i,j=0}^{N^2-1} c_{ij}(t) F_i \rho(0) F_j^\dagger,$$

with $c_{ij}(t) = \sum_k \langle\langle F_i | A_k \rangle\rangle \langle\langle A_k | F_j \rangle\rangle$. Note that time evolution is now absorbed into the coefficients; the operators F_i are static. Then, by computing

$$\partial_t \rho(t) = \lim_{\delta t \to 0} \frac{\sum_{i,j} c_{ij}(\delta t) F_i \rho(t) F_j^\dagger - \rho(t)}{\delta t}, \tag{1.35}$$

and comparing to Eq. (1.34), it is straightforward, yet too elaborate for this introduction, to show the *Lindblad equation*

$$\begin{aligned} \mathcal{L}[\rho(t)] &= -\mathrm{i}[H, \rho(t)] + \mathcal{D}[\rho(t)], \\ \mathcal{D}[\rho(t)] &= \sum_{k=1}^{N^2-1} \gamma_k \left(L_k \rho(t) L_k^\dagger - \frac{1}{2} \{ L_k^\dagger L_k, \rho(t) \} \right), \end{aligned} \tag{1.36}$$

with $\{\cdot, \cdot\}$ the anti-commutator. Comparing this equation to Eq. (1.30), the way in which the Lindblad equation forms a generalization of unitary time evolution is manifest.

In the Lindblad equation, the Hermitian operator $H \in \mathcal{B}(\mathcal{H})$, the general *Lindblad operators* $L_k \in \mathcal{B}(\mathcal{H})$, and the $\gamma_k \geq 0$ for all k, can all be expressed explicitly in terms of the $c_{ij}(t)$ and F_i. For details, see Ref. [26]. However, the whole point of the current introduction to the Lindblad equation is not to show how the H, L_k and γ_k are obtained, but rather to to give the most general *form* of the generator of a quantum dynamical semigroup. In some physical considerations the Lindblad equation is even used as a starting point rather than a result. As long as H is Hermitian and $\gamma_k \geq 0$ [there are no restrictions on L_k other than $L_k \in \mathcal{B}(\mathcal{H})$], the family that is generated by the Lindbladian is automatically a semigroup with convex linear, trace preserving and completely positive elements.

How should we think about semigroup dynamics in the context of a system and a bath and unitary time evolution? The family of quantum channels $\mathcal{A}(t)$ arising from Eq. (1.27) can be obtained by the following procedure. 1) Append a bath in a state $|\varphi\rangle$ to the current system state, 2) evolve the whole with a time evolution operator $U(t)$, 3) trace out the bath. This map does not satisfy the semigroup property. This is because $\mathcal{A}(t_1)\mathcal{A}(t_2)$ introduces a reset of the bath to the state $|\varphi\rangle$ just after t_1, but $\mathcal{A}(t_1 + t_2)$ does not.

By Eq. (1.35), approximate Lindblad evolution can be seen as the following procedure. 1) Append a bath in the state $|\varphi\rangle$ to the current system state, 2) evolve the whole with a time evolution operator $U(\delta t)$, 3) trace out the bath and reset it to $|\varphi\rangle$, 4) repeat steps 1-3 $T/\delta t$ times. Exact Lindblad evolution is recovered by sending δt to zero in the above procedure. Note that this procedure does satisfy the semigroup property for all $t_1, t_2 > 0$.

Hence, the physical conditions that lead to Lindblad-like time evolution may be realized in physical systems if the dynamics of the bath are much faster than those of the system, quickly carrying away any excitations that occur near the system, and if furthermore these excitations never return to the system. This is only possible if the bath is infinitely large, for otherwise excitations are carried back to the system before or at some finite recurrence time.

1.4.7 Decoherence: a simple example

Decoherence is the loss of information about a quantum state due to its interaction with the environment. In this subsection, we consider, as a simple example, a single qubit of which we successively lose more and more information about the relative phase between the states $|0\rangle$ and $|1\rangle$. The situation where there is only loss of phase information is also described as *pure decoherence* because, as we will see in this subsection, it solely affects the coherences of the density operators (see Sec. 1.4.2).

Consider a qubit initially in the state $|+\rangle$. Assume that after every time step it gets a phase kick ϕ with probability 1/2, or it does not get a phase kick at all (with the same probability). A phase kick of $|+\rangle$ with angle ϕ means that we rotate $|+\rangle$ around the z-axis with angle ϕ. After k phase kicks, the state $|+\rangle$ has changed in to $|\psi_k\rangle = (|0\rangle + \mathrm{e}^{i\phi k}|1\rangle)/\sqrt{2}$. After m time steps, the probability of k phase kicks is $p_k(m) = (1/2)^k(1/2)^{m-k}\begin{pmatrix} m \\ k \end{pmatrix}$. So, if we do not have any information about k, after m time steps the state of the qubit is given by

$$\begin{aligned}\rho(m) &= \sum_{k=0}^{m} p_k(m)\,|\psi_k\rangle\langle\psi_k| \\ &= \frac{1}{2}\sum_k p_k(m)\left(|0\rangle\langle 0| + |1\rangle\langle 1| + \mathrm{e}^{-\mathrm{i}\phi k}\,|0\rangle\langle 1| + \mathrm{e}^{\mathrm{i}\phi k}\,|1\rangle\langle 0|\right) \\ &= \frac{1}{2}\begin{pmatrix} 1 & s^*(m) \\ s(m) & 1 \end{pmatrix}, \end{aligned} \tag{1.37}$$

with $s(m) = \sum_k p_k(m) \mathrm{e}^{\mathrm{i}\phi k}$.

As an aside, note that, for general states, a single time step can be described as the quantum channel $\mathcal{A}$ with Kraus operators

$$E_0 = \mathbb{1}/\sqrt{2}, \qquad E_1 = RZ(\phi)/\sqrt{2},$$

[See Sec. 1.4.6.2 and Eq. (1.6)]. Hence, it is possible to come up with a bath B, a system S, and a unitary on SB such that $\mathcal{A}$ is obtained by unitary evolution of SB and a partial trace over B. The quantum channel for m time steps is just $\mathcal{A}$ applied m times, $\mathcal{A}^m$. Note that $\mathcal{A}^m$ approaches a quantum dynamical semigroup for large m and small ϕ, and can hence, in the appropriate limit, be described by a Lindbladian (see Sec. 1.4.6.3).

Let us here, however, stay with the discrete description of Eq. (1.37). We see the populations are static, but that the two coherences are time-dependent. The moduli of the latter are equal, and are computed as

$$\begin{aligned} |s(m)| &= \left| \sum_k \left(\frac{1}{2}\right)^m \begin{pmatrix} m \\ k \end{pmatrix} \mathrm{e}^{\mathrm{i}\phi k} \right| \\ &= \left| \left(\frac{1}{2} + \frac{\mathrm{e}^{\mathrm{i}\phi}}{2} \right)^m \right| \\ &= \left[\cos^2 \left(\frac{\phi}{2} \right) \right]^{m/2}. \end{aligned}$$

Therefore, the qubit suffers exponential loss of coherence on a time scale set by $1/\log[\cos^2(\phi/2)]$.

As m goes to infinity, $\rho(m)$ goes to $\mathbb{1}$. This latter state is indistinguishable from a classical mixture of the classical states $|0\rangle$ and $|1\rangle$. Remarkably, however, if we were now to learn that the qubit has suffered k_0 phase kicks, there is a classical 'collapse' of $\rho(m)$ to $|\psi_{k_0}\rangle$.

1.5 Selected topics in quantum computing

In this section, we use concepts from Sec. 1.4 to extend upon the picture of quantum computation as given in Sec. 1.3. Again, the topics covered here are similar to those in standard textbooks [108, 119, 34]. This section provides additional conceptual background that complements the rest of this thesis, and may be skipped at first reading.

1.5.1 Gate implementation

Quantum gates are performed by turning on a certain Hamiltonian for a certain time. For example, one way of acting with an $RZ(\theta) = \mathrm{e}^{-\mathrm{i}\theta Z/2}$ gate on qubit i, is to turn on a Hamiltonian $V = Z_i/2$, where Z_i acts only on qubit i, for a time $t = \theta$. In turn, a Z_i Hamiltonian can be turned on by creating an energy difference between the states $|0\rangle$ and $|1\rangle$ of qubit i.

For two-qubit gates, a Hamiltonian is turned on that couples the two qubits. Consider, for example, a quantum dot quantum computer, where the spin degree of electrons is used to implement qubits. Two spins in different dots interact according to the Heisenberg Hamiltonian

$$H = J\ \mathbf{S}_0 \cdot \mathbf{S}_1,$$

with $\mathbf{S}_i = (X_i, Y_i, Z_i)^T/2$, and where $J > 0$ depends on the overlap of the spatial part of the wave function of the two spins. Thus, by temporarily lowering a high potential energy barrier between two dots, each hosting one electron, a two-qubit gate of the form $\mathrm{e}^{-\mathrm{i}\theta(X_0X_1+Y_0Y_1+Z_0Z_1)}$ with $\theta \in \mathbb{R}$ can be realized.

In many physical implementation of qubits, there is a constant 'background' time evolution of all qubits. For example, in a superconducting qubit, the states $|0\rangle$ and $|1\rangle$ generally differ in energy by some value Δ. This causes them to continuously evolve along the background Hamiltonian $H_b = \frac{\Delta}{2}(|0\rangle\langle 0| - |1\rangle\langle 1|) = \frac{\Delta}{2}Z$, leading to $|\psi(t)\rangle = \mathrm{e}^{-\mathrm{i}t\Delta Z/2}\,|\psi(0)\rangle$, even when no gate is being applied.

This redundant time evolution can be removed from our description of the state by going to the *rotating frame*. This is a specific version of the interaction picture, where H_0 is the background Hamiltonian H_b, and $V = 0$ for as long as no gate is being applied. This leads to $|\psi(t)\rangle^I = |\psi(0)\rangle^I = |\psi(0)\rangle$ by the definition of $\rho^I(t)$ [Eq. (1.24)].

1.5.2 Quantum simulation

1.5.2.1 Dynamic quantum simulation

Here we show how quantum computers can efficiently simulate the dynamics of a quantum mechanical system with Hamiltonian H. We may assume that H is k-local (see Sec. 1.4.4). This is because all common Hamiltonians are k-local. These include those of quantum electrodynamics, and the Coulomb, electronic structure, Ising, Heisenberg, Rydberg, James-Cummings, and Hubbard Hamiltonians. Furthermore, for simplicity, here we assume H is a Hamiltonian on n spin-1/2 degrees

of freedom. Quantum computers can also efficiently simulate other types of systems, such as fermionic systems. This, however, requires a mapping from the physical Hamiltonian in question to an Hamiltonian on qubits, which is something we want to omit here for the sake of brevity. Under the above assumptions, we may write $H = \sum_{i=1}^{m} H_m$ with $m = \operatorname{poly} n$.

The ultimate goal of dynamical quantum simulation is to learn classical data about future states of a system given an efficient classical description of an initial state of that system. On a quantum computer, we may do so by evolving an initial state by $U(t)$. This yields the state $|\psi(t)\rangle$, from which classical data may be extracted by repeated preparation and measurement. For example, one may be interested in how the spin-spin correlation function $\langle\psi(t)| Z_i Z_j |\psi(t)\rangle$ evolves as a function of the parameter t, with $|\psi(0)\rangle = |\uparrow\uparrow \ldots \uparrow\rangle = |00\ldots0\rangle$.

In this section we focus on a method for implementing $U(t)$ using only two-body gates, and assuming all-to-all connectivity. It is called *Trotterization*. Even though H is k-local, the time evolution operator $\mathrm{e}^{-\mathrm{i}tH}$ is not. Therefore, it is not clear a priori how to implement it using only two-qubit gates. Evolution along any single term in the Hamiltonian, $\mathrm{e}^{-\mathrm{i}tH_i}$, however, is k-local. Thus, given the universal gate set $\{U(\alpha, \tilde{\theta}, \tilde{\phi}), \mathrm{CNOT}\}$ (Sec. 1.3.2.5) any $\mathrm{e}^{-\mathrm{i}tH_i}$ can be implemented using $O(k^2 4^k)$ gates, which is independent of n, t and H_i. The idea of Trotterization is that $\mathrm{e}^{-\mathrm{i}tH} \approx \Pi_i \mathrm{e}^{-\mathrm{i}tH_i}$ for t small. To obtain $|\psi(t)\rangle$ on a quantum computer, we could thus divide the time interval t up into r smaller pieces of length t/r and apply the unitary $\Pi_i \mathrm{e}^{-\mathrm{i}\frac{t}{r}H_i}$ to $|\psi(0)\rangle$ a total of r times.

All r steps introduce some error (even on a perfect quantum computer), and the question is how this error accumulates. It can be shown that, in every step, there is an error

$$\left\| \mathrm{e}^{-\mathrm{i}\frac{t}{r}H} - \Pi_i \mathrm{e}^{-\mathrm{i}\frac{t}{r}H_i} \right\| = O\left[\left(\textstyle\sum_i \|H_i\|\right)^2 (t/r)^2 \right]$$

as the argument of O goes to zero [30]. Since errors in a product of unitaries add up at most linearly [119], we have, after r steps, a total error of $O\left[\left(\sum_i \|H_i\|\right)^2 t^2/r \right]$. Thus, if we demand the error is at most ε, a number of steps $r = O[(\sum_i \|H_i\|)^2 t^2/\varepsilon]$ suffices. Every step costs $O(m)\, O(k^2 4^k)$ gates. So, the total cost of implementing $\mathrm{e}^{-\mathrm{i}tH}$ on a quantum computer up to error ε is n qubits and

$$O(m)\, O(k^2 4^k)\, O\left[(\textstyle\sum_i \|H_i\|)^2 t^2/\varepsilon \right]$$

gates.

1.5.2.2 Static quantum simulation

Next to the *dynamic* quantum simulation discussed above, there is another type of quantum simulation, which could be called *static quantum simulation*. The goal of the latter is to find (the properties of) the lowest energy eigenstate of a given Hamiltonian. The dynamic and static types of quantum simulation can be related via a routine that is called quantum phase estimation.

Consider a unitary U on the space of n qubits. Since U is unitary, we may write its eigenvalue equation as $U|\psi_i\rangle = \mathrm{e}^{\mathrm{i}2\pi\varphi_i}|\psi_i\rangle$ with $\varphi_i \in [0,1)$. Consider a quantum computer with an m-qubit data register, initialized to $|00\ldots0\rangle$, and a second register holding an eigenstate $|\psi_i\rangle$. Assume for simplicity that all φ_i can be represented exactly by a binary fraction with m bits of precision, and define the bitstring $\tilde{\varphi}_i$ by the binary representation of φ_i, $\varphi_i = 0.\tilde{\varphi}_{i(m-1)}\tilde{\varphi}_{i1}\tilde{\varphi}_{i0}$.[5][6] *Quantum phase estimation* is a quantum algorithm that maps

$$|00\ldots0\rangle|\psi_i\rangle \mapsto |\tilde{\varphi}_i\rangle|\psi_i\rangle\,,$$

A precise description of the steps that are involved in the implementation of the phase estimation algorithm are outside the scope of this introduction. Nevertheless, it is worth noting that one of the essential requirements for the implementation of the phase estimation algorithm is the ability to implement the unitary U.

When we apply phase estimation using an initial state that contains a superposition of eigenstates, that is, on $|00\ldots0\rangle|\Psi\rangle = \sum_i c_i|00\ldots0\rangle|\psi_i\rangle$, we obtain the state $\sum_i c_i|\tilde{\varphi}_i\rangle|\psi_i\rangle$. If we now measure the data register, the total state collapses to $|\tilde{\varphi}_i\rangle|\psi_i\rangle$ with probability $|c_i|^2$ (also see Sec. 1.4.1). In this way, we can use phase estimation as a routine for sampling phases according to a distribution that is determined by the amplitudes of the initial state of the second register.

To see how this can be used to translate from dynamic simulation to static simulation of physical systems, the first step is to find a good candidate ground state $|\Psi\rangle$. This could, for example, be obtained by mean-field theory. Take $U = \mathrm{e}^{\mathrm{i}\tilde{H}2\pi}$, with $\tilde{H}$ some Hamiltonian on n spins, obtained by normalizing and shifting a spin Hamiltonian H such

[5] It is straightforward to generalize the binary representation of the integers (Sec. 1.3.1) to fractions; the $(M+m)$-bit bitstring $x = x_{M-1}\ldots x_1x_0\,.\,x_{-1}\ldots x_{-m+1}x_{-m}$ with a '1' only at position $i \in \{M-1,\ldots,-m+1,-m\}$ represents the number 2^i. For example, 0.1 (binary representation) equals 0.5 (decimal representation).

[6] If the φ_i are arbitrary real numbers, we can still perform phase estimation. A measurement of the data register will collapse the output state to $|\tilde{\varphi}_i\rangle|\psi_i\rangle$, where $0.\tilde{\varphi}_i$ is the closest m-bit binary fraction to φ_i, with high probability.

a way that the minimum and maximum eigenvalues of $\tilde{H}$ lay between 0 and 1, respectively. (A priori, we do not know the minimum and maximum eigenvalues of H, but a respective lower and upper bound suffice.) This unitary U can be implemented efficiently using dynamic quantum simulation. Note that if $|\psi_i\rangle$ is an eigenvector of $\tilde{H}$ with eigenvalue φ_i, then $|\psi_i\rangle$ is an eigenvector of U with eigenvalue $e^{\mathrm{i}2\pi\varphi_i}$. Then, using the phase estimation routine, we can sample from the spectrum of $\tilde{H}$ according to the amplitudes squared of $|\Psi\rangle$.

There is no guarantee that $|\Psi\rangle$ has large overlap with the true ground state of $\tilde{H}$. Additionally, phase estimation does not give you any guarantee that, out of m runs of phase estimation, the lowest $\tilde{\varphi}_i$ out of those runs is the ground state energy of $\tilde{H}$. So, actually, static quantum simulation seems to be much harder than dynamic quantum simulation. (In terms of complexity classes, dynamic quantum simulation is in BQP, whereas the static problem is QMA complete.)

So, we have shown how to go from dynamic to static quantum simulation. In Chapter 4 of this thesis, we consider a method that is initially intended for approximate static quantum simulation. In that chapter we show how this method can be used for dynamical simulation as well.

1.5.3 Feynman path integral and quantum circuits

The Feynman path integral, which finds its origin in theoretical physics, offers an interesting perspective on quantum circuits. Vice versa, quantum circuits, and especially those for dynamic quantum simulation, offer an interesting perspective on the path integral in theoretical physics. Consider n qubits initially in the computational basis state $|i_0\rangle$ and a depth-T quantum circuit $C = U_T U_{T-1} \dots U_1$. The amplitude that is on a computational basis state $|i_T\rangle$ after the circuit C is given by $\langle i_T| C |i_0\rangle$. By inserting a resolution of the identity after every layer of the circuit, this can be rewritten as

$$\begin{aligned}\langle i_T| C |i_0\rangle &= \langle i_T| \left(\sum_{i'_T, i_{T-1}, \dots, i_1} \left|i'_T\right\rangle \left\langle i'_T\right| U_T |i_{T-1}\rangle \dots \langle i_2| U_2 |i_1\rangle \langle i_1| U_1 \right) |i_0\rangle \\ &= \sum_{i_{T-1}, \dots, i_1} \langle i_T| U_T |i_{T-1}\rangle \dots \langle i_2| U_2 |i_1\rangle \langle i_1| U_1 |i_0\rangle . \end{aligned} \tag{1.38}$$

Even though we have trivially inserted some identities, the equation above offers a whole new perspective on quantum circuits.

To see this, imagine a directed, weighted graph $G = (V, E, w)$ with vertices $V = \{0, 1, \dots, 2^n - 1\}^{\times(T+1)}$. The vertex V_{ti} represents $|i_t\rangle$ in

Eq. (1.38), and these two ways of notation will be used interchangeably. Put a directed edge $(V_{ti}, V_{t+1,j})$ for all possible t, i and j, and assign it the complex weight $w[(V_{ti}, V_{t+1,j})] = \langle i_{t+1}| U_{t+1} |i_t\rangle$. Denote the product of all weights along a given path through G as $c(\text{path})$. Then, Eq. (1.38) reads

$$\langle i_T| C |i_0\rangle = \sum_{\text{paths from } |i_0\rangle \text{ to } |i_T\rangle} c(\text{path}). \tag{1.39}$$

This is the Feynman path integral form of $\langle i_T| C |\psi\rangle$. For a general initial state $|\psi\rangle = \sum_{i_0} \psi_{i_0} |i_0\rangle$,

$$\langle i_T| C |\psi\rangle = \sum_{i_0} \psi_{i_0} \sum_{\text{paths from } |i_0\rangle \text{ to } |i_T\rangle} c(\text{path}). \tag{1.40}$$

These equations do not contain an integral over paths, but rather a sum. The term 'integral' originates from the path integral's original context of continuous time evolution, where the sum over paths becomes an integral over paths. The technically more correct term 'Feynman path sum' is also encountered.

Equation (1.40) contains a sum of all the amplitudes that flow from the initial state onto the basis vector $|i_T\rangle$. If this sum vanishes even though its terms do not, it is said that *destructive interference* occurs at $|i_T\rangle$. If, on the other hand, all terms have the same complex phase and hence add up, it is said that *constructive interference* occurs at $|i_T\rangle$. This is analogous to interference in a double-slit experiment.

As an example of interference in quantum circuits, consider the simple circuit

$$|0\rangle \text{ —— } \boxed{H} \text{ —— } \boxed{RZ(\theta)} \text{ —— } \boxed{H} \text{ —— } C|0\rangle\,. \tag{1.41}$$

It is straightforward to show that $C|0\rangle = \frac{1+e^{i\theta}}{2}|0\rangle + \frac{1-e^{i\theta}}{2}|1\rangle$. A subgraph of the graph G that corresponds to the circuit C is displayed in Fig. 1.5. The subgraph contains only paths from $|0\rangle$ to $|0\rangle$. The amplitudes in the initial and final state are given on the left and right part of the figure, respectively. We see there are two non-trivial paths that end up at $|0\rangle$ in the final state. One carries the amplitude $1/2$, the other an amplitude of $e^{i\theta}$. At the final state, the two paths interfere in a way that depends on the phase shift θ that was induced by the $RZ(\theta)$ gate.

The design of new quantum algorithms can be seen as the art of creating (approximate) constructive interference at basis states corresponding to the correct output of some computational problem instance

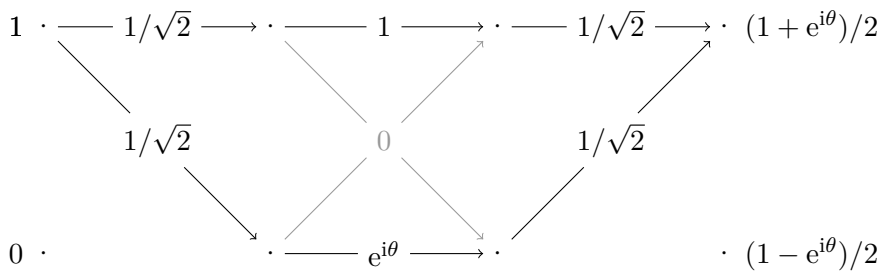

Figure 1.5: The flow of amplitudes from $|i_0\rangle = |0\rangle$ to $|i_T\rangle = |0\rangle$ as caused by Circuit (1.41).

(e.g. a prime factor of some large input integer), and (approximate) destructive interference at other basis states. Then, measurement of the final quantum state of the computation will yield a correct output with high probability.

To store the state of n qubits on a classical computer requires $O(2^n)$ classical memory bits. Remarkably, the Feynman path integral makes it manifest that quantum computations on n qubits can be simulated by a classical computer using only poly n bits if memory. To be more precise, let me first introduce *decision problems*. These are problems that have a yes/no answer. Many problems that initially are not decision problems can be cast into one. For example, instead of asking: 'what are the prime factors of N?', one could ask: 'is there a prime factor of N smaller than m?'. It is easy to show that if one can efficiently solve the latter decision problem, one can efficiently solve the former problem as well. The model of quantum computations as introduced in Circuit (1.11) can also be used to describe quantum computers that solve decision problems. In the model, one can choose to only measure the first qubit and take the outcome as the answer to the decision problem. We could say the outcome '1' means 'yes' and '0' means 'no'. It is for this type of problem that we are going to show the memory requirement of classical computers simulating a quantum computer.

If a quantum computer runs a circuit C on the input state $|0^n\rangle \equiv |0\rangle^{\otimes n}$, the probability of 'yes' after measurement of the first qubit equals

$$p_{\text{yes}} = \sum_{i' \in \{0,1\}^{n-1}} |\langle 1, i'| \, C \, |0^n\rangle|^2. \tag{1.42}$$

Every amplitude $\langle 1, i'| \, C \, |0^n\rangle$ can be written as a path integral [Eq. (1.38)]. Note that since C can be assumed to consist of one-

and two-qubit gates only, every weight $\langle i_{t+1}| U_{t+1} |i_t\rangle$ can be computed using $\operatorname{poly} n$ bits. Hence $c(\text{path})$ can be computed classically using $\operatorname{poly} n$ bits. Therefore, using an additional classical register that holds partial sums, p_{yes} can be computed classically using $\operatorname{poly} n$ bits.[7]

Note, however, that we did not escape an exponential overhead in simulating quantum computers using classical computers. This is because, even though $c(\text{path})$ can be computed for every path using only $\operatorname{poly} n$ bits, there are exponentially many paths. Hence, we have not shown that also the time complexity of simulating an n-qubits is $\operatorname{poly} n$. It is generally believed this is impossible.[8]

***

[7] This shows BQP⊆PSPACE.

[8] That is, it is believed that BPP≠BQP.

Chapter 2

Variational quantum eigensolver for the kagome lattice

Abstract

The Heisenberg anti-ferromagnet (HAFM) on the kagome lattice forms a model for the magnetic properties of real-world materials. The phase of the ground state of the HAFM on the kagome lattice is notoriously hard to find using classical computers. Quantum computers have already been shown to outperform classical computers in practice, but thus far not for real-world problems. We give a detailed proposal for a Variational Quantum Eigensolver (VQE) that solves for the ground state properties of the HAFM on the kagome lattice on a quantum computer. This VQE is well-suited for Near-term Intermediate Scale Quantum (NISQ) technology because the structure of the problem is intimately related to the structure of NISQ hardware itself and because of the known inherent noise-resilience of VQEs. We classically emulate a noiseless quantum computer with the connectivity of a 2D square lattice and show that the ground state energy of a 20-site patch, as found by the VQE, approaches the true ground sate energy exponentially as a function of the circuit depth of the VQE. Our simulations can be used to benchmark the performance of real quantum devices running this VQE for small patches.

2.1 Introduction

Despite decades of developments in numerical methods, the ground state phase of the Heisenberg anti-ferromagnet (HAFM) on the kagome lattice remains elusive. Approaches towards solving this problem include diagonalization of finite-size patches [89] and the density matrix renormalization group (DMRG) method [145]. Proposals for the ground state phase include a Valence Bond Crystal (VBC) [100, 109, 133, 134, 42] and a quantum spin liquid [69, 145, 9]. (See Ref. [89] and references therein for a more complete overview.) All classical methods for finding the ground state phase of the kagome HAFM are ultimately limited, for example by the inability to treat large patches (exact diagonalization), or the inability to describe highly entangled states (DMRG).

Quantum computation is a new player in this field that brings with it entirely novel possibilities. One method for finding ground states on a quantum computer is the Variational Quantum Eigensolver (VQE) [102, 117]. VQEs are especially suited for Near-term Intermediate Scale Quantum (NISQ) [120] devices because of their relatively mild circuit depth requirements and inherent noise-resilience [102, 117, 113, 125]. As any variational method, a VQE uses parametrized states. To every setting of the parameters, the corresponding energy of the corresponding state can be calculated, creating an 'energy landscape'. A classical minimization algorithm tries to find the global minimum of that landscape, but generally no guarantees exists that the global minimum is indeed obtained. Properties of the optimal state found by the optimization routine can be extracted by calculating expectation values of observables.

What sets the VQE apart from classical variational methods is that the parametrized state is obtained by applying a parametrized quantum circuit to some easy to prepare reference state of the quantum computer's register. The energy of the resulting state is obtained by performing measurements on many copies of that state. Note that the task of state preparation and measurement is intractable on classical computers.[1] Information can be extracted from the terminal state of the VQE by measuring the value of desired observables on that state. Parameter variation an optimization is still performed by a classical routine. So, a VQE can be seen as a classical variational method that uses a quantum computer as a subroutine for its function calls to the

[1] This is true, unless, in terms of complexity classes, BPP=BQP. It is generally believed that BPP$\neq$ BQP, for otherwise classical computers could solve factoring efficiently [130].

energy landscape.

Quantum computers can already perform tasks that are intractable on classical computers [11, 153], and have hence obtained what is called 'quantum supremacy' or a 'quantum advantage'. However, the tasks for which quantum computers can currently outperform classical computers have no known application; these tasks were designed purely for showing a quantum advantage. The milestone of a *useful* quantum advantage, where a quantum computer performs a useful task that can not be performed on any classical computer, is still ahead.

In this chapter, we design a VQE for the HAFM on the kagome lattice as an explicit proposal for showing a useful quantum advantage on NISQ devices. Henceforth, we refer to this VQE as KVQE for short. The experimental realization of this proposal would impact the fields of condensed matter and quantum computing alike.

KVQE uses the Hamiltonian Variational Ansatz (HVA), which was introduced in Ref. [142]. In the HVA, to find the ground state of a Hamiltonian H_1, the ansatz state is obtained by first preparing some known, easy-to-prepare ground state of a Hamiltonian H_{init}. Thereafter, this state is evolved sequentially by terms in the Hamiltonian. (Commuting terms may be evolved by simultaneously.) Every gate corresponds to time evolution according to a term in the Hamiltonian, where the parameter of that gate is set by the time duration of that evolution. The HVA itself does not specify H_{init} nor the sequence of terms in the Hamiltonian that the initial state is evolved by.

In our ansatz, H_{init} is formed by pairing up all vertices of the Kagome lattice (where two vertices are only paired if they are adjacent on the kagome lattice), and defining the Heisenberg interaction on every pair. The ground state of the HAFM on two spins is a singlet state. Thus, our initial state is a dimer covering of the kagome lattice, where every dimer is a singlet state. The parametrized circuit that is applied to the initial state consists of a cycle of gates c that is repeated p times. We define the gate HEIS(α) as time evolution along a single term in the Heisenberg Hamiltonian for a time α. (Sometimes we omit the explicit dependence on α for brevity.) In one cycle, all terms in the Hamiltonian are evolved by exactly once. Every HEIS gate in the circuit has its own parameter. See Fig. 2.1 for details. References [100, 109, 133, 134, 42] propose a Valence Bond Crystal (VBC) with a 36-site unit cell as the ground state of the HAFM on the kagome lattice. For patches with more than 36 sites, we propose to use this VBC as the initial state. For this initial state, also the gate sequence detailed in Fig. 2.1 can be used. Due to the large unit cell classical emulations using this initial state are outside the capabilities of our

classical emulator.

For NISQ VQE algorithms to give an advantage over purely classical methods, it is essential that the structure of the problem is close to the quantum hardware the VQE is run on [49]. KVQE is close to NISQ hardware for three reasons. Firstly, because the Hamiltonian of the kagome HAFM is a spin Hamiltonian, it is directly a Hamiltonian defined on qubits. In contrast, many Hamiltonians for which VQEs are proposed are Fermionic. Examples include those in quantum chemistry [117, 113, 60], and the Fermi-Hubbard model [142, 28, 125, 12]. In order for a VQE using the HVA to solve for the ground state of a Fermionic Hamiltonian, the Hamiltonian first needs to be mapped to a spin Hamiltonian, for example by the Jordan-Wigner [107], Bravyi-Kitaev [25] or ternary tree [70] transformations. Fermion to spin maps either increase the non-locality of terms in the Hamiltonian or they introduce additional qubits, in any case leading to an overhead in quantum resources.

A second reason that KVQE is close to NISQ hardware is that its gates are essentially native on multiple NISQ architectures. The HVA requires time evolution generated by terms in the Hamiltonian. For the HAFM, this amounts to turning on an exchange interaction between qubits, which is native on quantum dot architectures [35, 15, 99, 63]. In Sec. 2.5, we show this interaction can also be realized on the superconducting hardware by Google AI quantum [48] using a single native two-qubit gate and at most four single-qubit gates. (If a two-qubit gate is equal to a single native gate up to single-qubit rotations, we call the former gate 'essentially native'.)

Next to the HVA, a well-known type of ansatz is the Hardware-Efficient Ansatz (HEA). The HEA is hardware-inspired; the circuit generating the ansatz state consists, by definition, of gates native to the hardware, avoiding the need to compile the ansatz into native gates. However, the HEA suffers from the 'barren plateau' problem: the gradient of the energy cost function is exponentially small in the number of parameters [101]. The HVA, on the other hand, is problem-inspired, and there is some evidence that it does not suffer from the barren plateau problem [143]. However, for execution on a quantum computer, gates in the HVA generally need to be compiled to gates native to that quantum computer. This increases the circuit depth, which is undesirable for NISQ devices. For KVQE, such compilation is not required on quantum dot architectures, and only minimal compilation that does not increase the number of two-qubit gates is needed on Google's hardware. So, to summarize, KVQE quantum dot or Google's superconducting hardware has the unique property that the HVA is essentially equal to the Hardware Efficient Ansatz (HEA) [74, 117].

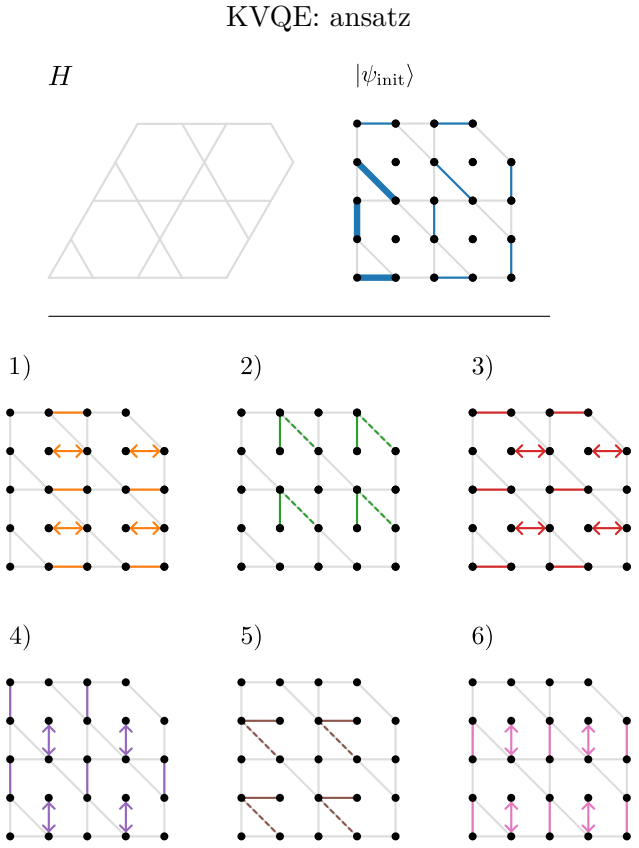

Figure 2.1: (**Top left**) The 20-site open patch simulated by KVQE, with spin-1/2 particles on the vertices and the Heisenberg interaction defined along the edges. (**Top right**) The initial state $|\psi_{\text{init}}\rangle$. Black dots represent qubits and solid blue lines represent singlets. A sheered kagome lattice is added in grey as a guide to the eye. The bold solid lines form one unit cell of the dimer covering that can be used to extend the current ansatz to systems of arbitrary size. For open systems some patching of the regular dimer covering is needed. In the present case this consists of the two singlets at the far right. (**Bottom**) The cycle c, with numbers indicating the order of the layers. Solid coloured lines represent HEIS gates, and two-headed arrows indicate SWAP gates. Dashed, coloured lines are added as guide to the eye and indicate along which bond of the kagome lattice the HEIS gates of that layer are acting effectively. The unit cell of the cycle as a whole is equal to the unit cell of the Kagome lattice itself, and can hence be straightforwardly extended to larger system sizes. No patching is needed at the edges.

Lastly, KVQE is close to NISQ hardware because it runs on hardware with the connectivity of a 2D square lattice (henceforth referred to as grid connectivity) with minimal overhead. This is the connectivity that is also required for the surface code [47]. Therefore, much effort is put in designing platforms with grid connectivity [64, 8, 139, 11, 63]. In Sec. 2.4, we show by an explicit construction how the limitation from all-to-all connectivity to grid connectivity increases the overall circuit depth of KVQE only by a factor of approximately 3/2.

We test KVQE by using it to simulate a 20-site open patch of the kagome lattice. We assume a noiseless 24-qubit quantum computer with grid connectivity and the ability to natively implement the exchange interaction, $\sqrt{Z}$ and X gates. We emulate this quantum computer classically, as is detailed in Sec. 2.2.4. The optimal state obtained by KVQE is compared to the exact ground state of the 20-site patch, the latter of which is obtained by exact diagonalization. We find that the optimal energy obtained by KVQE approaches the true ground state energy exponentially as a function of the number of cycles p. Also, the fidelity (overlap squared) between the optimal state and the true ground state approaches unity exponentially fast in p. A fidelity of $>99.9\%$ is reached at $p = 16$, corresponding to a circuit of depth 99.

As an intermediate goal towards finding the ground sate of the kagome HAFM, we propose to use a similar method for finding the ground state of the HAFM on a periodic chain, see Fig. 2.2. Henceforth we refer to this VQE as CVQE for short. CVQE is a suitable benchmark problem for quantum hardware because, in contrast to the kagome lattice, the ground state of the HAFM on the chain can be computed efficiently classically by means of the Bethe ansatz [22, 50, 29]. This opens the possibility to compare the optimal energy found by the VQE running on a quantum computer against the exact ground state energy even for chains with hundreds of sites.

CVQE is similar to the VQE of the HAFM on the chain of Ref. [65]. Differences are that we simulate a periodic chain instead of an open chain and that we use one parameter per gate instead of one parameter per layer, and that we go to larger system sizes and circuit depth. Under the same hardware assumptions of the previous paragraph, we classically emulate CVQE for a 20-site periodic chain. The fidelity and energy of the optimal state found by the VQE again improve exponentially as a function of circuit depth. The optimal state found by the VQE reaches an overlap of $>99.9\%$ after $p = 8$ cycles, corresponding to a circuit of depth 19.

CVQE: ansatz

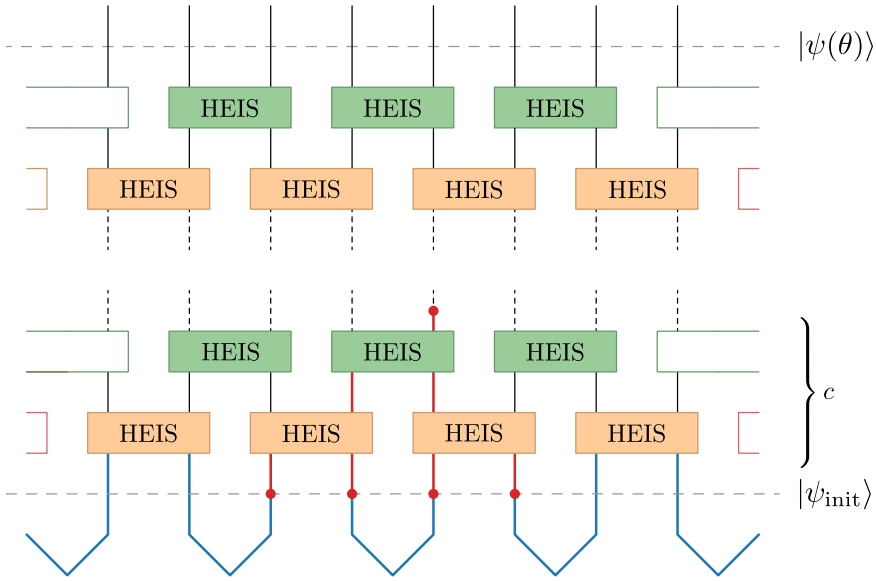

Figure 2.2: Part of the ansatz for CVQE, with time running from bottom to top. The initial state $|\psi_{\text{init}}\rangle$ consists of $n/2$ contiguous singlet states, displayed in blue. The circuit C that is applied sequentially consists of p repetitions of a cycle c, each time with new parameters, and with one parameter per gate. The HEIS gate is evolution according to the Heisenberg exchange interaction for a time given by its parameter. For one of the qubits the past light cone that is due to a single cycle c (excluding the singlet generation) is displayed in red. (Further information on the past light cone in Sec. 2.3).

2.2 Methods

2.2.1 VQE

The problem of finding the ground state energy of k-local Hamiltonians (Sec. 1.4.4) is believed to be intractable on classical computers [84, 118, 3]. Because quantum computers are themselves quantum mechanical, one could hope that this problem is in fact tractable for quantum computers. In general, however, the problem is believed to be intractable even for quantum computers. (That is, the local Hamiltonian problem is QMA-complete [84, 118, 3]). Nevertheless, there may be problem instance classes for which quantum computers could in fact solve for the ground state efficiently.

A proposed method for finding ground states on quantum computers is the Variational Quantum Eigensolver (VQE). A VQE is a variational method, and hence relies on the variational principle. Consider a quantum mechanical system with Hilbert space $\mathcal{H}$ of dimension N, Hamiltonian H with ground state energy E_0, and a subset of parametrized states $\{|\theta\rangle\} \subseteq \mathcal{H}$, with $\theta \in \mathbb{R}^m$. To describe all of $\mathcal{H}$, it is necessary that $m = O(N)$. The variational principle states that

$$E(\theta) = \langle\theta| H |\theta\rangle \geq E_0 \tag{2.1}$$

for all $|\theta\rangle \in \mathcal{H}$. For reasons of scalability, in variational methods, one generally takes $m = \operatorname{polylog} N$. Variational methods, like the VQE, seek to minimize $E(\theta)$ to hence establish a upper bound for the ground state energy.

A VQE is fed an efficient classical description of a Hamiltonian on n spin-1/2 particles,

$$H = \sum_{i=1}^{l} h_i H_i,$$

with the h_i real coefficients and H_i Hermitian operators. For k-local Hamiltonians, $l = \operatorname{poly} n$ [see Sec. 1.4.4]. Often, the Hamiltonian is not of the above form [117, 113, 60, 142, 28, 125, 12], in which case it first needs to be cast into that form using classical preprocessing.

A VQE proceeds as follows. First, an initial set of parameters θ is chosen. These initial parameters may be chosen at random, or may be inspired by a classical approximate solution to the ground state, for example by the Hartree-Fock ground state [136] in quantum chemistry problems. Then, a criterion is chosen, for example that a maximum number of iterations has not been reached, or that $E(\theta)$ has not reached a value below a given threshold. The VQE proceeds as follows.

1. While the criterion is true, repeat:
   (a) *Prepare the ansatz* $|\theta\rangle$.
   Prepare some easy-to-prepare initial state $|\psi_{\text{init}}\rangle$. Apply a parametrized circuit $C(\theta)$ to obtain the state $|\theta\rangle = C(\theta)|\psi_{\text{init}}\rangle$. The circuit $C(\theta)$ usually consists out of gates on fixed positions, where every or some of the gates are parametrized.
   (b) *Measure and store* $E(\theta)$.
   By linearity, $E(\theta) = \sum_i c_i \langle\theta|H_i|\theta\rangle$. Each expectation value $\langle\theta|H_i|\theta\rangle$ can be estimated by measuring the operator H_i repeatedly (each measurement requires a new preparation of $|\theta\rangle$) and taking the statistical average. See Ref. [102] for the expected number of measurements using this method, or Ref. [66], and references therein, for more efficient methods.
   (c) *Update* θ.
   Based on $E(\theta)$ and previous outcomes of $E(\theta)$, update θ according to some classical optimization algorithm.
2. Return the θ^* that achieved the smallest energy.

Physically relevant information, such as correlation functions, can now be extracted from $|\theta^*\rangle$ by repeatedly preparing and performing measurements on $|\theta^*\rangle$. Different VQEs differ in the way circuits are parametrized, how (an estimate for) $E(\theta)$ is obtained, and what specific optimization routine is used. These will be detailed in the subsequent sections of this chapter for KVQE and CVQE.

2.2.2 Ansatz

In the Hamiltonian Variational Ansatz (HVA) [142], the initial state $|\psi_{\text{init}}\rangle$ is the ground state of a Hamiltonian H_{init}. The Hamiltonian H_{init} is chosen so that its ground state is known and easy to prepare. The ansatz state $|\theta\rangle$ is obtained by sequentially evolving along terms in the Hamiltonian to be simulated, H, according to some fixed sequence i,

$$|\theta\rangle = \exp(-\mathrm{i}\theta_M H_{i_M}) \dots \exp(-\mathrm{i}\theta_2 H_{i_2}) \exp(-\mathrm{i}\theta_1 H_{i_1}).$$

The M parameters are formed by the time duration of the M evolutions. Often (not limited to Refs. [65, 142, 143, 28]), C consists out of p cycles of a smaller circuit c, each time defined by the same sequence i of terms in the Hamiltonian. Every cycle gets its own set

of m parameters. It is convenient to write θ as $\theta = (\theta_1, \ldots, \theta_p)$, with $\theta_j = (\theta_{j_1}, \ldots, \theta_{j_m})$. Then, a single cycle reads

$$c(\theta_j) = \exp(-\mathrm{i}\,\theta_{j_m} H_{i_m}) \ldots \exp(-\mathrm{i}\,\theta_{j_2} H_{i_2}) \exp(-\mathrm{i}\,\theta_{j_1} H_{i_1}), \tag{2.2}$$

and so

$$|\theta\rangle = c(\theta_p) \ldots c(\theta_1)\, |\psi_{\text{init}}\rangle\,. \tag{2.3}$$

We call this commonly used type of HVA the *cyclic* HVA. The cyclic HVA shows a close relation between static quantum simulation and dynamic quantum simulation (Sec. 1.5.2); choosing $i = (1, \ldots, l)$ (or a permutation thereof) and $\theta_j = (t/p, \ldots, t/p)$, the cyclic HVA implements quantum time evolution for a target time t with p Trotter steps. In a similar way, the cyclic HVA can mimic (but is more general than) adiabatic time evolution. Given that no gap closes between H_{init} and H, the HVA thus ensures that the ground state of H can in fact be prepared with the ansatz. This formed the initial motivation for the HVA in VQEs [142].

The Heisenberg anti-ferromagnetic Hamiltonian (HAFM) reads

$$H = \sum_{\langle ij \rangle} \mathbf{S}_i \cdot \mathbf{S}_j, \tag{2.4}$$

where $\mathbf{S}_i = (X_i, Y_i, Z_i)^T/2$ with X, Y, Z the Pauli matrices, and where the sum is over the edges $\langle i, j \rangle$ of some graph G. In this work, G is either kagome lattice (Fig. 1.3) or a periodic chain. Then, according to the HVA, we need to be able to evolve by what we call the HEIS gate. In the computational basis of two qubits (with e.g. $\langle 00|\,\mathrm{HEIS}(\alpha)\,|00\rangle$ the top left entry), it reads

$$\begin{aligned}\mathrm{HEIS}(\alpha) &\equiv \mathrm{e}^{-\mathrm{i}\alpha/4} \mathrm{e}^{-\mathrm{i}\alpha \mathbf{S}_0 \cdot \mathbf{S}_1} \\ &= \begin{pmatrix} \mathrm{e}^{-\mathrm{i}\alpha/2} & 0 & 0 & 0 \\ 0 & \cos(\alpha/2) & -\mathrm{i}\sin(\alpha/2) & 0 \\ 0 & -\mathrm{i}\sin(\alpha/2) & \cos(\alpha/2) & 0 \\ 0 & 0 & 0 & \mathrm{e}^{-\mathrm{i}\alpha/2} \end{pmatrix}.\end{aligned}$$

In a parametrized circuit [Eq. (2.3), Figs. 2.1 and 2.2], every instance of the HEIS gate gets its own parameter $\alpha = \theta_{j_k}$.

In this work, we will always assume that every Heisenberg gate in the ansatz gets its own parameter; we have One parameter Per Gate (OPG). Another possibility would be to have multiple HEIS gates per cycle share the same parameter. We call this One parameter Per Slice (OPS). We say the qubits sharing the same parameter are in the same 'slice'.

A possible advantage of OPS is that is possible to encode some of the symmetries we may believe the ground state to have directly into the circuit; by choosing proper slices, we can assure that the state produced by the circuit has the desired lattice symmetries. At the same time, this would make the search space smaller by only restricting to states with the desired lattice symmetry.

Nevertheless, OPG has advantages over OPS. With OPS ground states we may overlook symmetry broken ground states. For example, it is not known whether the ground state of the kagome lattice is symmetry broken [89]. Secondly, even if the ground state does not break the symmetry of the Hamiltonian, the depth of the OPG circuit for that state may be lower than the depth of the OPS circuit that produces the same state. (For any state, the optimal OPG circuit depth is a lower bound for the optimal OPS circuit depth obtaining that same state.) For NISQ devices it is imperative to keep circuit depths as low as possible. Finally, the inherent noise-resilience of VQEs may be compromised by choosing OPS over OPG. As an illustration, say we are given a noiseless quantum computer, a Hamiltonian and a minimal-depth OPS circuit that produces the ground state of that Hamiltonian. Suppose that now a static but random over-rotation is added to every HEIS gate. Then it is very unlikely that the OPS circuit can still produce the correct ground state, no matter its parameters. When we lift the restriction that the qubits in every slice share the same parameter, and hence go to a OPG circuit, the over-rotations can be absorbed into the parameters, and hence the ground state can in principle still be produced with the same depth.

2.2.3 Analysis

We assess the effectiveness of KVQE an CVQE by running them for fixed system sizes but a varying number of cycles p. For every p, we plot the relative energy error $\mathcal{E}$ between the true ground state energy, E_0, and the optimal energy found by the VQE, $E(\theta^*)$,

$$\mathcal{E} = \left| \frac{E(\theta^*) - E_0}{E_0} \right|. \tag{2.5}$$

Additionally, we plot the infidelity $\mathcal{I}$ between the true ground state $|E_0\rangle$ and the optimal state obtained by the VQE, $|\theta^*\rangle$,

$$\mathcal{I} = 1 - \mathcal{F} \equiv 1 - |\langle E_0|\theta^*\rangle|^2,$$

with $\mathcal{F}$ the fidelity between $|E_0\rangle$ and $|\theta^*\rangle$. Even in plots showing the infidelity, the corresponding VQE uses a routine that optimizes the

energy, not the infidelity. The infidelity is a useful figure of merit because it upper bounds the relative error in expectation value of any observable [16],

$$\frac{|\langle E_0| O |E_0\rangle - \langle \theta^*| O |\theta^*\rangle|}{\|O\|} \leq 4\sqrt{\mathcal{I}}, \tag{2.6}$$

with $\|\cdot\|$ the operator norm.

We obtain E_0 and $|E_0\rangle$, and thus $\mathcal{E}$ and $\mathcal{I}$, by exact diagonalization. For large system sizes, such as those needed for quantum advantage experiments, this is no longer possible.

2.2.4 Classical implementation

We emulate the quantum circuits in this chapter using the home-grown, optionally GPU-accelerated, classical quantum emulator `HeisenbergVQE`. Documentation, source code and all generated data are freely available online [76]. `HeisenbergVQE` is tailored to running VQEs for the Heisenberg model on any graph. It is written in Python [46], with performance critical code delegated to C via NumPy [62] if GPU acceleration is off, and CUDA via CuPy [110] if GPU acceleration is on.

We exploit the full access to the wave function, granted by classical emulation, in the computation of the energy of ansatz states. Furthermore, we assume a noiseless quantum computer. This allows us to use gradient-based optimization methods. A gradient-based method, in turn, allows us to use backward-mode automatic differentiation, which is a standard technique in the context of neural networks, and is much faster than finite-difference methods [106]. We use an implementation from Chainer [137].

For optimization of the cost function $E(\theta)$, we first choose initial parameters uniformly at random in the interval $[-10^{-3}, 10^{-3})$. (I.e. $\theta_{j_k} \in_R [-10^{-3}, 10^{-3})$ for every integer $1 \leq j \leq p$ and $1 \leq k \leq m$, where parameters are distributed according to the descriptions in Figs. 2.1 and 2.2.) There is some evidence that suggests that for the HVA, points close to the origin in parameter space are good starting points for local optimization [143]. We then use the BFGS algorithm, as implemented in SciPy [140], to find a local minimum. At every step of the BFGS routine the energy and the gradient of the energy are calculated. Here, we call these two steps together one *function call*. The steps of random parameter generation and local optimization (one 'round') are repeated a variable number of times. The parameters that achieve the lowest energy out of all local minimization rounds, θ^* is outputted together

with $E(\theta^*)$. Starting many rounds of local optimization from unrelated starting points has the benefit that they can be run in parallel, even without the need of communication between the processes. (Such a parallelization is called 'embarrassingly parallel'.)

`HeisenbergVQE` computes exact ground states using SciPy's wrapper of ARPACK, which implements the Implicitly Restarted Lanczos Method [91]. Operator-vector multiplication is optionally GPU accelerated. The energy of the exact ground state and the exact ground state vector itself are used as a reference of the performance of the VQEs in this chapter. We note that such reference is not possible for system sizes for which a quantum computer might obtain a useful quantum advantage.

`HeisenbergVQE`'s online resource [76] also includes data and plots for systems and ansätze not reported in this chapter, including other system sizes, simulations that use one parameter per slice (see Sec. 2.2.2), periodic patches, ansätze that assume all-to-all connectivity, and runs where we use the infidelity as the cost function. Using the infidelity as a cost function is impractical on quantum computers (or even impossible if the ground state is not known), but may be used by classical computers to obtain further data on the theoretically attainable performance of an ansatz. For all systems, data was stored in human-readable format. Fields include: the number of calls to the cost function by the BFGS routine, the wall-clock time of the classical emulation, the initial parameters, and the parameters, energy, and infidelity of the local minima.

2.3 Chain

Here, we detail our ansatz for the VQE for the HAFM [Eq. (2.4)] on a periodic chain (CVQE) and show its results for a chain of 20 sites.

A Quantum Processing Unit (QPU) with grid-connectivity naturally embeds subsets of qubits with (at least) the connectivity of a periodic chain. In contrast to the HAFM on the kagome lattice, it is known how to efficiently classically compute the ground state energy and correlation functions of the HAFM on the periodic chain. This is done via the Bethe ansatz [22, 50], as implemented in, for example, the ABACUS library [29]. Because of the classical tractability of the HAFM on the chain we can use it as a benchmark problem for real hardware. It is only for systems up to ~ 50 qubits [89] that similar benchmarks can be made for the HAFM on the kagome lattice.

The ansatz is depicted in Fig. 2.2. We assume n an even number

of qubits, and take $H_{\text{init}} = \sum_{i \text{ even}} \mathbf{S}_i \cdot \mathbf{S}_{i+1}$ (the first qubit is at $i = 0$), resulting in a ground state $|\psi_{\text{init}}\rangle = |s\rangle^{\otimes n/2}$, with $|s\rangle \equiv (|01\rangle - |10\rangle)/\sqrt{2}$ a singlet state. The cycle c is build up out of two layers. In the first layer, we place HEIS gates between qubits i and $(i+1) \bmod n$, with i odd. In the second, we place HEIS gates between qubits i and $(i+1) \bmod n$ with i even. Because every gate gets its own parameter, the total number of parameters is $M = np$. The energy landscape is optimized by running 32 local optimization routines, starting from 32 random initial points (see Sec. 2.2.4).

Results are displayed in Fig. 2.3. Both the relative energy error $\mathcal{E}$ and the infidelity $\mathcal{I}$ (Sec. 2.2.3) initially decrease exponentially as a function of p, reaching an energy that is below the first exited state for $p \geq 2$. Both functions show a sudden improvement after $p_{\text{crit}} = 5$. From p_{crit} to $p_{\text{crit}} + 1$, $\mathcal{E}$ drops by an order of magnitude, and $\mathcal{I}$ drops by two orders of magnitude. For $p > 5$, both functions again decrease roughly exponentially with a slope that is greater in magnitude than before. At the same time, the number of function calls (as defined in Sec. 2.2.4, data not shown in the plot but available at [76]) grows polynomially with p. A fidelity of >99.9% is reached for $p \geq 8$. Assuming HEIS gates are native and that singlets can be created with a circuit of depth 3 (Sec. 2.5), $p = 8$ amounts to a circuit with $20/2 \times 3 = 30$ gates for the preparation of singlets and $20 \times 8 = 160$ HEIS gates, giving a total of 190 gates and 160 parameters. The depth of the circuit is $3+8\times2 = 19$. The optimization routine for finding the 32 local minima at $p = 8$ used 104,890 function calls. A fidelity of >99,99% is reached at $p = 11$ cycles, using a total of 197,685 function calls.

We observe a sudden improvement of the performance of CVQE after $p_{\text{crit}} = 5$ cycles. A plausible explanation is in terms of the past light cone. The past light cone of a qubit q after a circuit C consists of all qubits q' for which there exists a past-directed path through C that connects q to q'. It is only when q' is in the past light cone of q that C can build up entanglement between q and q'.

The ground state of the HAFM on the chain shows long-range entanglement [88]. The sudden improvement of performance is a clear sign of a ground state with long-range entanglement. After p_{cirt}, for the first time the past light cone of every qubit at the end of C (as defined in Sec. 2.2.2 and Fig. 2.2) covers the entire chain. However, at p_{crit}, the past light cone of every qubit already covers the entire chain if we continue the light cone through the gates that generate the singlet states. It so seems that the first three unparametrized layers that generate the singlets cannot create the right type of entanglement.

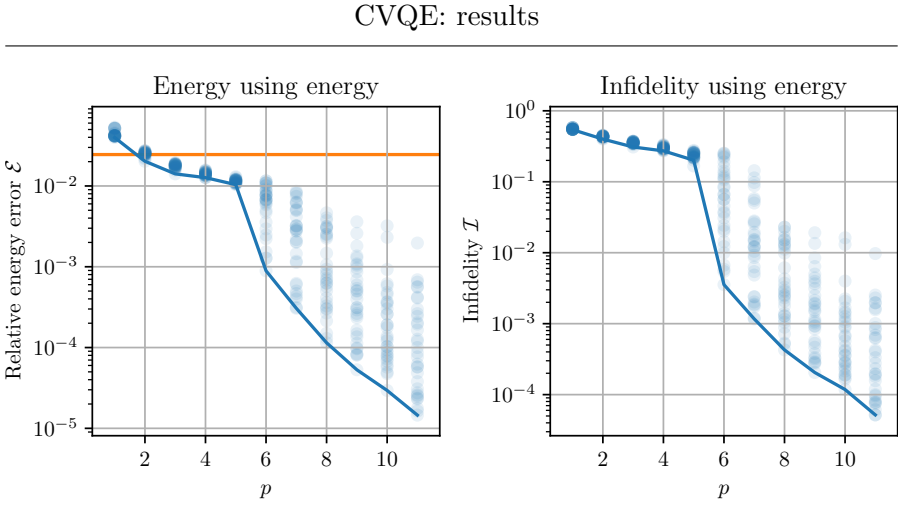

Figure 2.3: (**Left**) Semi-log plot of the relative energy error [Eq. (2.5)] obtained by CVQE (Fig. 2.2) for 20 sites as a function of the number of cycles p. Every translucent point represents one of the 32 local minima that were found per value of p. The solid line connects the lowest local minima $E(\theta^*)$. An orange horizontal line is drawn at the value of the first exited state. (**Right**) Semi-log plot of the infidelities of the states corresponding to the local minima in the left plot. The solid line connects the points that, for a given p, are lowest in *energy*. Although it occurs regularly, these points need not have the lowest infidelity. One such exception is visible at $p = 5$. In both the left and the right plot we see a sudden improvement of performance at $p_{\text{crit}} = 5$.

2.4 Kagome

Here, we detail our ansatz for the VQE of the HAFM on the Kagome lattice (KVQE), and show its performance in simulating a 20-site open patch. It uses 20 data qubits to represent the 20 sites of the patch, and an additional 4 qubits as 'swapping stations', used to realize kagome connectivity on a grid architecture. The restriction of grid connectivity increases the circuit depth per cycle (assuming HEIS gates are native) from 4 to 6, and (in the limit of large system sizes) introduces one ancilla qubit per three qubits.

Results are displayed in Fig. 2.4. The relative energy error $\mathcal{E}$ decreases roughly exponentially for all considered p. Again, the number of function calls scales polynomially with p (data available at [76]). KVQE finds an energy lower than the energy of the first exited state for $p \geq 5$. There is no clear critical p after which $\mathcal{E}$ and/or $\mathcal{I}$ improve drastically. Nevertheless, $\mathcal{I}$ transitions to an improved exponential decay rate somewhere between $p = 3$ and $p = 5$, reaching a fidelity of >99,9% at $p \geq 16$. Under the assumptions of the previous section (Sec. 2.3) and the additional assumption that the SWAP gate is native, $p = 16$ amounts to $3 \times 10 = 30$ gates for the generation of the singlets, $16 \times 30 = 480$ HEIS gates, and $16 \times 16 = 256$ SWAP gates, giving a total of 766 gates and 480 parameters. The total depth equals $3 + 16 \times 6 = 99$. To obtain the 10 local minima at $p = 16$ a total of 82,466 function calls were made.

In contrast to the chain, there is no clear critical p after which there is a sudden improvement of performance for the current kagome patch. The past light cone effect can explain this difference: not all qubits' past light cones cover the entire system for the first time at the same number of cycles. Let us lay out a coordinate system over the 24 qubits used in Fig. 2.1 (top right). We put the origin (0,0) at the bottom left qubit, the the qubit directly above at (0,1), and the qubit directly to the right of the origin at (1,0). At $p = 2$, there is no qubit whose past light cone in C covers the entire system. At $p = 3$, there are qubits, such as the bottom right (4,0), bottom left (0,0), top left (0,4) and middle (2,2) qubit, whose past light cone in C covers the entire system. There are, however, still some qubits for which this is not the case, such as the qubits at (3,4), (4,3) and the top middle (2,0). At $p = 4$, the past light cone of the latter qubits covers the entire system, except for the qubit at (3,4). It is only after $p = 5$ cycles that its past light cone covers the entire system.

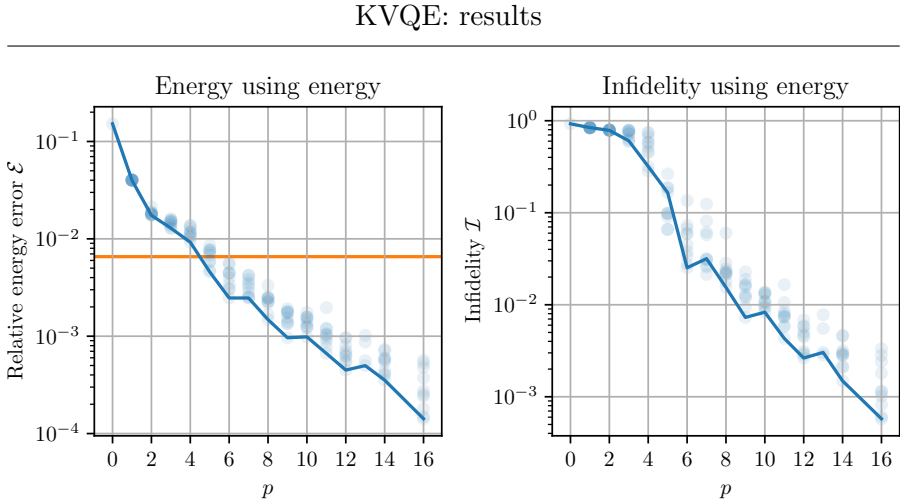

Figure 2.4: (**Left**) Semi-log plot of the relative energy error [Eq. (2.5)] obtained by KVQE for 20 sites (Fig. 2.1), as a function of the number of cycles p. Translucent points represent the 10 local minima that were found by KVQE per p. Every cycle is a circuit of depth 6 and uses 30 parameters. The orange horizontal line is at the value of the first exited state. (**Right**) Semi-log plot of the corresponding infidelities. The solid line connects the points that are lowest in energy.

2.5 Hardware implementation

The HEIS gate is directly native on quantum dot architectures. This also allows native implementation of the SWAP gate on these devices since SWAP = i HEIS(π). The native, parametrized two-body gate of Google AI Quantum equals [48]

$$\mathrm{fSim}(\theta,\phi) = \begin{pmatrix} 1 & 0 & 0 & 0 \\ 0 & \cos(\theta) & -\mathrm{i}\sin(\theta) & 0 \\ 0 & -\mathrm{i}\sin(\theta) & \cos(\theta) & 0 \\ 0 & 0 & 0 & \mathrm{e}^{-\mathrm{i}\phi} \end{pmatrix}.$$

Here, we show how this gate can be used to implement HEIS(α) for any α.

The HEIS gate is periodic, up to an overall phase, with period 2π. For $-\pi \leq \alpha < \pi$, the fSim gate is related to the HEIS gate by

$$\mathrm{HEIS}(\alpha) = \mathrm{RZ}_0(\alpha/2)\mathrm{RZ}_1(\alpha/2)\mathrm{fSim}(\alpha/2,\alpha), \tag{2.7}$$

with $\mathrm{RZ}_0(\theta) = \mathrm{RZ}(\theta)\otimes\mathbb{1}$ and $\mathrm{RZ}_1(\theta) = \mathbb{1}\otimes\mathrm{RZ}(\theta)$, where $RZ(\theta) = \mathrm{e}^{-i\theta Z/2}$, and Z is the Pauli-Z operator. According to Eq. (2.7), for $0 \leq \alpha/2 \leq \pi/2$, a HEIS($\alpha$) gate can be directly implemented using two single-qubit RZ gates and one fSim gate. For parameter values that fall outside that range, the following identity can be used in conjunction with Eq. (2.7),

$$\mathrm{fSim}(\theta,\phi) = \begin{cases} Z_0 Z_1\,\mathrm{fSim}(\theta-\pi,\phi) & : -\pi \leq \theta < -\pi/2 \\ Z_0\,\mathrm{fSim}(-\theta,\phi)\,Z_0 & : -\pi/2 \leq \theta < 0 \\ \mathrm{fSim}(\theta,\phi) & : 0 \leq \theta < \pi/2 \\ Z_0\,\mathrm{fSim}(-\theta+\pi,\phi)\,Z_1 & : \pi/2 \leq \theta < \pi \end{cases}.$$

Here, $Z_0 = Z\otimes\mathbb{1}$ and $Z_1 = \mathbb{1}\otimes Z$.

The SWAP is related to the fSim gate by

$$\mathrm{SWAP} = \sqrt{Z_0}\sqrt{Z_1}\,\mathrm{fSim}(\pi/2,\pi).$$

The fSim gate in this equation can be implemented directly. Hence, a SWAP gate can be implemented by using one layer of RZ rotations and a single fSim gate. Assuming single qubit rotations are native, and a Heisenberg or fSim gate is native, singlets can be created between two adjacent qubits with a circuit of depth 3 (see Fig. 2.6).

So, to conclude, by adding up the angles of subsequent RZ rotations, ℓ layers of HEIS and/or SWAP gates can be implemented by at most ℓ layers of single-qubit RZ rotations and $\ell+1$ layers of fSim gates. Depending on the specific circuit, further reductions may be possible by using that $\mathrm{RZ}_0(\beta)\mathrm{RZ}_1(\beta)$ commutes with $\mathrm{fSim}(\theta,\phi)$ and addition of RZ rotation angles. For an example, see Fig. 2.5.

HEIS compilation

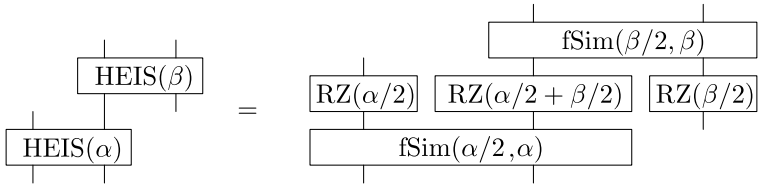

Figure 2.5: Example for compiling HEIS gates into fSim gates and single-qubit RZ rotations for $0 \leq \alpha/2 \leq \pi$.

Singlet preparation

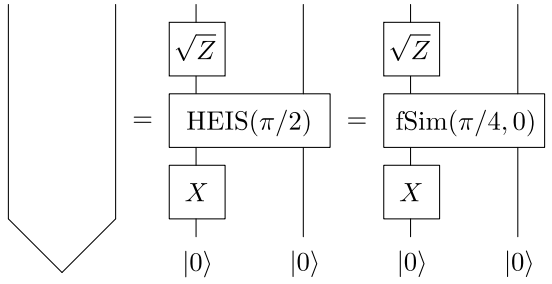

Figure 2.6: Circuits for preparing the singlet state up to a global phase (left), using gates native to quantum dots (middle) and gmons (right).

2.6 Discussion and outlook

Current hardware does not yet simultaneously have grid connectivity and the ability to implement the exchange interaction for all parameter values essentially natively. Quantum dot architectures can natively implement the exchange interaction, but are not yet available with grid connectivity. However, this connectivity may become available in the future [15, 35, 63, 92]. Google AI Quantum is able to implement the exchange interaction essentially natively for all parameter values (see Ref. [48] and Sec. 2.5), and is also able to demonstrate grid connectivity [11], but is not yet able to combine these two features in a single processor. They have, however, expressed this as a future goal (see Sec. C. of the supplementary material of Ref. [11]). Some of the current hardware can in principle already efficiently perform CVQE for small problem sizes of open [48] or closed chains [63]. In such experiments, the observation of a critical circuit depth forms an early goal.

For showing a quantum advantage with KVQE on a quantum computer, it is a prerequisite that it is first able run KVQE for a 20-site patch of the kagome lattice. In this work, we have set a performance baseline for this patch; we do not expect a quantum computer to perform as well as the noiseless emulations in this work. The extent to which a given quantum computer can approach this baseline forms an interesting assessment of its capabilities and prospects. Possible performance characteristics include the presence of exponential decay of the relative energy error as a function of the number of cycles, and the value of the relative energy error at which the experimental VQE saturates. (We see no such saturation in the noiseless classical emulation.)

Another baseline we have set in this work is the performance of a VQE for the HAFM on the periodic chain of 20 sites. Here, an additional performance characteristic is formed by the kink that the relative energy shows at the critical number of cycles $p_{\mathrm{crit}} = 5$. Observation of this kink would indicate the ability to generate and find ground states with system-wide entanglement. We expect KVQE for larger patches (of both the kagome lattice and the chain) to also show an exponential decay of the relative energy error as a function of the number of cycles. Due to the inherent limitations of classical emulation, a fully fledged system-size scaling study of the rate of this exponential decay is outside the scope of the current work. Further investigation, possibly on real quantum devices, is needed to show how rate of exponential decay changes with system size and noise levels.

***

Chapter 3

Conditions for superdecoherence

Abstract

In quantum computation, the decoherence rate per qubit is typically assumed to be constant. It is known, however, that quantum registers coupling to a single reservoir can show a decoherence rate per qubit that increases linearly with the number of qubits. This effect has been referred to as superdecoherence, and has been suggested to pose a threat to the scalability of quantum computation. Here, we show that a sufficient condition for the absence of superdecoherence is that the spectrum of the reservoir is a bounded function on momentum space. The reason of this absence, is that, as the number of qubits is increased, a quantum register inevitably becomes susceptible to an ever narrower bandwidth of frequencies in the reservoir. Furthermore, we show that for superdecoherence to occur in a reservoir with an unbounded spectrum, containing, for example, delta functions, one of the frequencies at which the spectrum diverges has to coincide exactly with the frequency the quantum register is most susceptible to. We thus fully resolve the conditions that determine the presence or absence of superdecoherence. We conclude that superdecoherence is easily avoidable in practical realizations of quantum computers.

3.1 Introduction

As we inch towards full-scale quantum computing, where we are already facing systems with on the order of a hundred qubits [120, 11, 152], the system size dependence of decoherence becomes of increasing importance. (See Sec. 1.4.7 for an elementary and intuitive introduction to decoherence.) A common simplified theoretical model for decoherence is the spin-boson model, where only the dephasing effects of the bosonic bath are taken into account [138, 115, 124, 26, 90, 147, 41, 17, 10, 1]. Henceforth, we will refer to this model as simply 'the dephasing model'. This model is exactly solvable, and at the same time broadly relevant because dephasing times are typically much shorter than relaxation times [124, 114, 17]. It should be noted, however, that there are situations where it does not accurately describe the decoherence process because of non-perturbative effects [114, 17]. If, in the dephasing model, each qubit is assumed to couple to its own, independent reservoir, the decoherence rate per qubit is constant. If, on the other hand, the qubits couple to single reservoir, the decoherence rate per qubit scales linearly with the number of qubits for certain states [115, 135, 20, 124, 26, 51, 31]. This effect has been referred to as superdecoherence, in analogy with superradiance.

Superdecoherence has been observed experimentally in an ion-trap quantum computer [104]. Although some states suffer superdecoherence, the probability of running into such a state during the course of an actual algorithm may be extremely small [20]. Additionally, if the decoherence is dominated by relaxation, rather than dephasing, is has been shown that superdecoherence does not occur for the Greenberger-Horne-Zeilinger (GHZ) and the Hadamard state [33]. Also the particular model of solid-state qubits coupling to a single phonon reservoir has been shown not to give rise to superdecoherence [68]. The latter approach focuses on a specific setting of the dephasing model: the geometry of the quantum register is assumed to be a linear array, and the phonon reservoir is assumed to be three-dimensional and thermal, with a continuous spectrum and a linear dispersion relation. Therefore, it is unable to reveal the general underlying physical reasons for the absence of superdecoherence. The reason why superdecoherence emerges in other settings of the single-reservoir dephasing model remained unknown.

Here, we fully resolve the physical conditions that determine the presence or absence of superdecoherence in the dephasing model, with all qubits coupling to a single bath. We do not make any assumptions about the geometry of the quantum register, the spatial dimension

d, the reservoir dispersion relation, or the directional dependence of the spin-boson interaction. For the reservoir state, we assume a very general initial condition that applies to practically relevant situations. In determining the conditions that prevent or allow superdecoherence, we find that the boundedness of the *spectral density* and the *occupation density* of the reservoir are essential directives.

The spectral density of the reservoir is the density of modes at a given frequency. If the reservoir admits only a discrete set of frequencies, such as the electromagnetic field in an ideal cavity, the spectral density is given by a sum of delta functions, and is hence unbounded. If, on the other hand, the reservoir admits a continuum of frequencies, such as the electromagnetic field in an imperfect cavity or free space, the reservoir spectral density is a bounded function of frequency.

The occupation density, on the other hand, tells us to what extent a given mode in the reservoir is exited. It is typically a bounded function of the mode frequency. However, if only a single frequency is excited, the occupation density is described by a delta function centred at that frequency. This is the case when the bosonic field is the electromagnetic field, and a mode is excited by a laser with vanishing spectral bandwidth. In contrast, if this laser has a non-zero spectral bandwidth, also the occupation density remains bounded.

We prove that boundedness of the reservoir spectral density and the reservoir occupation density is a sufficient condition for the absence of superdecoherence. Henceforth, we refer to reservoirs with a bounded spectral and occupation density as a *bounded reservoirs* for short (the dimension of the Hilbert space of the reservoir may still be infinite). An important physical quantity in the proof is the *dephasing susceptibility*, which we define as the only part of the decoherence rate that depends on the system. It is closely related to, but different from, the so-called array factor, which arises in classical antenna arrays [14], quantum antenna arrays [93], and interdigital transducers that couple to surface acoustic waves [105]. The dephasing susceptibility captures the extent to which a reservoir frequency contributes to the dephasing process if this frequency is present in the reservoir.

Superdecoherence may be exhibited when either the spectral density or the occupation density is unbounded. Depending on the state of the quantum register, there may be frequencies for which the dephasing susceptibility scales quadratically with the number of qubits. If one of these frequencies coincides with a frequency for which either the reservoir spectral density or the reservoir occupation density diverges, superdecoherence is exhibited. This is because, in this specific case, the decoherence rate scales with the system size in the same way as the

peak of the dephasing susceptibility.

The reason for the absence of superdecoherence in bounded reservoirs is that peaks in the dephasing susceptibility inevitably become narrower as the system size is increased. Specifically, we show that, if the dephasing susceptibility has a peak whose height scales as the square of the number of qubits, the width of this peak must scale inversely with the number of qubits. That is to say, the quantum register may be increasingly susceptible to a given reservoir frequency as the system size grows, but the bandwidth of this susceptibility must at the same time decrease. This effect mitigates the total decoherence rate, and the net effect is that superdecoherence is absent.

A subtle case occurs when the reservoir is in a thermal state. This is because, in that case, the occupation density of the reservoir diverges, but only algebraically. We show that, even though in this case the occupation density diverges, superdecoherence cannot occur. The only exception to this rule occurs when the reservoir is a so-called subohmic reservoir. In that case, the decoherence rate scales with the system size at a rate that is somewhere between regular decoherence (linear scaling) and superdecoherence (quadratic scaling).

In this chapter, we let L denote the number of spins, as opposed to n in other chapters. In the literature on dephasing [115, 135, 20, 124, 26, 51, 31], L is the more common notation.

3.1.1 A classical analogue

The cause of the inverse scaling of the bandwidth of the susceptibility, which is responsible for the absence of superdecoherence in bounded reservoirs, can be sketched with a classical analogue. We leave the treatment of the quantum dephasing susceptibility for Sec. 3.3. Consider L identical, classical, non-interacting electric dipoles in a linear array with spacing a, as depicted in Fig. 3.1 (top). (This geometry is chosen for explanatory reasons. Our results concerning the quantum dephasing susceptibility hold for general register geometries.) In the initial state of the array, all dipoles point upwards. For simplicity, consider only the electromagnetic modes whose momentum is collinear with the array and are polarized in the direction of the dipole moments. The dipoles couple to the electromagnetic field, giving an initial potential energy $V = C_1 \sum_{\ell=1}^{L} E_\ell$, where C_1 is some constant, E_ℓ is the electric field at the ℓth dipole, and k the wave number. In terms of the Fourier transform $E(k) := \sum_{\ell=1}^{L} e^{ikr_\ell} E_\ell$, where $r_\ell = a(\ell - 1)$ is the position of the ℓth qubit, the initial potential energy equals $V = \frac{aC_1}{2\pi} \int_{-\pi/a}^{\pi/a} \mathrm{d}k\, f(k) E(k)$, with $f(k) = \sum_{\ell=1}^{L} e^{-ikr_\ell}$ the coupling

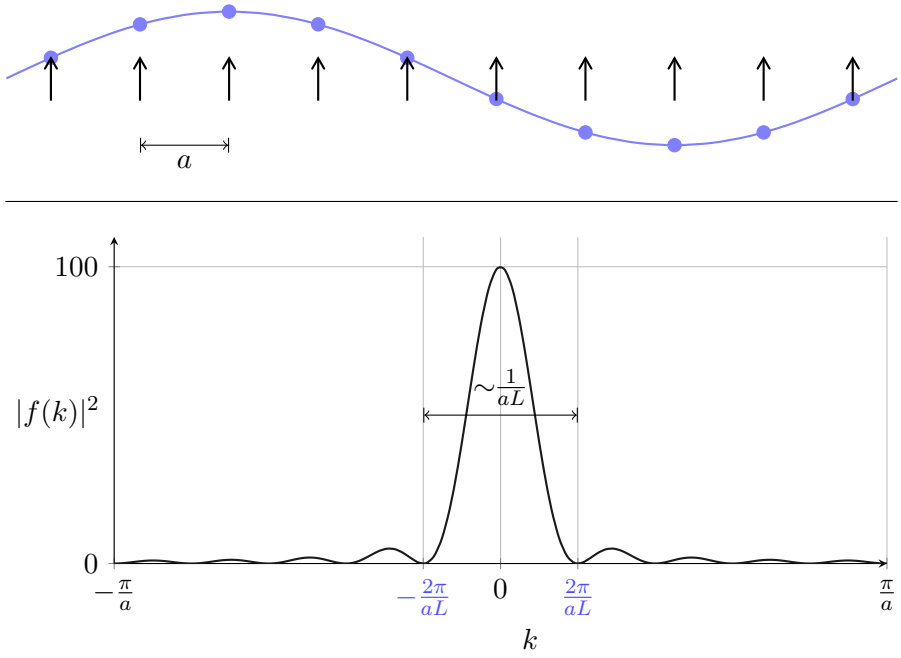

Figure 3.1: (**Top**) A classical analogue, where a linear array of classical dipoles, with lattice spacing a, is placed in the electromagnetic field. As a whole, the array couples strongly to the mode with wave number $k = 0$ (not shown). The array does not couple at all to modes with wave number $k = \pm 2\pi/(aL)$ (shown in blue). This is because, for these modes, all potential energies arising from the dipole-field interaction cancel exactly. (**Bottom**) The modulus squared of the coupling strength in the classical analogue, for $L = 10$, as a function of the wave number k. Two wave numbers of modes that do not couple to the array in displayed in blue. The array mainly couples to modes in a bandwidth less than $\Delta k = 4\pi/(aL)$.

strength between the array and the mode with wave number k. See Fig. 3.1 (bottom) for a plot of $|f(k)|^2$. From the previous expression for $f(k)$, and from the plot, we can see the array couples most strongly to the electromagnetic field mode with wave number $k = 0$. We can also see that the array does not couple at all to modes with wave number $\pm 2\pi/(aL)$. In real space, this is because, for this wave number, all potential energies cancel exactly [also see Fig. 3.1 (top)]. Thus, the bandwidth of modes to which the array couples strongly is at most $\Delta k = 4\pi/(aL)$, which scales inversely with the length of the array.

3.2 Spin-boson dephasing

In this section, we introduce the model of spin-boson dephasing, following references [115, 124, 26]. First, we consider the case of a single qubit coupling to a bosonic reservoir, and extend this to multiple qubits, each of which couples to its own, independent, bosonic reservoir. In both of these cases, superdecoherence cannot occur under any circumstance. Subsequently, this situation is contrasted with the scenario where all qubits couple to a single bosonic reservoir, in which case superdecoherence may in fact occur. Compared to aforementioned references, we make some generalizations concerning the initial reservoir state. The details of this generalization can be found in Sec. 3.A. We use units where $c = \hbar = k_B = 1$.

3.2.1 Single qubit

Consider a single qubit (the system S), with an internal Hamiltonian $H_S = \Delta J^z$, that is placed in a bosonic reservoir (the bath B, also see Sec. 1.4.3 for more background on open quantum systems). Here Δ is the level spacing and J^z the spin-z operator $Z/2$. We work in the computational basis, where this operator is diagonal, and has eigenstates $|1/2\rangle$ and $|-1/2\rangle$. The internal Hamiltonian of the reservoir is given by $H_B = \sum_{\mathbf{k}} \omega_{\mathbf{k}} N_{\mathbf{k}}$, with $N_{\mathbf{k}} = a^\dagger_{\mathbf{k}} a_{\mathbf{k}}$ the number operator of a bosonic mode with wave vector $\mathbf{k}$. Here $a_{\mathbf{k}}$ ($a^\dagger_{\mathbf{k}}$) is the bosonic annihilation (creation) operator of the mode with wave vector $\mathbf{k}$. The sum is over all $\mathbf{k}$ that are admitted by the reservoir. The set of $\mathbf{k}$s that are admitted by the reservoir depends on the physical details of the reservoir. The reservoir couples to the qubit via the interaction term $H_{SB} = \sum_{\mathbf{k}} J^z (g^*_{\mathbf{k}} a_{\mathbf{k}} + g_{\mathbf{k}} a^\dagger_{\mathbf{k}})$, with $g_{\mathbf{k}}$ the coupling strength between the qubit and the mode with wave vector $\mathbf{k}$. There are many explicit physical settings that may lead to this interaction term [37], but here, we

do not assume such a specific setting. Since the only system operator in the interaction term is J^z, H_{SB} causes dephasing only. Putting all terms together, the dephasing model of a single qubit reads

$$H_1 := \Delta J^z + \sum_{\mathbf{k}} \omega_{\mathbf{k}} N_{\mathbf{k}} + \sum_{\mathbf{k}} J^z (g_{\mathbf{k}}^* a_{\mathbf{k}} + g_{\mathbf{k}} a_{\mathbf{k}}^\dagger).$$

In this and the following sections, we assume that the overall system-reservoir state is a product state, $\rho(0) \otimes \rho_B(0)$. Here $\rho(0)$ (no subscript) is a general initial system state, and $\rho_B(0)$ is the initial reservoir state. The latter is assumed to be a product state of single-mode states, $\rho_B(0) = \bigotimes_{\mathbf{k}} \rho_{B,\mathbf{k}}(0)$, with $\rho_{B,\mathbf{k}}(0)$ the initial state of the mode with wave vector $\mathbf{k}$. The state $\rho_{B,\mathbf{k}}(0)$ is assumed to be a displaced thermal state, that is, $\rho_{B,\mathbf{k}}(0) = D(\alpha_{\mathbf{k}}) e^{-\omega_{\mathbf{k}} N_{\mathbf{k}}/T_{\mathbf{k}}} D^\dagger(\alpha_{\mathbf{k}})/\mathcal{Z}$, where $\alpha_{\mathbf{k}}$ is the displacement (which can be any complex number), $N_{\mathbf{k}}$ the number operator, $T_{\mathbf{k}}$ the ($\mathbf{k}$-dependent) temperature, $\mathcal{Z}$ the normalization, and D the displacement operator. (In Sec. 3.A we show displacement is irrelevant in the dephasing process, so we do not give an expression for D here.) Possible $\rho_{B,\mathbf{k}}(0)$ admitted by this parametrization include the regular single-mode thermal states ($T_{\mathbf{k}} \geq 0$ and $\alpha_{\mathbf{k}} = 0$), the coherent states ($T_{\mathbf{k}} = 0$, $|\alpha_{\mathbf{k}}| \geq 0$), and the vacuum state ($T_{\mathbf{k}} = 0$, $\alpha_{\mathbf{k}} = 0$). We call a reservoir *completely thermal* if the overall initial reservoir state $\rho_B(0)$ equals the regular thermal density matrix with temperature T, that is, if $\rho_B(0) = e^{-\omega_{\mathbf{k}} N_{\mathbf{k}}/T}/\mathcal{Z}'$. In our parametrization of initial reservoir states, this is the specific case where $\alpha_{\mathbf{k}} = 0$ and $T_{\mathbf{k}} = T$ for all $\mathbf{k}$. Our form of the initial reservoir state is a generalization of that used in references [138, 115, 124, 26, 41, 1, 20], where the assumption is that the initial reservoir state is completely thermal.

It can be shown that the absolute value of the i,jth entry (with $i,j \in \{-1/2, 1/2\}$) of the system density matrix, after time t, is given by

$$|\rho_{ij}(t)| = e^{-\Gamma_{i-j}(t)} |\rho_{ij}(0)|, \tag{3.1}$$

where $\Gamma_{i-j}(t)$ is the *decoherence function* (See Refs. [115, 124, 26],[1] and Sec. 3.A). In the current model, dephasing is the only decoherence mechanism. Therefore the *decoherence rate* can be defined as $1/T_2$, were T_2 is the dephasing time, here defined as the smallest time t for which $\Gamma_{i-j}(t) = 1$.

[1] These references give a derivation for the density operator in the interaction picture, $|\rho_{ij}^I(t)| = e^{-\Gamma_{i-j}} |\rho_{ij}^I(0)|$. In the dephasing model, $|\rho_{ij}^S(t)| = |\rho_{ij}^I(t)|$. Therefore, we drop the superscript indicating the picture in Eq. (3.1), keeping in mind that the equation holds in both pictures. The same applies to the system density operators in Sec. 3.2.2 and 3.2.3. See Sec. 1.4.5.3 and Sec. 1.4.6.1 for more background on the interaction picture in open quantum systems.

In general, the decoherence function only depends on the difference $\mathrm{d} = i - j$.[2] It is given by

$$\Gamma_{\mathrm{d}}(t) = \gamma_{\mathrm{d}} \sum_{\mathbf{k}} |g_{\mathbf{k}}|^2 \tau(t, \omega_{\mathbf{k}})(1 + 2\bar{N}_{\mathbf{k}}). \tag{3.2}$$

Here $\gamma_{\mathrm{d}} = |\mathrm{d}|$ and

$$\tau(t, \omega_{\mathbf{k}}) = \frac{1 - \cos(\omega_{\mathbf{k}} t)}{\omega_{\mathbf{k}}^2}. \tag{3.3}$$

Under the current assumptions on the initial reservoir state, the occupation number $\bar{N}_{\mathbf{k}}$ of the mode $\mathbf{k}$ is given by the Bose-Einstein distribution with ($\mathbf{k}$-dependent) temperature $T_{\mathbf{k}}$.[3] That is,

$$\bar{N}_{\mathbf{k}} = \frac{1}{e^{\omega_{\mathbf{k}}/T_{\mathbf{k}}} - 1}. \tag{3.4}$$

This need not be an isotropic function on k-space. For the specific case of the completely thermal reservoir (i.e. $T_{\mathbf{k}} = T$ and $\alpha_{\mathbf{k}} = 0$ for all $\mathbf{k}$), the occupation number is in fact isotropic, and depends on the mode energy only,

$$\bar{N}_{\omega}^{th} := \frac{1}{e^{\omega/T} - 1}. \tag{3.5}$$

We do not assume any particular dispersion relation, nor the reservoir to be completely thermal, unless stated otherwise.

3.2.2 Independent reservoirs

Now consider L copies of the system-reservoir combination described in the previous subsection. This setting is known as independent dephasing. The overall Hamiltonian reads $H_L^{\mathrm{ind}} = (H_1)^{\otimes L}$. This is depicted schematically in Fig. 3.2 (left).

We denote states in the computational basis of the L-qubit quantum register by $|\mathbf{i}\rangle \equiv |i_1, \ldots, i_L\rangle$. It can be shown that, under the evolution by H_L^{ind}, the absolute value of the $(\mathbf{i}, \mathbf{j})$th entry of the system density matrix equals $|\rho_{\mathbf{ij}}(t)| = e^{-\Gamma_{\mathbf{d}}(t)} |\rho_{\mathbf{ij}}(0)|$, with $\mathbf{d}$ the difference vector $\mathbf{d} = \mathbf{i} - \mathbf{j}$ and

$$\Gamma_{\mathbf{d}}(t) = \gamma_{\mathbf{d}} \sum_{\mathbf{k}} |g_{\mathbf{k}}|^2 \tau(t, \omega_{\mathbf{k}})(1 + 2\bar{N}_{\mathbf{k}})$$

[2] We use the italic d for dimension, and the straight d for the differences $\mathrm{d} = i - j$ and (for multiple qubits) $\mathbf{d} = \mathbf{i} - \mathbf{j}$.

[3] The initial state of the reservoir may still be a general thermal *displaced* state. Displacement of a mode does affect the expectation value of its number operator, but only the thermal part contributes to $\Gamma_{\mathbf{d}}(t)$. See Sec. 3.A for details.

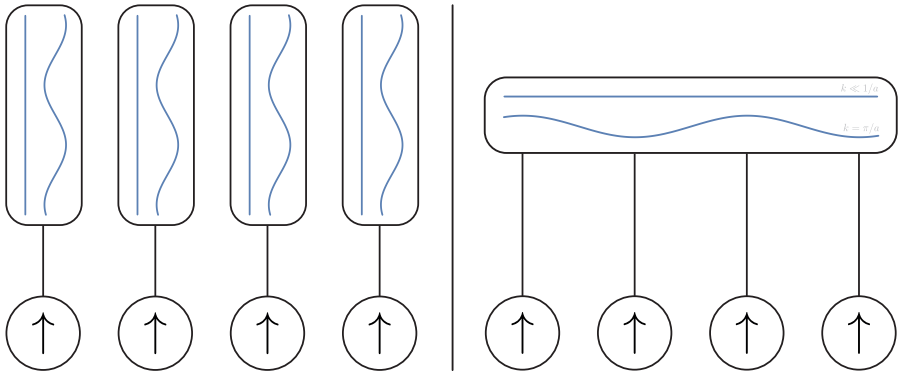

Figure 3.2: **(Left)** Qubits coupling to independent reservoirs. **(Right)** Qubits coupling to a single reservoir

the decoherence function. Here, we have singled out the factor $\gamma_{\mathbf{d}} = \sum_{\ell=1}^{L} |\mathbf{d}_\ell|$ for later reference. This factor is the only part of the decoherence function that depends on L, and it is at most proportional to L. Thus, for independent dephasing, the decoherence function scales at worst linearly with the system size,

$$\Gamma_{\mathbf{d}} \propto L.$$

That is, the decoherence rate per qubit is at most constant in the system size.

3.2.3 A single reservoir

Now consider the situation where all qubits couple to a single reservoir,

$$H = \Delta \sum_{\ell=1}^{L} J_\ell^z + \sum_{\mathbf{k}} \omega_{\mathbf{k}} N_{\mathbf{k}} + \sum_{\ell=1}^{L} \sum_{\mathbf{k}} J_\ell^z (g_{\mathbf{k}\ell}^* a_{\mathbf{k}} + g_{\mathbf{k}\ell} a_{\mathbf{k}}^\dagger), \tag{3.6}$$

as is depicted schematically in Fig. 3.2 (right). Again, $\mathbf{k}$ runs over all wave vectors that are supported by the reservoir. Now, the coupling constant $g_{\mathbf{k}\ell}$ depends on both the wave vector and the qubit location. If the reservoir consist of plane-wave modes, $g_{\mathbf{k}\ell} = g_{\mathbf{k}} e^{i\mathbf{k}\cdot\mathbf{r}_\ell}$. For single-reservoir dephasing, it can be shown that (Refs. [115, 124, 26], Sec. 3.A) the density matrix equals

$$|\rho_{\mathbf{ij}}(t)| = e^{-\Gamma_{\mathbf{i}-\mathbf{j}}(t)} |\rho_{\mathbf{ij}}(0)|,$$

as before, but now

$$\Gamma_{\mathbf{d}}(t) = \sum_{\mathbf{k}} \gamma_{\mathbf{d}}(\mathbf{k}) |g_{\mathbf{k}}|^2 \tau(t, \omega_{\mathbf{k}}) (1 + 2\bar{N}_{\mathbf{k}}), \tag{3.7}$$

with

$$\gamma_{\mathbf{d}}(\mathbf{k}) = \sum_{\ell m} \mathbf{d}_\ell \mathbf{d}_m \cos(\mathbf{k}\cdot\mathbf{r}_{\ell m}), \tag{3.8}$$

where $\mathbf{r}_{\ell m} \coloneqq \mathbf{r}_\ell - \mathbf{r}_m$ is the vector pointing from the location of qubit ℓ to that of qubit m. In contrast to the situation of independent dephasing, $\gamma_{\mathbf{d}}(\mathbf{k})$ now depends on $\mathbf{k}$ and contains a double sum over the qubit indices. The summand of $\gamma_{\mathbf{d}}(\mathbf{k})$ can at most equal unity, which is attained, for example, if $\mathbf{d}_\ell = 1$ for all ℓ, and $\mathbf{k} = \mathbf{0}$. Thus, if indeed $\mathbf{k} = \mathbf{0}$ is admitted by the reservoir,

$$\Gamma_{\mathbf{d}} \propto L^2$$

at worst. The possibility of quadratic, rather than linear scaling of the decoherence function with L is called *superdecoherence*. The decoherence rate per qubit can thus scale with the system size, which is problematic for error correction [59, 119].

3.2.4 The continuum limit

We may write Eq. (3.7) in a more meaningful form, starting by introducing $\mathcal{D} = \sum_{\mathbf{k}'} \delta(\mathbf{k}-\mathbf{k}')$, so that we may replace the sum by an integral,

$$\sum_{\mathbf{k}} \ldots \to \int_{\mathbb{R}^d} \mathrm{d}\mathbf{k}\, \mathcal{D}(\mathbf{k}) \ldots,$$

where d is the dimension of the reservoir. Here $\mathcal{D}(\mathbf{k})$ is a density of states on k-space, currently describing a discrete set of modes. Note that $\mathcal{D}$ is unbounded at those modes, and vanishes elsewhere. In the continuum limit, the peaks merge into a bounded and continuous density of states on k-space. We then have

$$\Gamma_{\mathbf{d}}(t) = \int_{\mathbb{R}^d} \mathrm{d}\mathbf{k}\, \mathcal{D}(\mathbf{k}) |g_{\mathbf{k}}|^2\, \gamma_{\mathbf{d}}(\mathbf{k})\, \tau(t,\omega_{\mathbf{k}})\, (1+2\bar{N}_{\mathbf{k}}), \tag{3.9}$$

where $\mathcal{D}$ is unbounded for discrete reservoirs, and bounded in the continuum limit. In the continuum limit, $\bar{N}_{\mathbf{k}}$ becomes an occupation density rather than an occupation number. Note $\mathcal{D}(\mathbf{k})$ is different from the usual density of states, because the latter is a function of frequency only. For the electromagnetic field in free space, without boundary conditions, $\mathcal{D}$ is proportional to a constant with length dimension d. Equation (3.9) is the most general form of the decoherence function in the dephasing model because it can describe both discrete and continuous reservoirs. We will work with this form from now on.

One feature of Eq. (3.9) (and the preceding, less general forms) is that we can easily separate the vacuum contributions from those that are due to reservoir excitations. That is, we may write

$$\Gamma_{\mathbf{d}}(t) =: \Gamma_{\mathbf{d}}^{(vac)}(t) + \Gamma_{\mathbf{d}}^{(ex)}(t), \tag{3.10}$$

with

$$\Gamma_{\mathbf{d}}^{(vac/ex)}(t) := \int_{\mathbb{R}^d} \mathrm{d}\mathbf{k}\, \gamma_{\mathbf{d}}(\mathbf{k}) \xi^{(vac/ex)}(t, \mathbf{k}), \tag{3.11}$$

where

$$\xi^{(vac)}(t, \mathbf{k}) := \mathcal{D}(\mathbf{k}) |g_{\mathbf{k}}|^2 \tau(t, \omega_{\mathbf{k}}), \tag{3.12}$$

$$\xi^{(ex)}(t, \mathbf{k}) := \mathcal{D}(\mathbf{k}) |g_{\mathbf{k}}|^2 \tau(t, \omega_{\mathbf{k}})\, 2\bar{N}_{\mathbf{k}}. \tag{3.13}$$

For the dephasing susceptibility to be well-defined, the integral in Eq. (3.9) has to converge. This is guaranteed by a high frequency cutoff. Physically, this arises because, as a function of $\omega_{\mathbf{k}}$, either $\mathcal{D}$ goes to zero, or the coupling strength $g_{\mathbf{k}}$ goes to zero, or a combination of both. Here, we assume that after some cutoff frequency ω_c, the product $\mathcal{D}(\mathbf{k})|g_{\mathbf{k}}|^2$ is suppressed at least exponentially,

$$\mathcal{D}(\mathbf{k}) |g_{\mathbf{k}}|^2 = O(e^{-\omega_{\mathbf{k}}/\omega_c}) \tag{3.14}$$

as $e^{-\omega_{\mathbf{k}}/\omega_c}$ goes to zero. At this point, this cutoff does not impose any restriction on the physical systems described because ω_c can be arbitrarily large.

Even in continuous reservoirs, it is possible in theory that a single mode $\mathbf{k}'$ is excited, but no modes in its neighbourhood (in k-space). Then, the occupation density is unbounded at that mode, $\bar{N}_{\mathbf{k}} \propto \delta(\mathbf{k} - \mathbf{k}')$. We call a reservoir *continuous* if, in contrast, both $\mathcal{D}(\mathbf{k})|g_{\mathbf{k}}|^2$ and $\bar{N}_{\mathbf{k}}$ are bounded functions of $\mathbf{k}$.

A common assumption [115, 124, 26], that we will only make occasionally, is that $\mathcal{D}(\mathbf{k})|g_{\mathbf{k}}|^2$ and $\bar{N}_{\mathbf{k}}$ are isotropic, and that the reservoir dispersion relation is linear. For a linear dispersion relation, $\omega_{\mathbf{k}} = v|\mathbf{k}|$ for some constant v. Working in units where $v = 1$ for notational convenience, we may then transform to spherical coordinates and write

$$\Gamma_{\mathbf{d}}(t) = \int_0^\infty \mathrm{d}\omega\, J(\omega) \tilde{\gamma}_{\mathbf{d}}(\omega) \tau(t, \omega)(1 + 2\bar{N}_\omega), \tag{3.15}$$

with

$$\tilde{\gamma}_{\mathbf{d}}(\omega) := \int \mathrm{d}\Omega\, \gamma_{\mathbf{d}}(\omega, \theta).$$

Here, Ω is the $d-1$ dimensional solid angle, and θ the $d-1$ dimensional angle of $\mathbf{k}$. The function $J(\omega) = \omega^{d-1}\mathcal{D}(\omega)|g_\omega|^2$ is called the *spectral density* of the reservoir. A common form is [138, 115, 124, 26, 90, 18, 27, 141, 7, 82, 1]

$$J(\omega) = \alpha_d \omega^d e^{-\omega/\omega_c}, \tag{3.16}$$

with α_d a constant with length dimension $d-1$, and ω_c the cutoff frequency. This expression is often extended to include even non-integer d, which may be encountered in reservoirs with fractal properties [90]. Depending on the dimension, these reservoirs are called subohmic ($d < 1$), Ohmic ($d = 1$), or superohmic ($d > 1$). In this chapter, we do not assume isotropy, unless stated otherwise, and we will mainly work with the general form of the decoherence function [Eq. (3.9)].

In the following sections, we study the qualitative system-size scaling of the decoherence function. For completeness, however, in Sec. 3.C we show explicit solutions for $\Gamma_L^{(vac)}$, and derive simplified approximate solutions in the regimes $t \ll 1$ and $t \to \infty$.

3.3 Dephasing susceptibility

In this section, we identify $\gamma_{\mathbf{d}}(\mathbf{k})$ as an important physical quantity and derive some of its properties, especially regarding its system size dependence. Namely, $\gamma_{\mathbf{d}}(\mathbf{k})$ is determined solely by the system, and at the same time it is the only part of the decoherence function that depends on the system. So it fully captures the influence of the system on the decoherence function. The function $\gamma_{\mathbf{d}}(\mathbf{k})$ weighs the severity of the influence of the mode $\mathbf{k}$ if this mode was to be 'offered' by the reservoir, and depends on the system geometry and the index $(\mathbf{i}, \mathbf{j})$. We call it the *dephasing susceptibility* of the reservoir.

To illustrate the qualitative behaviour of the dephasing susceptibility, we first consider the *array model*, the classical analogue of which was treated in Sec. 3.1.1. It consists of a linear array of L non-interacting qubits with spacing a that couple to a single reservoir with dimension $d = 1$. Two system states we consider are

$$\begin{aligned} |\mathrm{GHZ}\rangle &= \tfrac{1}{\sqrt{2}} \left|\tfrac{1}{2}, \tfrac{1}{2}\right\rangle^{\otimes L/2} + \tfrac{1}{\sqrt{2}} \left|-\tfrac{1}{2}, -\tfrac{1}{2}\right\rangle^{\otimes L/2}, \\ |\mathrm{GHZ}'\rangle &= \tfrac{1}{\sqrt{2}} \left|\tfrac{1}{2}, -\tfrac{1}{2}\right\rangle^{\otimes L/2} + \tfrac{1}{\sqrt{2}} \left|-\tfrac{1}{2}, \tfrac{1}{2}\right\rangle^{\otimes L/2}. \end{aligned} \tag{3.17}$$

Both states are of the form $(|\mathbf{i}\rangle + |\mathbf{j}\rangle)/\sqrt{2}$, and thus have only a single non-zero matrix element in the upper right triangle of their density

matrix. That is, in the computational basis,

$$\rho_{\mathrm{GHZ}} = \frac{1}{2}\begin{pmatrix} 1 & 0 & \dots & 0 & 1 \\ 0 & 0 & \dots & 0 & 0 \\ \vdots & \vdots & \ddots & \vdots & \vdots \\ 0 & 0 & \dots & 0 & 0 \\ 1 & 0 & \dots & 0 & 1 \end{pmatrix}, \tag{3.18}$$

and similarly for the density matrix associated with $\left|\mathrm{GHZ}'\right\rangle$.

The difference vectors $\mathbf{d} = \mathbf{i} - \mathbf{j}$ belonging to these off-diagonal matrix elements are

$$\mathbf{d}_{\mathrm{GHZ}} = (1, 1, 1, 1, \dots), \tag{3.19}$$

$$\mathbf{d}_{\mathrm{GHZ}'} = (1, -1, 1, -1, \dots). \tag{3.20}$$

Thus, with Eq. (3.8), we find[4]

$$\gamma_{\mathrm{GHZ}}(k) = \frac{\sin^2(akL/2)}{\sin^2(ak/2)}, \tag{3.21}$$

$$\gamma_{\mathrm{GHZ}'}(k) = \frac{\sin^2(akL/2)}{\cos^2(ak/2)}, \tag{3.22}$$

for L even. Here, we write γ_{GHZ} instead of $\gamma_{\mathbf{d}_{\mathrm{GHZ}}}$ for conciseness, and similarly for $\gamma_{\mathrm{GHZ}'}$. Plots of $\gamma_{\mathrm{GHZ}'}(k)$ for various L can be found in Fig. 3.3.

Note there are values of k for which $\gamma_{\mathrm{GHZ}'}(k) = 0$. This occurs when $\sin^2(akL/2) = 0$ but $\cos^2(ak/2) \neq 0$. That is, when $ak = \pi + n\,2\pi/L$ for integer values of n, excluding n that are multiples of $L/2$. (I.e. $n \in \mathbb{Z}\backslash\{m \in \mathbb{Z} \,|\, m = \ell L/2 \wedge \ell \in \mathbb{Z}\}$.) If the reservoir only supports these modes, the off-diagonal matrix element of $\left|\mathrm{GHZ}'\right\rangle$ does not diminish as a function of time at all. In this situation the two basis states that compose $\left|\mathrm{GHZ}'\right\rangle$ [Eq. (3.17)] are in the same decoherence-free subspace [115, 40, 41, 151, 147, 95, 97, 83].

The dephasing susceptibility $\gamma_{\mathrm{GHZ}'}$ is dominated by the peak at $ak = \pi$, whose height is L^2. Depending on the reservoir, this may result in superdecoherence. From Eq. (3.7), we see that if the reservoir is discrete and supports the mode $ak = \pi$, the decoherence function scales as L^2, even in the vacuum. We stress that, as shown by this simple example, superdecoherence is possible even when the coupling constants

[4] These closed form formulas are ill-defined when the denominator vanishes. The original form [Eq. (3.8)] does not have this anomaly. It is to be understood that at these points, the closed form formulas are determined by their limit values. Then the resulting functions are smooth.

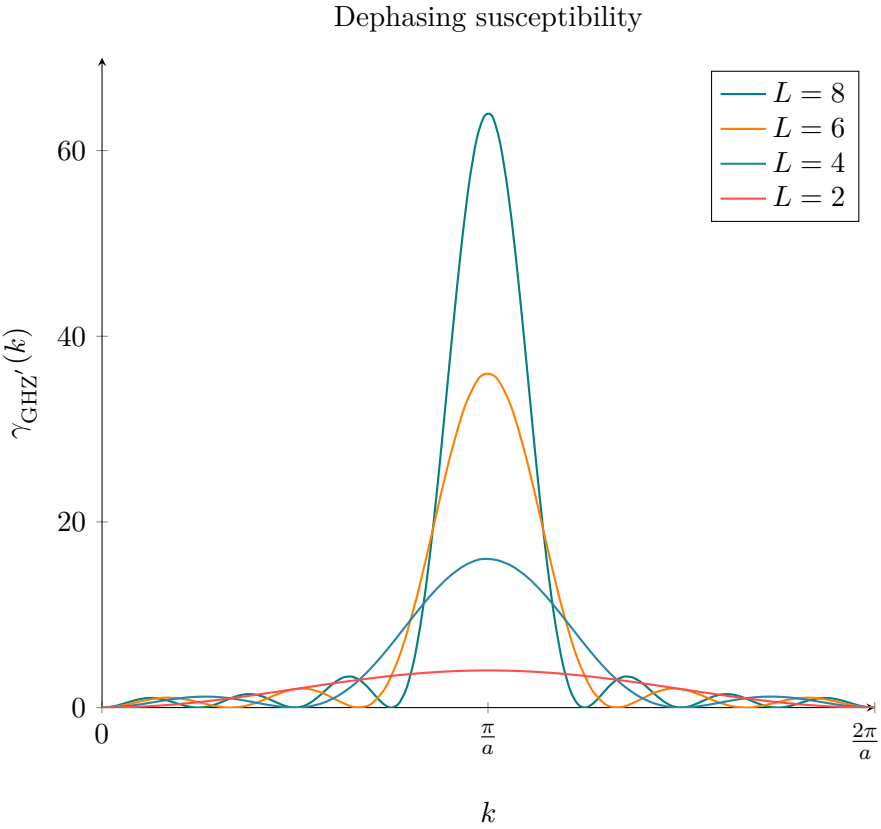

Figure 3.3: The dephasing susceptibility of the off-diagonal matrix element of $|\mathrm{GHZ}'\rangle$, for system sizes $L = 2, 4, 6, 8$. The peaks have height L^2 and width $\sim 1/(aL)$. For the off-diagonal matrix element of the state $|\mathrm{GHZ}\rangle$, the entire graph is translated in such a way that the peaks lie above $k = 0$.

$g_{\mathbf{k}\ell}$ depend on the the qubit location. Hence permutation symmetry of the Hamiltonian is not a prerequisite for superdecoherence.

Consider the two points around the peak where $\gamma_{\mathrm{GHZ}'} = 0$. The previous equations about the minima show that the distance between these points equals $\Delta k = 4\pi/(aL)$. Thus, the bandwidth of modes the off-diagonal matrix element of $|\mathrm{GHZ}'\rangle$ is most susceptible to scales inversely with the system size.

This decreasing bandwidth is shown by the dephasing susceptibility in general. This is because, mathematically, $\gamma_{\mathbf{d}}(\mathbf{k})$ is the spectral density of the difference vector $\mathbf{d}$. That is,

$$\begin{aligned}\gamma_{\mathbf{d}}(\mathbf{k}) &= \sum_{\ell m} \mathbf{d}_\ell \mathbf{d}_m \{\cos(\mathbf{k}\cdot\mathbf{r}_{\ell m}) + i\sin(\mathbf{k}\cdot\mathbf{r}_{\ell m})\} \\ &= \sum_{\ell m} \mathbf{d}_\ell \mathbf{d}_m e^{i\mathbf{k}\cdot\mathbf{r}_{\ell m}} \\ &= |\tilde{\mathrm{d}}(\mathbf{k})|^2, \end{aligned} \tag{3.23}$$

with $\tilde{\mathrm{d}}(\mathbf{k}) := \sum_{\ell=1}^{L} e^{-i\mathbf{k}\cdot\mathbf{r}_\ell}\mathbf{d}_\ell$ the Fourier transform of $\mathbf{d}$. Here the sine vanishes because it is antisymmetric under exchange of ℓ and m. If the qubits are placed on a lattice, the dephasing susceptibility is periodic in $\mathbf{k}$.

The summand in the original definition of $\gamma_{\mathbf{d}}(\mathbf{k})$ [Eq. (3.8)] is at most unity. This is achieved, for example, when $\mathbf{d}_n = 1$ for all $n \in \{1, \ldots, L\}$ and $\mathbf{k} = 0$. Thus,

$$0 \leq \gamma_{\mathbf{d}}(\mathbf{k}) \leq L^2. \tag{3.24}$$

Nevertheless, the integral of the dephasing susceptibility over one reciprocal unit cell $\mathcal{C}$ is bounded by $2\pi L/V$, where V is the volume one real-space unit cell. This follows directly from the fact that the dephasing susceptibility is the spectral density function of $\mathbf{d}$, and Parseval's theorem,

$$\begin{aligned}\int_{\mathcal{C}} \mathrm{d}\mathbf{k}\, \gamma_L(\mathbf{k}) &= \int_{\mathcal{C}} \mathrm{d}\mathbf{k}\, |\tilde{\mathrm{d}}(\mathbf{k})|^2 \\ &= \frac{2\pi}{V} \sum_{m=1}^{L} |\mathbf{d}_m|^2,\end{aligned}$$

with $|\mathbf{d}_m| = |\mathbf{i}_m - \mathbf{j}_m| \leq 1$. Therefore

$$\int_{\mathcal{C}} \mathrm{d}\mathbf{k}\, \gamma_L(\mathbf{k}) \leq \frac{2\pi L}{V}. \tag{3.25}$$

This shows that if the dephasing susceptibility has a peak of height L^2, the width of that peak must scale as $1/L$. As we show in the following section, this relation causes a mitigation of the dephasing process, causing the absence of superdecoherence in bounded reservoirs.

A related question about the dephasing susceptibility is how large $\gamma_{\mathbf{i}-\mathbf{j}}(\mathbf{k})$ is typically if we fix $\mathbf{k}$ and L and vary $(\mathbf{i},\mathbf{j})$. In Sec. 3.B, we show that the distribution of $\gamma_{\mathbf{i}-\mathbf{j}}(\mathbf{k})$ over $(\mathbf{i},\mathbf{j})$ is approximated by a Gaussian, with a standard deviation that is at most $L/(2\pi)$. This means $\gamma_{\mathbf{i}-\mathbf{j}}(\mathbf{k})$ is typically on the order of L and that there are few $\mathbf{i}-\mathbf{j}$ such that $\gamma_{\mathbf{i}-\mathbf{j}}(\mathbf{k}) \approx L^2$.

3.4 Asymptotic system size scaling

In this section, we derive our main results, which are upper bounds on the system size scaling of the decoherence function. An important quantity herein is the dephasing susceptibility, because this is the only factor in the integrand of the decoherence function that depends on the system size. In turn, the dephasing susceptibility depends on L because L is the length of the vector $\mathbf{d}$. The exact scaling of $\Gamma_{\mathbf{d}}$ with L depends on how entries are added to $\mathbf{d}$ as the L is increased. In principle, this can be done according to any prescription.

For example, we could consider the dephasing associated with $\mathbf{d}$, where $\mathbf{d}$ increases in length by adding a random number for every qubit we add. A more physically relevant situation, is for example to consider the coherence of the state $|\mathrm{GHZ}\rangle$ or $|\mathrm{GHZ}'\rangle$, as a function of the system size. The results in this section hold for any description, unless stated otherwise, but some descriptions may arise more naturally than others.

To tidy up notation, and to highlight L dependence, we will now write $\gamma_L(\mathbf{k})$ instead of $\gamma_{\mathbf{d}}(\mathbf{k})$ and likewise $\Gamma_L(t)$ instead of $\Gamma_{\mathbf{d}}(t)$. At the same time, we use $\gamma_{\mathrm{GHZ}}(\omega)$ and $\gamma_{\mathrm{GHZ}'}(\omega)$ for the dephasing susceptibilities of the off-diagonal matrix elements of $|\mathrm{GHZ}\rangle$ and $|\mathrm{GHZ}'\rangle$, respectively. Likewise, we write Γ_{GHZ} and $\Gamma_{\mathrm{GHZ}'}$.

The starting point of our derivation is the most general form of the decoherence function, in which the vacuum contributions are separated from the excitation contributions [Eq. (3.10)]. Both contributions are of the form of Eq. (3.11). Assume $t = t_0$ is fixed. The mathematical property that the integral of γ_L over one reciprocal unit cell scales linearly with the number of qubits [Eq. (3.25)] ensures that also $\Gamma_L^{(vac/ex)}$ scales linearly with the number of qubits, provided that $\xi^{(vac/ex)}$ is bounded.

This is shown as follows. Assume $\xi^{(vac/ex)}(t_0,\mathbf{k})$ is bounded. The

integral $\Gamma_L^{(vac/ex)}$ equals a sum of integrals, where each domain of integration is one reciprocal unit cell $\mathcal{C}$,

$$\Gamma_L^{(vac/ex)}(t_0) = \sum_{\mathcal{C}} \int_{\mathcal{C}} \mathrm{d}\mathbf{k}\, \gamma_L(\mathbf{k}) \xi^{(vac/ex)}(t_0, \mathbf{k}).$$

Each term is upper bounded by the integral of $\gamma_L(\mathbf{k})$ over a single reciprocal unit cell after the integral is rescaled by the maximum of $\xi^{(vac/ex)}(t_0, \mathbf{k})$ on that unit cell,

$$\Gamma_L^{(vac/ex)}(t_0) \leq \sum_{\mathcal{C}} \max_{\mathbf{k}\in\mathcal{C}} \left[\xi^{(vac/ex)}(t_0, \mathbf{k})\right] \int_{\mathcal{C}} \mathrm{d}\mathbf{k}\, \gamma_L(\mathbf{k}).$$

By Eq. (3.25),

$$\Gamma_L^{(vac/ex)}(t_0) \leq \frac{2\pi L}{V} \sum_{\mathcal{C}} \max_{\mathbf{k}\in\mathcal{C}} \left[\xi^{(vac/ex)}(t_0, \mathbf{k})\right].$$

The high-frequency cutoff [Eq. (3.14)] ensures the sum converges, no matter the value of the cutoff ω_c. Thus, we obtain the main mathematical result of this chapter: if $\xi^{(vac/ex)}(t_0, \mathbf{k})$ is bounded, then

$$\Gamma_L^{(vac/ex)} = O(L). \tag{3.26}$$

The relevant physical question then, is when $\xi^{(vac/ex)}(t_0, \mathbf{k})$ is bounded. First, consider the vacuum contribution $\xi^{(vac)}(t_0, \mathbf{k}) = \mathcal{D}(\mathbf{k})|g_\mathbf{k}|^2 \tau(t_0, \omega_\mathbf{k})$ [Eq. (3.12)]. The temporal factor $\tau(t_0, \omega_\mathbf{k})$ is a bounded function of $\omega_\mathbf{k}$ for every t_0. The remaining factor $\mathcal{D}(\mathbf{k})|g_\mathbf{k}|^2$ is bounded for bounded reservoirs (see Sec. 3.2). Therefore, in bounded reservoirs,

$$\Gamma_L^{(vac)} = O(L). \tag{3.27}$$

This says that in bounded reservoirs, vacuum fluctuations cannot cause superdecoherence.

Now consider the excitation contribution $\xi^{(ex)}(t_0, \mathbf{k}) = \mathcal{D}(\mathbf{k})|g_\mathbf{k}|^2 \tau(t_0, \omega_\mathbf{k})\, 2\bar{N}_\mathbf{k}$ [Eq. (3.13)]. It is bounded if both $\mathcal{D}(\mathbf{k})|g_\mathbf{k}|^2$ and $\bar{N}_\mathbf{k}$ are bounded. By Eq. (3.26) we have, in that case,

$$\Gamma_L^{(ex)} = O(L).$$

Together with Eq. (3.27), this says there is no superdecoherence in bounded reservoirs.

Conversely, we can consider the situations in which $\xi^{(vac/ex)}$ is unbounded. First, consider $\xi^{(vac)}$. It is unbounded if the reservoir is

discrete, that is, if $\mathcal{D}(\mathbf{k}) = \sum_{\mathbf{k}' \in D} \delta(\mathbf{k} - \mathbf{k}')$. Even though, in this case, the conditions of Eq. (3.26) are not satisfied, this does not lead to superdecoherence per se. It is clear that $\Gamma_L^{(vac)}$ scales superlinearly with L only if one of the modes in D coincides exactly with a mode to which the matrix element is superlinearly susceptible. This is also illustrated by Fig. 3.3 and Eq. (3.7): there is superdecoherence in the array model when the state is $\left|\mathrm{GHZ}'\right\rangle$, and $\pi/a \in D$. If, in the array model, $\pi/a \notin D$, but instead $\pi/a + \delta \in D$, with $0 < |\delta| \ll 1$, there is no superdecoherence. Note this in an asymptotic statement, and that, in the latter situation ($\pi/a \notin D$, $\pi/a + \delta \in D$), and for finite L, linear scaling of Γ_L with L only occurs after $1/L$ is approximately smaller than $|\delta|$. Further discussion on finite-size effects can be found in Sec. 3.5.

Secondly, consider $\xi^{(ex)}$. It is unbounded if the reservoir is discrete, like in the previous paragraph. It may additionally be unbounded if $\bar{N}_{\mathbf{k}}$ is unbounded. This happens when a mode $\mathbf{k}$ is excited but no modes in its neighbourhood are excited. Again, this does not need to lead to superdecoherence per se. It is only when $\mathbf{k}$ coincides exactly with a mode the matrix element is highly susceptible to that superlinear scaling of $\Gamma_{\mathbf{i}-\mathbf{j}}^{(ex)}$ is possible.

3.4.1 Completely thermal reservoirs

If the reservoir has a continuous spectrum, and the initial reservoir state is completely thermal, $\xi^{(ex)}(t_0, \mathbf{k})$ [Eq. (3.13)] is possibly unbounded because $\bar{N}_\omega^{th}$ [Eq. (3.5)] has an algebraic divergence at the origin. In this subsection, we show this nevertheless does not lead to superdecoherence (i.e. it does not lead to quadratic scaling of the decoherence function with the system size). However, superlinear scaling may be obtained, but only in subohmic reservoirs at non-zero temperature.

The at most linear scaling of the decoherence function for Ohmic ($d = 1$) and superohmic ($d > 1$) continuous thermal reservoirs is shown as follows. Consider $\xi^{(ex)}$ with $\bar{N}_{\mathbf{k}} = \bar{N}_\omega^{th}$. Note that τ [Eq. (3.3)] is constant to first order at the origin, so that it cannot contribute to the divergence. Thus, $\xi^{(ex)}$ is bounded near the origin if $\mathcal{D}(\mathbf{k})|g_{\mathbf{k}}|^2$ goes to zero fast enough near the origin. In the remainder of this subsection, we will assume the isotropic setting of Eq. (3.15), with $J(\omega)$ as in Eq. (3.16). Then the condition for bounded $\xi^{(ex)}$ becomes $d \geq 1$. This means there is no superlinear scaling of the decoherence function for Ohmic and superohmic continuous thermal reservoirs.

3.4.1.1 Subohmic thermal reservoirs

For subohmic reservoirs ($d < 1$), $\xi^{(ex)}$ in fact diverges at the origin. Here, we show how this can only lead to superlinear scaling of $\Gamma_L^{(ex)}$ with L when γ_L scales superlinearly with L near the origin. Even if γ_L scales superlinearly with L near the origin, quadratic scaling may be approached, but not attained.

Let us first single out the divergence near the origin by defining $\Gamma_L^{(ex)} = \mathcal{I}_L + \mathcal{J}_L$, with

$$\mathcal{I}_L = \int_0^\varepsilon \mathrm{d}\omega\, \gamma_L(\omega)\, \xi^{(ex)}(t_0, \omega), \tag{3.28}$$

$$\xi^{(ex)}(t_0, \mathbf{k}) = J(\omega)\tau(t_0, \omega_{\mathbf{k}})\, 2\bar{N}_\omega^{th}, \tag{3.29}$$

and $\mathcal{J}_L$ the remainder of the integral. Note $\xi^{(ex)}(t_0, \omega)$ now contains the thermal occupation density explicitly.

The integral $\mathcal{J}_L$ is $O(L)$ because, on the domain of integration, $\xi^{(ex)}$ is bounded [also see Eq. (3.26)]. We now turn to $\mathcal{I}_L$. Given an ε, there exists a constant C_2 such that $\xi^{(ex)} \leq C_2\omega^{d-1}$ on $(0, \varepsilon]$. Thus,

$$\mathcal{I}_L \leq C_2 \int_0^\varepsilon \mathrm{d}\omega\, \gamma_L(\omega)\omega^{d-1}.$$

Since ω^{d-1} is monotonically decreasing, the largest possible value of $\mathcal{I}_L$ occurs when $\gamma_L(\omega)$ is peaked at low ω. Herein it is constrained by $\gamma_L(\omega) \leq L^2$ [see Eq. (3.24)] and $\int_0^{2\pi/V} \mathrm{d}\omega\, \gamma_L(\omega) \leq 2\pi L/V$ [Eq. (3.25)]. Under these constraints $\mathcal{I}_L$ is largest when $\gamma_L(\omega)$ is a bump function, where the bump height is L^2, the left of the bump coincides with the origin, and the width of the bump is $2\pi/(VL)$. Therefore,

$$\begin{aligned}
\mathcal{I}_L &\leq C_2 L^2 \int_0^{2\pi/(VL)} \mathrm{d}\omega\, \omega^{d-1} \\
&= C_2 L^2 \frac{1}{d} \left(\frac{2\pi}{VL}\right)^d \\
&= O\left(L^{2-d}\right).
\end{aligned} \tag{3.30}$$

Thus, quadratic scaling of $\Gamma_L^{(ex)}(t_0)$, and thereby quadratic scaling of $\Gamma_L(t_0)$, cannot be obtained in subohmic continuous thermal reservoirs.

To approach superlinear scaling, it is essential that a superlinear peak of $\gamma_L(\omega)$ must be able to approach the origin arbitrarily closely as a function of L. In fact, if, on the contrary, there is a $\delta > 0$ such that $\gamma_L(\omega) = O(L)$ for all $0 \leq x \leq \delta$, then $\mathcal{I}_L = O(L)$. This is shown as

follows. Assume there is a $\delta > 0$ such that $0 < \delta < \varepsilon$ and $\gamma_L(\omega) = O(L)$ for all $0 \leq \omega \leq \delta$. Then because ω^{d-1} is finite on $[\delta, \varepsilon]$, and because there is a constant C_3 such that $\gamma_L(\omega) \leq C_3 L$ for all $[0, \delta)$, we have

$$\begin{aligned}\mathcal{I}_L &\leq C_2 \int_0^\delta \mathrm{d}\omega\, \gamma_L(\omega)\omega^{d-1} + C_2 \int_\delta^\varepsilon \mathrm{d}\omega\, \gamma_L(\omega)\omega^{d-1} \\ &\leq C_2 C_3 L \int_0^\delta \mathrm{d}\omega\, \omega^{d-1} + O(L) \\ &= O(L).\end{aligned}$$

An example in which this occurs is the array model, in the specific case that the dephasing susceptibility is given by $\gamma_{\mathrm{GHZ}'}(\omega)$ [Eq. (3.21)]. To show this, let $\delta = \pi/(2a)$. Then $\cos^2(a\omega/2) \geq \cos^2(\pi/4) \geq 1/2$ for all $0 \leq \omega \leq \delta$, and thus $\gamma_{\mathrm{GHZ}'} \leq 2\sin^2(a\omega L/2) \leq 2$ for all $0 \leq \omega \leq \delta$. This means that the off-diagonal matrix element of $|\mathrm{GHZ}'\rangle$ does not suffer from superdecoherence in subohmic thermal reservoirs, despite the fact that $\xi^{(ex)}$ is unbounded at the origin.

The result Eq. (3.30) is an upper bound, so the question remains if it may be attained. This is not clear a priori because a dephasing susceptibility cannot attain the form of a bump function as in the proof. This is because it is the spectral density of a vector with a finite number of elements [Eq. (3.23)]. We now show by explicit construction that the upper bound may also be attained. This construction is in the subohmic version of the array model (Sec. 3.3), with dephasing susceptibility γ_{GHZ} [Eq. (3.21)]. Roughly speaking, our strategy is to show that $\gamma_{\mathrm{GHZ}}(\omega)$ is a close enough approximation of the bump function. There are two main steps. The first is to show that for all $0 \leq \omega \leq 1/(2aL^2)$, we have $\gamma_{\mathrm{GHZ}}(\omega) \geq L^2 - 1$, or equivalently,

$$\gamma'_{\mathrm{GHZ}}(\omega) := 1 - \frac{\gamma_{\mathrm{GHZ}}(\omega)}{L^2} \leq \frac{1}{L^2}. \tag{3.31}$$

Consider the expansion of $\gamma'_{\mathrm{GHZ}}(\omega)$ in $a\omega$ around $a\omega = 0$. Using the original definition of the dephasing susceptibility [Eq. (3.8)], we have $\gamma'_{\mathrm{GHZ}}(\omega) = \sum_{j=2,4,\ldots} c_j (a\omega)^j$, with

$$|c_j| = \frac{1}{j!\, L^2} \sum_{mn} (m-n)^j < \frac{L^j}{j!}.$$

The radius of convergence of the expansion is infinite. Using the coef-

ficients, we have

$$\begin{aligned}\gamma'_{\mathrm{GHZ}}(\omega) &< \sum_{j=2,4,\ldots} \frac{L^j}{j!}\,(a\omega)^j \\ &= \sum_{j=1,2,\ldots} \frac{1}{(2j)!}(a\omega L)^{2j} \\ &\leq e^{(a\omega L)^2} - 1 \\ &\leq 4(a\omega L)^2. \qquad\qquad (0 \leq a\omega L \leq 1)\end{aligned}$$

The last step can be checked most easily by plotting both functions. The last inequality holds specifically for $a\omega \leq 1/(2L^2)$. After substitution, we have, therefore, that $\gamma'_{\mathrm{GHZ}}(\omega) \leq 1/L^2$ for all $0 \leq \omega \leq 1/(2aL^2)$.

The second step is to show that Eq. (3.31) enables us to approach quadratic scaling of $\mathcal{I}_L$ with L arbitrary closely. First, note that, from Eq. (3.28),

$$\mathcal{I}_L > \int_0^{1/(2aL^2)} \mathrm{d}\omega\, \gamma_{\mathrm{GHZ}}(\omega)\xi^{(ex)},$$

for $1/(2aL^2) < \varepsilon$. There exists an L_0 and a constant C_4 such that for all $L > L_0$, $\xi^{(ex)}(t_0, \omega) \geq C_4\omega^{d-1}$ on the entire domain of integration. Informally, this means that there is a C_4 such that, close enough to the origin, $\xi^{(ex)}(t_0, \omega) \geq C_4\omega^{d-1}$. Thus, for this C_4,

$$\mathcal{I}_L \geq C_4 \int_0^{1/(2aL^2)} \mathrm{d}\omega\, \gamma_{\mathrm{GHZ}}(\omega)\omega^{d-1}.$$

Now using Eq. (3.31), this leads to

$$\begin{aligned}\mathcal{I}_L &\geq C_4(L^2-1)\frac{1}{d}\left(\frac{1}{2aL^2}\right)^d \\ &= \Omega\left[L^{2(1-d)}\right].\end{aligned}$$

Here, the meaning of $\Omega(x)$ is similar to that of $O(x)$, but $\Omega(x)$ refers to a lower instead of an upper bound (see Sec. 1.3.3).

Thus, in the array model with a subohmic continuous thermal reservoirs, quadratic scaling of $\Gamma_L^{(ex)}$, and thereby Γ_L, may be approached arbitrarily closely by the off-diagonal matrix element of $|\mathrm{GHZ}\rangle$.

3.4.2 Infinite time limit

In our discussion of the system size scaling until now, we assumed the time t to be fixed. Here we consider the infinite time limit of the

isotropic case [Eq. (3.15)], with $J(\omega)$ as given in Eq. (3.16). In the following, we no longer assume $d < 1$ and $\bar{N}_\omega = \bar{N}_\omega^{th}$ as in the previous subsection. With $\partial_t \tau(t,\omega) = \sin(\omega t)/\omega$ [cf. Eq. (3.3)],

$$\lim_{t\to\infty} \partial_t \Gamma_L(t) = \frac{\pi}{2} \lim_{\omega\downarrow 0} J(\omega)\tilde{\gamma}(\omega)(1 + 2\bar{N}_\omega). \tag{3.32}$$

Thus, the infinite time behaviour of $\Gamma_L(t)$ depends only on the integrand at the origin, which is always non-negative. If the limit on the right hand side of Eq. (3.32) is positive, $\Gamma_L(t)$ keeps growing indefinitely as a function of t. If, on the other hand, this limit is zero, $\Gamma_L(t)$ increases at most sublinearly with t as t goes to infinity. We call this a quasi-plateau, which naturally includes proper plateaus. These proper plateaus are also referred to as incomplete dephasing [38] or coherence trapping [1]. In Sec. 3.C.3 we compute the height of the proper plateaus of $\Gamma_L^{(vac)}$ explicitly in the array model.

As an example, we can read off that for $\gamma_{\mathrm{GHZ}'}$, which is $O(\omega^2)$ as ω goes to zero [see Eq. (3.21)], in a completely thermal reservoir [Eq. (3.5)], a (quasi-)plateau is reached for all $T \geq 0$ and $d \geq 0$. From Eq. (3.32) alone we cannot infer anything about the height of the (quasi-)plateau.

3.5 Finite-size effects

In the previous section, we focused on the asymptotic system size scaling of the decoherence function. We saw that, in that case, a sharp delineation could be placed between cases of superlinear and linear scaling. For finite system sizes, the situation becomes less clear. This is because the decoherence function may scale quadratically up to some potentially large system size L_0, and show linear scaling only for $L > L_0$. Even though the main goal of this chapter is to investigate the asymptotic scaling of the decoherence function with the system size, we discuss some finite-size effects in this section.

3.5.1 Role of time in finite-size effects

Assume, for simplicity, a linear, isotropic dispersion relation, $\omega_{\mathbf{k}} = \omega = |\mathbf{k}|$, in units where the proportionality constant equals unity. Consider the temporal factor $\tau(t,\omega_{\mathbf{k}})$ [Eq. (3.3)] as a function of $\mathbf{k}$. The function is peaked at the origin, with height $t^2/2$. Away from the origin, it drops to zero at $|\mathbf{k}| = 2\pi/t$ and remains small afterwards [$O(1/|\mathbf{k}|^2)$]. Thus, for large t, τ gives large weight to wave vectors with a length below $2\pi/t$, and ever smaller weight to wave vectors with a length above $2\pi/t$.

In Sec. 3.3, we showed that, if $\gamma_L(\mathbf{k})$, as a function of $\mathbf{k}$, has a peak of height L^2, the support of that peak must scale as $1/L$. This effect causes the absence of superdecoherence in bounded reservoirs. However, if this peak is located at the origin, but t is such that the peak of $\tau(t, \omega_{\mathbf{k}})$ is much narrower than that of $\gamma_L(\mathbf{k})$, we have that $\gamma_L(\mathbf{k})$ is approximately constant on the interval where $\tau(t, \omega_{\mathbf{k}})$ is non-negligible. Thus, the reducing bandwidth of $\gamma_L(\mathbf{k})$ is only guaranteed to have an effect if

$$aL \gtrsim t. \tag{3.33}$$

Therefore, the actual scaling of Γ_L as a function of L may approach its asymptotic scaling only at times small compared to the system size. In Sec. 3.C, we derive explicit closed-form expressions for the vacuum contribution to the dephasing function. This gives possibilities for the study of the explicit interplay between time and system size.

Equation (3.33) seems to form an important caveat to our asymptotic results. However, it only applies in special cases. Firstly, $\gamma_L(\omega)$ needs to scale superlinearly as a function of L near the origin, which is rarely the case (Sec. 3.B). Secondly, even if $\gamma_L(\omega)$ scales superlinearly, the remaining factors $\xi^{(ex)}$ and $\xi^{(vac)}$ may kill the entire integrand around the origin [see Eq. (3.11)], for example when $\xi^{(vac)}(t, \omega) = O(\omega^d)$ and $\xi^{(ex)} = O(\omega^d)$ as $\omega \to 0$, with $d \geq 1$. Then for every $\gamma_L(\omega)$ that scales superlinearly at the origin and fixed L_0, there is a continuous crossover from superlinear to linear behaviour in L around L_0 as a function of d. See Fig. 3.4 for two concrete examples.

3.5.2 Peaked occupation density

A similar finite-size effect occurs if the occupation density has a peak that coincides with a superlinear peak of the dephasing susceptibility. To separate this effect from the one in the previous subsection, consider as an example the state $|\mathrm{GHZ}'\rangle$, in the array model, with a Gaussian occupation density $\bar{N}_\omega = \bar{N}_{tot}\exp[-(\omega - \pi/a)^2/(2\sigma^2)]/(\sqrt{2\pi}\sigma)$, with mean π/a, variance σ, and an integrated number of bosons $\bar{N}_{tot} := \int_{-\infty}^{\infty} \mathrm{d}\omega\, \bar{N}_\omega$. Similar to in the previous subsection, the mitigating effect of the $1/L$ bandwidth of the dephasing susceptibility has an effect only after the peak of the dephasing susceptibility becomes narrower than that of the occupation density. That is, we only expect linear scaling of the decoherence function for

$$\frac{2\pi}{aL} < \sigma.$$

See Fig. 3.5 for plots of the leading order in time of the decoherence function $\Gamma_{\mathrm{GHZ}'}$ that is obtained in the current case.

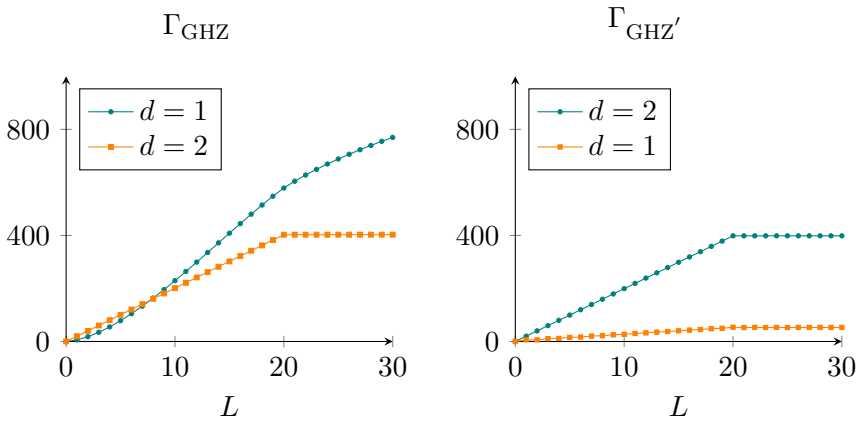

Figure 3.4: The decoherence function in the array model (Sec. 3.3), as a function of L, for the off-diagonal matrix element of $|\mathrm{GHZ}\rangle$ (left) and $|\mathrm{GHZ}'\rangle$ (right). In both plots, we use units where $a = 1$, and set $t = 20$, $J(\omega) = \alpha_d \omega^d e^{-\omega/\omega_c}$, with $\alpha_d = 1$ (for both $d = 1$ and $d = 2$), $\omega_c = 20$, and $\bar{N}_\omega = 0$. For these plots, we have used the analytical expressions for the decoherence function derived in Sec. 3.C. (**Left**) For $d = 1$ the decoherence function increases quadratically initially, after which it scales (sub)linearly. For $d = 2$ there is no quadratic scaling, even for $aL \ll t$. (**Right**) No superlinear scaling for any t, L and d (including d other than $d = 1, 2$, which are not shown). The lines for $d = 2$ in the left and right plot are similar, but not exactly equal.

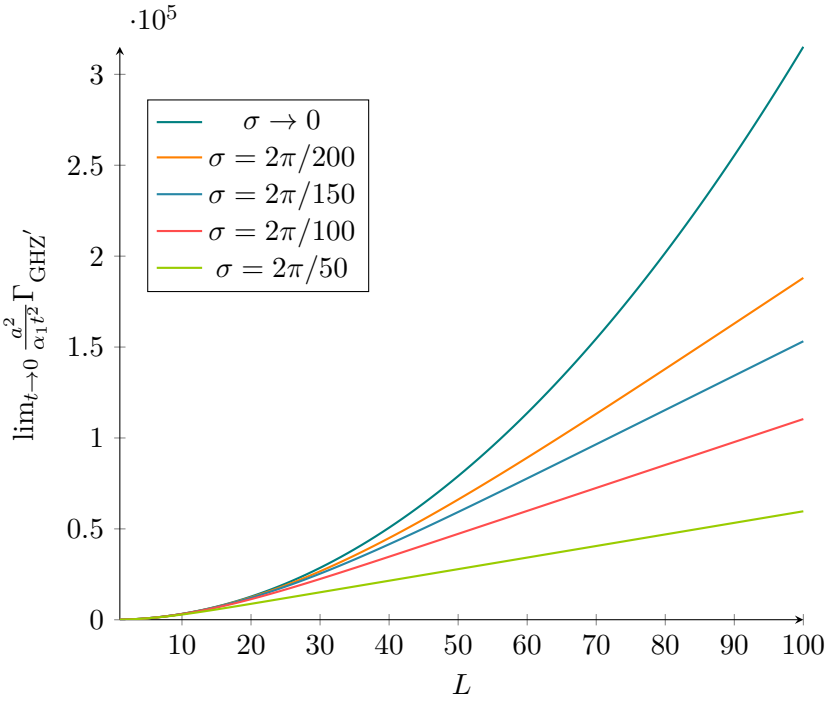

Figure 3.5: The leading order in time of the decoherence function of the off-diagonal matrix element of $|\mathrm{GHZ}'\rangle$, as a function of the system size L. The setting is that of the array model (Sec. 3.3), with $d = 1$. In units where $a = 1$, the occupation density $\bar{N}_\omega$ is taken to be a Gaussian, with mean $\omega_0 = \pi$, standard deviation σ and integrated occupation $\bar{N}_{tot} = 10$. We see linear scaling with L is obtained for $1/L \lesssim \sigma$. In the limit $\sigma \to 0$, the occupation density becomes unbounded, and consequently, it is only in the limit that the decoherence function scales as L^2 for all L. The plot uses an analytic solution of Eq. (3.15), with $J(\omega) = \frac{\alpha_1}{2}\omega[1 - \Theta(\omega - 2\pi)]$, where Θ is the step function. This form of the spectral density is chosen to accentuate the finite-size effects; the function $\gamma_{\mathrm{GHZ}'}(\omega)$ has peaks at $\omega = \pi, \pi + 2\pi, \ldots$, whereas, in this example, $\bar{N}_\omega$ only has a peak at $\omega_0 = \pi$. Finite-size effects only occur at places where the two peaks overlap, and including frequencies higher than 2π into $J(\omega)$ means including more effects that scale with L rather than L^2.

Again, in many situations, the effect discussed in this subsection does not have significant effects. Firstly, note that the integral in Eq. (3.15) is over infinitely many periods of the dephasing susceptibility. In the example above, the peak of the occupation density occurs only at a single frequency. In this case, the effect described in this subsection will thus only occur at one of the periods of $\gamma_{\mathrm{GHZ}'}(\omega)$. Secondly, the centre of the peak of the occupation density has to coincide exactly with the peak of the dephasing susceptibility.

The latter situation, where there is a single peak in the occupation density that overlaps exactly with the peak in the dephasing susceptibility, occurred in the ion-trap experiment by Monz et al., where the model of single-reservoir dephasing is applicable [104]. The state $|\mathrm{GHZ}\rangle$ was prepared in a semi-static, semi-uniform magnetic field, which was produced with a Helmholtz coil. Fluctuations of the field, caused by current fluctuations in the coil, excited long-wavelength modes (with $k \approx 0$). The dephasing susceptibility of the off-diagonal matrix element of $|\mathrm{GHZ}\rangle$ scales as L^2 at $k = 0$ (see Fig. 3.3), and exactly the modes $k \approx 0$ where heavily excited in the experiment. If modes were excited away from the origin, there would not have been superdecoherence. This follows from the explicit form of the dephasing susceptibility of the off-diagonal matrix element of $|\mathrm{GHZ}\rangle$ (also see Fig. 3.3). Furthermore, even if modes near the origin were excited, almost any matrix element other than the off-diagonal element of $|\mathrm{GHZ}\rangle$ would not have suffered superdecoherence (also see Sec. 3.B).

3.6 Conclusion and outlook

In this chapter, we studied superdecoherence in the model of single-reservoir spin-boson dephasing for asymptotic system sizes. We have shown that if the reservoir density of modes in k-space, $\mathcal{D}(\mathbf{k})$, and the reservoir occupation density $\bar{N}_{\mathbf{k}}$ are bounded, superdecoherence is not possible. This is because if there is a $\mathbf{k}$ such that the dephasing susceptibility scales quadratically with the system size, $\gamma_L(\mathbf{k}) \propto L^2$, the support of this peak in the dephasing susceptibility necessarily scales inversely with L.

Superdecoherence may thus only be obtained if $\mathcal{D}(\mathbf{k})$ or $\bar{N}_{\mathbf{k}}$ is unbounded. The former happens if the reservoir supports only a discrete set of modes. The latter happens if the reservoir supports a continuum of modes, but only perfectly isolated modes are excited. In both cases, for superdecoherence to occur, the unbounded point must coincide exactly with the mode for which the dephasing susceptibility $\gamma_L(\mathbf{k})$ scales

quadratically.

For completely continuous, thermal reservoirs, the occupation density $\bar{N}_\omega^{th}$ diverges algebraically at the origin. Nevertheless, it does not diverge fast enough to cause superdecoherence. There is one subtle situation. This is the subohmic continuous thermal reservoir with non-zero temperature, where, furthermore, the dephasing susceptibility must scale superlinearly (which includes quadratic scaling) at low frequencies. In this case, the decoherence function may approach, but not attain, quadratic scaling with the system size. Hence, only in this sub-case of thermal reservoirs, superdecoherence can be approached.

All effects discussed in this chapter can be observed experimentally. One could compare the effects of narrow-band versus broadband noise at a frequency to which the system is highly susceptible. Or, the system could be placed in a high-Q cavity in the vacuum state, that supports exactly the mode the system is highly susceptible to. This is to be compared to a situation where the cavity is slightly off-resonant.

Other applications lie in quantum metrology, in which superdecoherence can be used as a means of enhancing sensitivity. In this context, it is well-known that the GHZ state is highly susceptible to long-wavelength modes [56, 57]. The dephasing susceptibility, as defined in this chapter, offers an effective way to extend metrology to other states and wavelengths; any state for which there is a ω_0 such that $\gamma_L(\omega_0) \propto L^2$ is suitable for quantum metrology of the mode with wavelength ω_0. An example is a linear array of qubits, with spacing a, in the state $\left|\mathrm{GHZ}'\right\rangle$ [Eq. (3.17)]. This system is highly susceptible to the staggered mode $\omega_0 = \pi/a$. The dephasing susceptibility shows the added benefit that with increasing system size, the array becomes less sensitive to frequencies other than ω_0.

Appendix

3.A Spin-boson dephasing for arbitrary reservoir states

In this section, we generalize the decoherence function of single-reservoir dephasing, as derived in Refs. [115, 124, 26], to more general reservoir states. We pay specific attention to Gaussian states, Gaussian product states, and a product of displaced thermal states. The latter solution is included in the main text as Eqs. (3.2) and (3.7).

For a completely general reservoir state, it can be shown that [115,

124, 26]

$$|\rho_{\mathbf{ij}}(t)| = |\tilde{\chi}(\lambda)|\ |\rho_{\mathbf{ij}}(0)|, \tag{3.34}$$

where $\tilde{\chi}$ is the *characteristic function* of the reservoir state,

$$\tilde{\chi}(\lambda) := \left\langle e^{\sum_{\mathbf{k}\in D}(\lambda_{\mathbf{k}} a^\dagger - \lambda_{\mathbf{k}}^* a_{\mathbf{k}})} \right\rangle_{\rho_B(0)}. \tag{3.35}$$

Equations (3.34) and (3.35) hold for the interaction as well as the Schrödinger picture density operators. The set D contains all wave vectors that are supported by the reservoir.

The argument of the characteristic function, $\lambda \in \mathbb{C}^{|D|}$, depends on the matrix index $(\mathbf{i}, \mathbf{j})$ and the time t, but the notation of this dependence is suppressed. The $\mathbf{k}$th entry of λ is given by [115, 124, 26]

$$\lambda_{\mathbf{k}} = g_{\mathbf{k}}\, \tilde{\mathrm{d}}^*(\mathbf{k})\, \frac{1 - e^{i\omega_{\mathbf{k}} t}}{\omega_{\mathbf{k}}}, \tag{3.36}$$

with $\tilde{\mathrm{d}}$ the Fourier transform of $\mathbf{d} = \mathbf{i} - \mathbf{j}$ [see Eq. (3.16)]. The exponent in Eq. (3.36) stems from the internal time evolution of the reservoir. Equations (3.34) and (3.35) give the most general form of the absolute value of the time evolved reduced density matrix in the single-reservoir dephasing model.

For the class of *Gaussian states* [43, 2], the absolute value of the characteristic function is given by

$$|\tilde{\chi}(\lambda)| = e^{-\Gamma(\lambda)},$$

with

$$\Gamma(\lambda) = \frac{1}{2}\Lambda^T \sigma \Lambda. \tag{3.37}$$

This is the most general form of the decoherence function. Here, writing $\lambda_{\mathbf{k}_i}$ as λ_i for short,

$$\Lambda^T = \sqrt{2}\, \left(\mathrm{Re}\,\lambda_1, \mathrm{Im}\,\lambda_1, \ldots, \mathrm{Re}\,\lambda_{|D|}, \mathrm{Im}\,\lambda_{|D|}\right).$$

The $2|D| \times 2|D|$ matrix σ is the *covariance matrix*,

$$\sigma_{mn} = \tfrac{1}{2}\langle\{\hat{R}_m, \hat{R}_n\}\rangle - \langle\hat{R}_m\rangle\langle\hat{R}_n\rangle. \tag{3.38}$$

The expectation value is with respect to the Gaussian initial reservoir state $\rho_B(0)$. The vector $\hat{R}$ is defined by

$$\hat{R}^T = (\hat{q}_1, \hat{p}_1, \ldots \hat{q}_{|D|}, \hat{p}_{|D|}),$$

with $\{\cdot,\cdot\}$ the anti-commutator. To avoid confusion about operators versus numbers, in this section we write operators (and vectors containing operators) with hats, as opposed to in the main text. The quadrature operators $\hat{q}_m$ and $\hat{p}_m$, in turn, are defined by

$$\hat{q}_m = \frac{1}{\sqrt{2}}(\hat{a}_m + a_m^\dagger), \qquad \hat{p}_m = \frac{1}{i\sqrt{2}}(\hat{a}_m - \hat{a}_m^\dagger).$$

To obtain the decoherence function as a function of time and the density matrix index $(\mathbf{i},\mathbf{j})$, the expression for λ [Eq. (3.36)] has to be inserted into Eq. (3.37).

We may consider various simplifications of the decoherence function as it is given in Eq. (3.37). If the reservoir modes are unentangled, that is, $\rho_B(0) = \bigotimes_{\mathbf{k}} \rho_{B,\mathbf{k}}(0)$ with all $\rho_{B,\mathbf{k}}(0)$ Gaussian, the covariance matrix is block-diagonal. Each block corresponds to a 2×2 single-mode covariance matrix, which we denote by $\sigma_{\mathbf{k}}$. In this case, we may write

$$\Gamma(\lambda) = \sum_{\mathbf{k}} (\mathrm{Re}\lambda_{\mathbf{k}}, \mathrm{Im}\lambda_{\mathbf{k}})\, \sigma_{\mathbf{k}} \begin{pmatrix} \mathrm{Re}\lambda_{\mathbf{k}} \\ \mathrm{Im}\lambda_{\mathbf{k}} \end{pmatrix}, \tag{3.39}$$

where, by Eq. (3.38), the entries of the single-mode covariance matrix read

$$\begin{aligned}
(\sigma_{\mathbf{k}})_{11} &= \langle \hat{q}_{\mathbf{k}}^2 \rangle - \langle \hat{q}_{\mathbf{k}} \rangle^2 \\
(\sigma_{\mathbf{k}})_{22} &= \langle \hat{p}_{\mathbf{k}}^2 \rangle - \langle \hat{p}_{\mathbf{k}} \rangle^2 \\
(\sigma_{\mathbf{k}})_{12} &= \frac{1}{2}\langle \{\hat{q}_{\mathbf{k}}, \hat{p}_{\mathbf{k}}\} \rangle - \langle \hat{q}_{\mathbf{k}} \rangle \langle \hat{p}_{\mathbf{k}} \rangle \\
(\sigma_{\mathbf{k}})_{21} &= (\sigma_{\mathbf{k}})_{12}.
\end{aligned}$$

If the mode $\mathbf{k}$ is initially in the thermal state, with temperature $T_{\mathbf{k}}$, its density matrix reads $\rho_{B,\mathbf{k}}(0) \propto e^{-\omega_{\mathbf{k}} \hat{a}_{\mathbf{k}}^\dagger \hat{a}_{\mathbf{k}}/T_{\mathbf{k}}}$. In this case, the single-mode covariance matrix is diagonal,

$$\sigma_{\mathbf{k}} = \mathrm{diag}\left(\bar{N}_{\mathbf{k}} + \tfrac{1}{2},\, \bar{N}_{\mathbf{k}} + \tfrac{1}{2}\right), \tag{3.40}$$

with $\bar{N}_{\mathbf{k}}$ the occupation number [Eq. (3.4)]. A special thermal state is the vacuum, where $\bar{N}_{\mathbf{k}} = 0$.

If the reservoir modes are unentangled, and every mode is thermally excited with its own temperature, we have from combining Eqs. (3.39) and (3.40) that

$$\Gamma(\lambda) = \sum_{\mathbf{k}} |\lambda_{\mathbf{k}}|^2 (\bar{N}_{\mathbf{k}} + \tfrac{1}{2}). \tag{3.41}$$

Inserting the equation for $\lambda_{\mathbf{k}}$ [Eq. (3.36)], we obtain Eq. (3.7).

In general, a single-mode Gaussian state can also be represented as a squeezed and displaced thermal state [43],

$$
\begin{aligned}
(\sigma_{\mathbf{k}})_{11} &= (\bar{N}_{\mathbf{k}} + \tfrac{1}{2})[\cosh(2r) + \sinh(2r)\cos(\varphi)] \\
(\sigma_{\mathbf{k}})_{22} &= (\bar{N}_{\mathbf{k}} + \tfrac{1}{2})[\cosh(2r) - \sinh(2r)\cos(\varphi)] \\
(\sigma_{\mathbf{k}})_{12} &= -(\bar{N}_{\mathbf{k}} + \tfrac{1}{2})\sinh(2r)\sin(\varphi) \\
(\sigma_{\mathbf{k}})_{21} &= (\sigma_{\mathbf{k}})_{12}.
\end{aligned}
$$

Here r is the squeezing magnitude, and φ the squeezing angle. Note these expressions are invariant under displacement. Therefore, the decoherence function of a displaced thermal state is equal to Eq. (3.41), with $\bar{N}$ the regular Bose-Einstein distribution. Squeezing, on the other hand, does affect the covariance matrix, and would alter Eq. (3.41) straightforwardly. In the main text, we assume for simplicity that the reservoir modes are not squeezed.

Displaced vacuum states are precisely the coherent states. Thus, even if a reservoir mode is in a highly excited coherent state, this mode does not contribute more to the dephasing process than the same mode in the vacuum state would have done. A mixture of coherent states does lead to extra dephasing. However, the only mixture that can be described in the Gaussian state formalism is the thermal state.

To summarize, in single-reservoir dephasing, the decoherence process of the system is completely determined by the reservoir characteristic function; $|\tilde{\chi}(\lambda)| = |\rho_{\mathbf{ij}}(t)|/|\rho_{\mathbf{ij}}(0)|$. The argument of the characteristic function, λ, is a complex vector which depends on the matrix index $(\mathbf{i},\mathbf{j})$ and time [Eq. (3.36)]. For completely general reservoir states, the characteristic function is given by Eq. (3.35). For general Gaussian reservoir states, $|\tilde{\chi}(\lambda)| = e^{-\Gamma(\lambda)}$, with $\Gamma(\lambda) = \frac{1}{2}\Lambda^T\sigma\Lambda$ the decoherence function.. In case the reservoir modes are unentangled, $\Gamma(\lambda)$ may be written using a single sum over $\mathbf{k}$ [Eq. (3.39)]. If, furthermore, each of these modes is a (possibly) displaced thermal state, the decoherence function simplifies to Eq. (3.41). It is this form of the decoherence function that we use in the main text. Surprisingly, displacing a reservoir state has no effect on the dephasing process. For example, this means that it does not matter for the dephasing process if a mode is in a highly excited coherent state or the vacuum state.

3.B Typical values of the dephasing susceptibility

Here, we ask the question if there many $\mathbf{i}-\mathbf{j}$ such that $\gamma_{\mathbf{i}-\mathbf{j}}(\mathbf{k}) \approx L^2$, given fixed values for L and $\mathbf{k}$. We show this is not the case: as we go over all $(\mathbf{i},\mathbf{j})$, the values of $\gamma_{\mathbf{i}-\mathbf{j}}(\mathbf{k})$ are distributed according to a Gaussian that has a standard deviation that is at most $L/(2\pi)$. This means that, for a random $(\mathbf{i},\mathbf{j})$, $\gamma_{\mathbf{i}-\mathbf{j}}(\mathbf{k})$ is typically on the order of $L/(2\pi)$, or less.

To show this, fix L and $\mathbf{k}$, and consider the function $D_{\mathbf{ij}} := \sqrt{\gamma_{\mathbf{i}-\mathbf{j}}(\mathbf{k})} = \|\sum_\ell (\mathbf{i}_\ell - \mathbf{j}_\ell) e^{i\mathbf{k}\cdot\mathbf{r}_\ell}\|$. Consider the frequency distribution of this function. This is a table that, per possible value D_0 of $D_{\mathbf{ij}}$, shows the number of inputs $(\mathbf{i},\mathbf{j})$ such that $D_{\mathbf{ij}} = D_0$. To obtain this distribution, we see D as the distance from the origin of a random walker on the complex plane. The walker takes L steps, where the ℓth step is given by $\mathbf{d}_\ell e^{i\mathbf{k}\cdot\mathbf{r}_\ell}$, with $\mathbf{d} = \mathbf{i}-\mathbf{j}$. For the ℓth step, the walker has a probability $1/2$ to make no step at all, a probability of $1/4$ to take the step $+e^{i\mathbf{k}\cdot\mathbf{r}_\ell}$, and a probability of $1/4$ to take the step $-e^{i\mathbf{k}\cdot\mathbf{r}_\ell}$. After L steps, the walker is a distance $D_{\mathbf{ij}}$ away from the origin of the complex plane.

Naturally, the variance in the distances from the origin is largest if the walker is restricted to move on a single line, which happens if $\mathbf{k} = \mathbf{0}$. Let us therefore put $\mathbf{k} = \mathbf{0}$, keeping in mind that, at worst, we are overestimating the variance of $D_{\mathbf{ij}}$ for other values of $\mathbf{k}$. For a 1D random walker that can take the steps $+1$ and -1 with equal probability, it is well-known that, after L steps, the distribution of distances from the origin is well approximated by a Gaussian with standard deviation $\sqrt{2L/\pi}$. In our situation, half of the time the 1D walker does not take a step at all. Therefore, the distribution of D will be approximated by a Gaussian with variance $\sqrt{L/(2\pi)}$. Since $\gamma_{\mathbf{i}-\mathbf{j}} = (D_{\mathbf{ij}})^2$, the distribution of $\gamma_{\mathbf{i}-\mathbf{j}}$ over $(\mathbf{i},\mathbf{j})$ is approximated by a Gaussian with standard deviation $L/(2\pi)$. This means that for fixed L and $\mathbf{k}$, and given a random $(\mathbf{i},\mathbf{j})$, the decoherence function is, at most, typically on the order of $L/(2\pi)$. Additionally, it means that, if we are given a random $(\mathbf{i},\mathbf{j})$, where also the dimension L of $\mathbf{i}$ and $\mathbf{j}$ is random but equal, the probability that $\gamma_{\mathbf{i}-\mathbf{j}} \geq \kappa L^2$ goes to zero as L goes to infinity, for all $\mathbf{k}$ and $\kappa > 0$.

3.C Explicit expressions for the vacuum contribution

Here, we derive, for the first time, the explicit solution of the vacuum part of the decoherence function, $\Gamma_{\mathbf{d}}^{(vac)}(t)$, in the array model of Sec. 3.3. This gives a better understanding between the interplay of time and system-size dependence. For simplicity we assume that the qubits form a linear array with spacing a and that they couple to a one-dimensional reservoir via the single-reservoir dephasing Hamiltonian. The spectral density of the reservoir is assumed to be given by Eq. (3.16).

In principle, in the array model, $d = 1$, but we will analytically extend our solutions to arbitrary d. After absorbing the integral over the solid angle, which in $d = 1$ dimensions gives a factor of 2, into α_d, the vacuum decoherence function reads

$$\Gamma_{\mathbf{d}}^{(vac)}(t) = \int_0^\infty \mathrm{d}\omega\, J(\omega)\gamma_{\mathbf{d}}(\omega)\tau(t,\omega), \tag{3.42}$$

with

$$\begin{aligned} J(\omega) &= \alpha_d \omega^d e^{-\omega/\omega_c}, \\ \gamma_{\mathbf{d}}(\omega) &= \sum_{\ell m} \mathbf{d}_\ell \mathbf{d}_m \cos[\omega a(\ell - m)], \\ \tau(t,\omega) &= \frac{1-\cos(\omega t)}{\omega^2}. \end{aligned}$$

In this section, we derive the full solution of Eq. (3.42). Additionally, we derive simplified approximate solutions for the limits of infinitesimal and infinite time. For infinitesimal times, we find

$$\Gamma_{\mathbf{d}}^{(vac)}(t) \approx \frac{1}{2}\alpha_d \|\mathbf{d}\|^2 \tilde{\Gamma}(1+d)\omega_c^{d-1}(t\omega_c)^2,$$

where $\tilde{\Gamma}$ is the regular gamma function $\tilde{\Gamma}(j+1) = j!$, not to be confused with the decoherence function. In the infinite time limit, $\Gamma_{\mathbf{d}}^{(vac)}(t)$ reaches a plateau for all $d > 1$. For $d \geq 2$, we show that the height this plateau equals

$$\lim_{t\to\infty} \Gamma_{\mathbf{d}}^{(vac)}(t) \approx \alpha_d \|\mathbf{d}\|^2 \tilde{\Gamma}(d-1)\omega_c^{d-1}.$$

This result extends that of Sec. 3.4.2 for the current, specific setting. Note that, because $\|\mathbf{d}\|^2 \leq (\sqrt{1^2+1^2+\ldots+1^2})^2 \leq L$, the decoherence function scales at most linearly with L in the limits of infinitesimal and infinite time, in accordance with the results in the main text.

3.C.1 General solution

We start by rewriting $\gamma_{\mathbf{d}}(\omega)$ as

$$\gamma_{\mathbf{d}}(\omega) = \sum_{r=0}^{L-1} f_{\mathbf{d}r} \cos(a\omega r), \tag{3.43}$$

where

$$f_{\mathbf{d}r} = (2 - \delta_{0r}) \sum_{m=1}^{L-r} \mathbf{d}_m \mathbf{d}_{m+r}. \tag{3.44}$$

Written this way, $\gamma_{\mathbf{d}}(\omega)$ is the cosine transform of $f_{\mathbf{d}r}$. For later reference, we note that for the states $|\mathrm{GHZ}\rangle$ and $|\mathrm{GHZ}'\rangle$,

$$f_{\mathbf{d}r} = \begin{cases} L & : r = 0 \\ 2(L-r)\zeta^r & : r > 0 \end{cases},$$

where $\zeta = 1$ for $|\mathrm{GHZ}\rangle$ and $\zeta = -1$ for $|\mathrm{GHZ}'\rangle$.

Going back to the general case, we have from Eqs. (3.42) and (3.43), and $f_{\mathbf{d}0} = \|\mathbf{d}\|^2$, that

$$\Gamma_{\mathbf{d}}^{(vac)}(t) = \alpha_d \|\mathbf{d}\|^2 I_0 + \alpha_d \sum_{r=1}^{L-1} f_{\mathbf{d}r} I_r, \tag{3.45}$$

with

$$I_r(t) = \int_0^\infty \mathrm{d}\omega\, \omega^d \tau(t,\omega)\, e^{-\omega/\omega_c} \cos(a\omega r). \tag{3.46}$$

This integral is solved using standard identities for Gaussian integrals. For $d > 0$, $d \neq 1$,

$$\begin{aligned} I_r(t) =& \frac{a^{1-d}}{4} \tilde{\Gamma}(d-1) \\ & \times \left[2(Q_{r0})^{1-d} - (Q_{r,-1})^{1-d} - (Q_{r1})^{1-d} \right] \\ & + c.c, \end{aligned} \tag{3.47}$$

Here *c.c.* stands for the complex conjugate of the preceding term, and

$$Q_{rj} := \mathrm{i}(jt/a - r) + \frac{1}{a\omega_c}, \tag{3.48}$$

with i the imaginary unit. For $d = 1$,

$$\begin{aligned} I_r(t) =& \frac{1}{4} \left[-2 \log(Q_{r0}) + \log(Q_{r,-1}) + \log(Q_{r1}) \right] \\ & + c.c. \end{aligned} \tag{3.49}$$

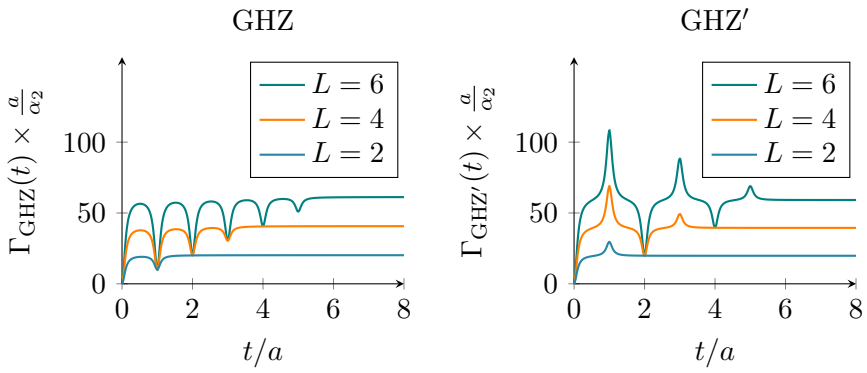

Figure 3.6: The decoherence function of the off-diagonal matrix element of the density matrix of $|\mathrm{GHZ}\rangle$ (left) and $|\mathrm{GHZ}'\rangle$ (right) in $d = 2$ dimensions, with $\omega_c = 10/a$ and $T = 0$. We observe $L1$ pronounced extrema, at $t/a = 0, 1, 2, \ldots, L-1$. The time interval between these extrema is equal to the time required by the mode to travel a distance a. There are no extrema after the mode has had the time to travel the distance aL, which is the total length of the array. For $|\mathrm{GHZ}'\rangle$, the extrema are alternating local maxima and minima. For $|\mathrm{GHZ}\rangle$, there are only local minima at these points. After the series of extrema, Γ_{GHZ} and $\Gamma_{\mathrm{GHZ}'}$ reach the same plateaus, the height of which is given by Eq. (3.58). Plots for higher L, and odd L, show the same behaviour.

We now have $\Gamma_{\mathbf{d}}^{(vac)}(t)$ in closed form, except for the sum over a single index in Eq. (3.45). Using this analytic solution, Γ_{GHZ} and $\Gamma_{\mathrm{GHZ}'}$ are plotted in Fig. 3.6.

3.C.2 Infinitesimal time limit

The leading, second order in time of the integral in Eq. (3.46) equals

$$\frac{1}{2}t^2 \int_0^\infty \mathrm{d}\omega\, e^{-\omega/\omega_c}\omega^d \cos(a\omega r).$$

Solving this integral, we obtain, for $r = 0$,

$$I_0(t) = \omega_c^{d-1}\left\{\frac{1}{2}\tilde{\Gamma}(1+d)(t\omega_c)^2 + O\left[(t\omega_c)^4\right]\right\}. \tag{3.50}$$

For $r > 0$, we find

$$I_{r>0}(t) = a^{1-d}\frac{1}{4}\tilde{\Gamma}(1+d)(t/a)^2[(Q_{r0})^{-(d+1)} + c.c.] + a^{1-d}O\left[(t/a)^4\right].$$

These two solutions hold for all $d > 0$. Up to a factor $\alpha_d\|\mathbf{d}\|^2$, the first term of the decoherence function in Eq. (3.45) is given by Eq. (3.50). For the remaining terms, with $r > 0$, note that $|f_{\mathbf{d}r}| \leq 2f_{\mathbf{d}0} = 2\|\mathbf{d}\|^2$. Thus,

$$\alpha_d\left|\sum_{r=1}^{L-1} f_{\mathbf{d}r}I_r(t)\right| \leq 2\alpha_d\|\mathbf{d}\|^2\sum_{r=1}^{L-1}|I_r(t)|. \tag{3.51}$$

Note $|I_r(t)|$ is proportional to

$$\begin{aligned}\left|(Q_{r0})^{-(d+1)} + c.c.\right| &< 2|Q_{r0}|^{-(d+1)} \\ &= 2\left(r^2 + \frac{1}{(a\omega_c)^2}\right)^{-(d+1)} \\ &< 2\,r^{-2(d+1)}.\end{aligned}$$

Therefore,

$$\begin{aligned}\sum_{r=1}^{L-1}\left|(Q_{r0})^{-(d+1)} + c.c.\right| &< 2\sum_{r=1}^{L-1} r^{-2(d+1)} \\ &< 4.\end{aligned}$$

Thus, we obtain

$$\begin{aligned}\alpha_d\left|\sum_{r=1}^{L-1} f_{\mathbf{d}r}I_r\right| &< 2\alpha_d\|\mathbf{d}\|^2a^{1-d}\tilde{\Gamma}(1+d)(t/a)^2 \\ &\quad + \alpha_d\|\mathbf{d}\|^2a^{1-d}O(t/a)^4.\end{aligned} \tag{3.52}$$

There are extra factors of L hiding in the $O(t/a)^4$ term. We can disregard this L dependence because, in this subsection, we are interested in the limit of infinitesimal time. Then for any L there is a $t/a \ll 1$ such that the second term in Eq. (3.52) is negligible.

Thus, for small times and $d > 0$, the final result is

$$\Gamma_{\mathbf{d}}^{(vac)}(t) = \frac{1}{2}\alpha_d\|\mathbf{d}\|^2\tilde{\Gamma}(1+d)\omega_c^{d-1}(t\omega_c)^2 + \mathcal{E}, \tag{3.53}$$

where $\mathcal{E}$ contains both the error from the $\alpha\|\mathbf{d}\|^2 I_0$ term, and all of the remaining terms in Eq. (3.45),

$$\begin{aligned}\mathcal{E} &= \alpha_d\|\mathbf{d}\|^2\omega_c^{d-1}O(t\omega_c)^4 \\ &\quad + 2\alpha_d\|\mathbf{d}\|^2 a^{1-d}\tilde{\Gamma}(1+d)(t/a)^2 \\ &\quad + \alpha_d\|\mathbf{d}\|^2 a^{1-d}O(t/a)^4.\end{aligned}$$

Given an L and $\omega_c a \gg 1$, the relative error

$$\begin{aligned}\tilde{\mathcal{E}} &:= \frac{\mathcal{E}}{\frac{1}{2}\alpha_d\|\mathbf{d}\|^2\tilde{\Gamma}(1+d)\omega_c^{d-1}(t\omega_c)^2} \\ &< O(t\omega_c)^2 + \frac{4}{(a\omega_c)^{d+1}} + \frac{1}{a\omega_c(t\omega_c)^2}O(t/a)^4,\end{aligned}$$

is negligible for t small compared to $1/\omega_c$ and a.

3.C.3 Infinite time limit

If $d > 1$ and $j \neq 0$, the function $(Q_{rj})^{1-d}$ vanishes in the limit that t goes to infinity. For $j = 0$, on the other hand, $(Q_{rj})^{1-d}$ is time-independent and non-zero. Thus, from Eq. (3.42),

$$\lim_{t\to\infty} I_r(t) = \frac{1}{2}a^{1-d}\tilde{\Gamma}(d-1)(Q_{r0})^{1-d} + c.c, \tag{3.54}$$

for $d > 1$. Therefore, $\lim_{t\to\infty}\Gamma_{\mathbf{d}}^{(vac)}(t)$ exists for $d > 1$, and its value can be found by substituting Eq. (3.54) into Eq. (3.45). The existence of this limit means the vacuum decoherence function always reaches a proper plateau for $d > 1$ (cf. Sec. 3.4.2).

We now show the height of this plateau scales linearly with L for $d \geq 2$, and, for these d, simplify the exact expression for the height of the plateau. (This result need not imply superlinear scaling of the height of the plateau for $d < 2$.) Firstly,

$$\lim_{t\to\infty}\Gamma_{\mathbf{d}}(t) = \alpha_d\sum_{r=0}^{L-1} f_{\mathbf{d}r}\lim_{t\to\infty} I_r. \tag{3.55}$$

With $f_{\mathbf{d}0}{=}\|\mathbf{d}\|^2$, Eq. (3.54), and $Q_{00} = 1/(a\omega_c)$, the first term ($r = 0$) equals

$$\alpha_d\|\mathbf{d}\|^2\lim_{t\to\infty} I_0{=}\alpha_d\|\mathbf{d}\|^2\tilde{\Gamma}(d-1)\omega_c^{d-1}.$$

The remaining terms in Eq. (3.55) can be neglected. This is because they are upper bounded by

$$\begin{aligned}\mathcal{E} := \alpha_d \left| \sum_{r=1}^{L-1} f_{\mathbf{d}r} \lim_{t\to\infty} I_r \right| &< 2\alpha_d \|\mathbf{d}\|^2 \sum_{r=1}^{L-1} \left| \lim_{t\to\infty} I_r \right| \\ &\leq 2\alpha_d \|\mathbf{d}\|^2 \frac{1}{2} a^{1-d} \tilde{\Gamma}(d-1) \\ &\quad \times \sum_{r=1}^{L-1} \left| (Q_{r0})^{1-d} + c.c. \right| . \end{aligned} \tag{3.56}$$

For $r \geq 1$, $|Q_{r0}|>1$, and $d \geq 2$, we have

$$\begin{aligned}\left| (Q_{r0})^{1-d} + c.c. \right| &\leq \left| (Q_{r0})^{-1} + c.c. \right| \\ &= \frac{1}{a\omega_c} \frac{1}{r^2 + \frac{1}{(a\omega_c)^2}} \\ &< \frac{1}{a\omega_c} \frac{1}{r^2}. \end{aligned} \tag{3.57}$$

Thus, with $\sum_{r=1}^{L-1} 1/r^2 < 2$, we have for the sum in Eq. (3.56) that

$$\sum_{r=1}^{L-1} \left| (Q_{r0})^{1-d} + c.c. \right| < \frac{2}{a\omega_c}.$$

Therefore

$$\mathcal{E} < 2\alpha_d \|\mathbf{d}\|^2 a^{1-d} \tilde{\Gamma}(d-1) \frac{1}{a\omega_c}.$$

In conclusion, we have for $d \geq 2$,

$$\lim_{t\to\infty} \Gamma_{\mathbf{d}}^{(vac)}(t) = \alpha_d \|\mathbf{d}\|^2 \tilde{\Gamma}(d-1) \omega_c^{d-1} + \mathcal{E}, \tag{3.58}$$

with relative error

$$\begin{aligned}\tilde{\mathcal{E}} &:= \frac{\mathcal{E}}{\alpha_d \|\mathbf{d}\|^2 \tilde{\Gamma}(d-1) \omega_c^{d-1}} \\ &< \frac{2}{(a\omega_c)^d} \\ &< \frac{2}{a\omega_c}. \end{aligned}$$

The latter is negligible for $a\omega_c \gg 1$. Note that $\Gamma_{\mathbf{d}}^{(vac)}(t) = O(L)$ even if this condition does not hold.

***

Chapter 4

Dynamical fidelity susceptibility of decoherence-free subspaces

Abstract

In idealized models of a quantum register and its environment, quantum information can be stored indefinitely by encoding it into a decoherence-free subspace (DFS). Nevertheless, perturbations to the idealized register-environment coupling will cause decoherence in any realistic setting. Expanding a measure for state preservation, the dynamical fidelity, in powers of the strength of the perturbations, we prove stability to linear order is a generic property of quantum state evolution. The effect of noise perturbations is quantified by a concise expression for the strength of the quadratic, leading order, which we define as the dynamical fidelity susceptibility of DFSs. Under the physical restriction that noise acts on the register k-locally, this susceptibility is bounded from above by a polynomial in the system size. These general results are illustrated by three physically relevant examples. Knowledge of the susceptibility can be used to increase coherence times of future quantum computers.

4.1 Introduction

The biggest roadblock on the way to scalable quantum computation is decoherence [108, 138, 115]. Quantum error correction offers solutions to this problem [131, 96]. In active quantum error correction, errors have to be detected and corrected, whereas in passive error correction, the strategy is to avoid the errors by encoding. The two forms of error correction can be used in conjunction [94, 83], and can be described in the same mathematical framework [87].

An important player in the passive category is the decoherence-free subspace (DFS) [115, 40, 151, 147, 148, 95, 97, 83]. Although DFSs have been superseded theoretically by more general notions of passive error correction [24], they remain of interest both in theory and in practice [85, 23, 154]. In this technique, symmetries of the register-environment coupling are exploited to store quantum information in a register subspace whose reduced time evolution is purely unitary. In contrast to states outside of a DFS, those in it do not suffer from decoherence. Only register-environment models with enough symmetry allow for DFSs.

In real systems, there are small deviations from the idealized model of the interaction between the quantum register (the 'system') and the environment (the 'bath'). In particular, these may lead to superdecoherence (Chapter 3) even for states in a DFS. The quantification of the sensitivity of DFSs to perturbations has lead to the definition of the dynamical fidelity [95, 13].

The dynamical fidelity is a measure for the closeness of two states: (*i*) a state, possibly in a DFS, evolving in time under the original model, and (*ii*) the *same* initial state, evolving under the presence of an additional system-bath interaction whose strength is proportional to ε. At the initial time, the dynamical fidelity equals unity, but as time evolves the two states will start to diverge, decreasing the fidelity. The dynamical fidelity can be seen as a generalization of the Loschmidt echo [58] to open quantum systems, and is related the fidelity in the context of phase transitions [150, 146, 61]. In the latter, the fidelity measures the closeness between the ground states of Hamiltonians with different parameter values.

In an initial qualitative study [13], it was shown that the dynamical fidelity can only depend linearly on ε whenever the unperturbed system evolves unitarily on its own in a non-trivial way. This is so for non-degenerate logical states, or whenever the quantum register is used in a quantum computation. Conversely, they showed there is no term linear in ε whenever the quantum register does not evolve on

its own. This led to the conclusion that DFSs are 'robust' or 'stable' against perturbations when used as quantum memory, but not when used during a quantum computation [95, 13, 97, 6, 58, 39, 129, 128].

Here, we prove there never is a linear dependence on ε. In the parlance of the previous work, this means DFSs are also stable when used during a quantum computation. However, we show the result even holds for initial states outside of a DFS. In retrospect, the absence of a linear term in the expansion of the dynamical fidelity is a consequence of its definition, and not a property of DFSs. This can be considered positive for DFSs, because it shows states in a DFS do not react more strongly to perturbations than regular states. For the fidelity in the context of phase transitions the absence of a linear term was already known [150, 146, 61].

We go on to introduce the dynamical fidelity susceptibility of DFSs χ, 'susceptibility' for short (not to be confused with the characteristic function of Sec. 3.A), defined as the strength of the term in the dynamical fidelity proportional to $\varepsilon^2 t^2$.[1] As the first non-trivial term, the susceptibility quantifies the leading order sensitivity to perturbations of states in a DFS. Surprisingly, it does not depend on the unperturbed Hamiltonian, so the leading order behaviour of DFSs is as if there were no unperturbed system-bath interaction. Furthermore, it means our result can be used to study the behaviour of *any* state under perturbations, outside of the context of DFSs, as long as the unperturbed system-bath interaction vanishes because in that case the DFS of a quantum register is its entire Hilbert space. Even though physically the leading order in time is the most interesting, we later generalize to include all orders in time for completeness.

For general perturbations, we show the susceptibility is bounded from above by an exponential in the system size, $\chi = O(2^{4n})$, with n the number of qubits. A DFS for which the susceptibility increases exponentially should be considered non-scalable in any practical sense. However, noise can typically be described by a k-local Hamiltonian (Sec. 1.4.4), which enforces a more favourable scaling with n. The most commonly considered case is $k = 1$, which describes completely local noise [108]. For general k-local perturbing noise, the susceptibility is shown to be bounded from above by a polynomial, $\chi = O(n^{2k})$. This can be compared to the related result on active error correction by Preskill [121], and impacts the scalability of quantum computation [72,

[1] A quantity called the 'dynamical fidelity susceptibility' was also introduced in [103]. Despite the name, this refers to something different; it refers to the fidelity between a thermal state (under some Hamiltonian) and the same state after being time evolved by a perturbed Hamiltonian.

73] using DFSs.

To illustrate these results, we compute the susceptibility of a highly non-classical state, the GHZ state, in two types of DFS. The first protects against pure collective dephasing, the second additionally against collective emission and absorption. We find $\chi = n^2/4$ and $\chi = n/3$, respectively. Similar scaling laws were found before [115, 26, 104] for non-DFS states, and, in fact, DFSs were designed to prevent such scaling laws. Our work shows that these scaling laws are still present in practice. To connect to Chapter 3, we also compute the dynamical fidelity susceptibility caused by a general spin boson dephasing model. The result shows the relation between the dephasing susceptibility of Chapter 3 and the dynamical fidelity susceptibility of the current chapter.

4.2 The dynamical fidelity

Consider a system S in a bath B, as in Sec. 1.4.3. In the context of quantum computation, S is the collection of qubits, the quantum register, and B is the environment, such as the electromagnetic field. In general, the Hamiltonian on these systems can be written in the form

$$H_0 = H_S \otimes \mathbb{1} + \mathbb{1} \otimes H_B + H_{SB}, \tag{4.1}$$

where H_S (H_B) acts only on S (B) and H_{SB} is a system-bath interaction term. In an ongoing quantum computation, H_S includes the generators of the gates (also see Sec. 1.5.1).

Assume that at $t = 0$ we have a product state $\rho_{SB,\text{init}} = |\Psi\rangle\langle\Psi|$, with $|\Psi\rangle = |\psi\rangle \otimes |\varphi_0\rangle$. The reduced time evolution that is induced by the Hamiltonian (4.1) is detailed in Sec. 1.4.6. The essential aspects will be summarized here. For a non-trivial H_{SB} the Hamiltonian (4.1) will induce entanglement between S and B. Tracing out B, the pure system state $|\psi\rangle\langle\psi|$ at time $t = 0$ will generally be mapped to a mixed system state at $t > 0$ by time evolution. We denote this map, or quantum channel, by $\mathcal{A}(t) = \mathcal{A}$. For every $t \geq 0$ we have a quantum channel. The system state after time t equals $\rho_S(t) \equiv \mathcal{A}[|\psi\rangle\langle\psi|] = \text{tr}_B(e^{-itH}|\Psi\rangle\langle\Psi|e^{itH})$ in units where $\hbar = 1$. This can be rewritten by introducing the Kraus operators $A_i(t) \equiv \langle\varphi_i|e^{-itH}|\varphi_0\rangle$, where $\{|\varphi_i\rangle\}$ forms an orthonormal basis for $\mathcal{H}_B$, with $|\varphi_0\rangle$ the initial bath state. Since H_0 acts on both $\mathcal{H}_S$ and $\mathcal{H}_B$, and the $\{|\varphi_i\rangle\}$ are bath states, $A_i(t)$ acts non-trivially on $\mathcal{H}_S$ only. Thus the operator sum representation

(OSR) of $\mathcal{A}$ is obtained,

$$\mathcal{A}[|\psi\rangle\langle\psi|] = \sum_i A_i(t)\,|\psi\rangle\langle\psi|\,A_i^\dagger(t). \tag{4.2}$$

Because $\mathcal{A}$ is trace-preserving, we have the normalization condition $\sum_i A_i^\dagger(t)A_i(t) = \mathbb{1}$.

In general, $\mathcal{A}$ may map pure states to mixed states. A DFS, on the other hand, is defined as a subspace $D \subset \mathcal{H}_S$ for which, despite coupling to the bath via H, $\mathcal{A}[|\psi\rangle\langle\psi|] = e^{-\mathrm{i}tH_S}\,|\psi\rangle\langle\psi|\,e^{\mathrm{i}tH_S}$ for all $|\psi\rangle \in D$, where $e^{-\mathrm{i}tH_S}\,|\psi\rangle$ has to remain in D [151, 95]. Thus, pure states in a DFS are mapped to pure states in the same DFS by $\mathcal{A}$. In terms of the OSR, a necessary and sufficient condition for $|\psi\rangle \in D$ is $A_j\,|\psi\rangle = g_j e^{-\mathrm{i}tH_S}\,|\psi\rangle$ for all j, where $\sum_j |g_j|^2 = 1$ [97, 13]. We do not assume $|\psi\rangle \in D$ unless stated otherwise.

Consider the perturbation V to the Hamiltonian H_0,

$$H = H_0 + \varepsilon V, \tag{4.3}$$

where ε is a real parameter. (The ε-dependence of H is suppressed in the notation.) The system state after time t now also depends on ε, and the OSR of the map induced by H is $\rho_S(\varepsilon,t) \equiv \mathcal{A}_\varepsilon[|\psi\rangle\langle\psi|] = \sum_i A_i(\varepsilon,t)\,|\psi\rangle\langle\psi|\,A_i^\dagger(\varepsilon,t)$ with $A_i(\varepsilon,t) = \langle\varphi_i|\,e^{-\mathrm{i}tH}\,|\varphi_0\rangle$. Since the exponential map is analytic, the Kraus operators of the perturbed map may be expanded around $\varepsilon = 0$ as

$$A_i(\varepsilon,t) = A_i^{(0)}(t) + \varepsilon A_i^{(1)}(t) + \varepsilon^2 A_i^{(2)}(t) + O(\varepsilon^3). \tag{4.4}$$

Here, $A_i^{(1)}(t) = \langle\varphi_i|-\mathrm{i}tV - t^2(H_0V+VH_0)/2 + O(t^3)\,|\varphi_0\rangle$. The explicit form of $A_i^{(2)}(t)$ is of no interest because it will be eliminated. We do not allow qubits to leave the system, so even the perturbed quantum channel needs to be trace-preserving. Thus, $\sum_i A_i^\dagger(\varepsilon,t)A_i(\varepsilon,t) = \mathbb{1}$ for all real ε and t. After the expansion (4.4) is substituted this imposes

$$\sum_i \left(A_i^{(0)\dagger}(t)A_i^{(1)}(t) + A_i^{(1)\dagger}(t)A_i^{(0)}(t)\right) = 0, \tag{4.5}$$

$$\sum_i \left(A_i^{(0)\dagger}(t)A_i^{(2)}(t) + A_i^{(1)\dagger}(t)A_i^{(1)}(t) + A_i^{(2)\dagger}(t)A_i^{(0)}(t)\right) = 0. \tag{4.6}$$

Conditions involving higher orders of the expansion can be obtained similarly. The above relations are general, since they put constraints on perturbations to general quantum channels, applicable outside the present context. There are no separate conditions that follow from

the complete positivity of $\mathcal{A}_\varepsilon$; any map that has OSR is automatically completely positive. If one is interested in the effects of a perturbation of the Kraus operators rather than a perturbation of the Hamiltonian, Eq. (4.4) is the starting point.

In general, the fidelity between two states is defined as $F(\sigma,\eta) = \left[\mathrm{tr}\sqrt{\sqrt{\sigma}\eta\sqrt{\sigma}}\right]^2$ [71]. The effect of a perturbation on the dynamics may be quantified by the dynamical fidelity F, that is, the fidelity between the state as obtained after the unperturbed time evolution and the state after the perturbed time evolution, $F \equiv F[\rho_S(0,t),\rho_S(\varepsilon,t)]$. Often it is impractical to compute the fidelity because of the square roots. However, if $\rho_{S,\mathrm{init}} = |\psi\rangle\langle\psi|$, and $|\psi\rangle$ in in a DFS such that the state remains pure for all $t > 0$, the dynamical fidelity simplifies to

$$F = \langle\psi(t)|\,\rho_S(\varepsilon,t)\,|\psi(t)\rangle\,, \tag{4.7}$$

with $|\psi(t)\rangle = U(t)\,|\psi\rangle \equiv e^{-\mathrm{i}tH_S}\,|\psi\rangle$.

4.3 Expansion of the dynamical fidelity

The dynamical fidelity F is analytic in ε at $\varepsilon = 0$ because it is a composition of analytical functions of ε. A careful, elementary proof of this statement is given Sec. 4.A. Now, F may be expanded for small ε if the perturbation is weak,

$$F = 1 + \varepsilon F^{(1)} + \varepsilon^2 F^{(2)} + \ldots. \tag{4.8}$$

It has previously been shown that $F^{(1)} = 0$ whenever $H_S = 0$ and $|\psi\rangle$ in a DFS, which leaves open the possibility that $F^{(1)} \neq 0$ when $H_S \neq 0$, even though $|\psi\rangle$ is in a DFS [13].

However, $F^{(1)} = 0$ in all cases and at all times, even without assuming $|\psi\rangle$ to be in a DFS [as opposed to in Eq. (4.7)]. This is a direct consequence of the following theorem, together with the fact that $\rho_S(\varepsilon,t)$ is analytic in ε at $\varepsilon = 0$ for all t, as is clear from Eq. (4.4).

Theorem 4.3.1. *Let $\{\sigma(\varepsilon)\}$ be a family of finite-dimensional density matrices that is analytic at $\varepsilon = 0$, and let $F[\sigma(0),\sigma(\varepsilon)]$ denote the fidelity between $\sigma(0)$ and $\sigma(\varepsilon)$. Then $F^{(1)} \equiv \frac{d}{d\varepsilon}F[\sigma(0),\sigma(\varepsilon)]|_{\varepsilon=0} = 0$.*

Proof. $F[\sigma(0),\sigma(\varepsilon)]$ is analytic in ε at $\varepsilon = 0$. Because $0 \leq F \leq 1$ for any real ε, and $F[\sigma(0),\sigma(0)] = 1$, it follows that $F^{(1)}$ must always vanish. □

The theorem also follows from the connection of the fidelity to the Bures metric tensor [67, 116]. We elaborate more on this relation in Sec. 4.C. This relation of the theorem to the robustness of DFSs, which we make clear by the elementary considerations above, was not noticed before. In fact, it is opposite to previous suggestions that continue to proliferate in the literature [95, 13, 97, 6, 58, 39, 129, 128].

The theorem also applies when time evolution is generated by a Lindbladian $\mathcal{L}$, again even if the initial state is not in a DFS. See Sec. 1.4.6.3 for a detailed background on Lindbladians. We perturb the Lindbladian, as it is also done in [149, 5], by

$$H \to H + \varepsilon V,$$
$$L_k \to L_k + \varepsilon L'_k,$$

with H the Hamiltonian and L_k the Lindblad operators [Eq. (1.36)]. The effect on the Lindbladian is $\mathcal{L} \to \mathcal{L} + \varepsilon\mathcal{L}' + \varepsilon^2\mathcal{L}''$ for some finite, constant linear superoperators $\mathcal{L}'$ and $\mathcal{L}''$. The exponential map of an analytical matrix is analytical. When we see $\mathcal{L}$, $\mathcal{L}'$ and $\mathcal{L}''$ as matrices (see Secs. 1.4.6.2 and 1.4.6.3), it is evident that $\rho_S(\varepsilon, t) = e^{t(\mathcal{L}+\varepsilon\mathcal{L}'+\varepsilon^2\mathcal{L}'')}\rho_{S,\text{init}}$ is analytical in ε at $\varepsilon = 0$ for all $t \geq 0$. It is then a direct consequence of Theorem 4.3.1 that $F^{(1)} = 0$ also in the Lindblad-setting.

We now return to the OSR [Eq. (4.2)], and consider $F^{(2)}$. We stress that now we do assume $|\psi\rangle$ to be in a DFS. Combining Eqs. (4.2), (4.4), and (4.7), we find $F^{(1)} = \sum_i \langle\psi| A_i^{(0)\dagger}(t)A_i^{(1)}(t) + A_i^{(1)\dagger}(t)A_i^{(0)}(t) |\psi\rangle$ and $F^{(2)} = \sum_i \langle\psi| A_i^{(0)\dagger}(t)A_i^{(2)}(t) + A_i^{(2)\dagger}(t)A_i^{(0)}(t) |\psi\rangle + |\langle\psi| e^{itH_S} A_i^{(1)}(t) |\psi\rangle|^2$. At this point it seems that $F^{(1)} \neq 0$. By the normalization condition on perturbed Kraus operators [Eq. (4.5)], however, it follows that $F^{(1)} = 0$. The second condition [Eq. (4.6)] is crucial in obtaining a concise expression for $F^{(2)}$, as it can be used to eliminate $A_i^{(0)}(t)$ and $A_i^{(2)}(t)$. This yields

$$F^{(2)} = -\sum_i \sigma_\psi^2[U^\dagger(t)A_i^{(1)}(t)], \tag{4.9}$$

with $U(t) = e^{-itH_S}$, and $\sigma_\psi^2[O] \equiv \langle\psi| O^\dagger O |\psi\rangle - |\langle\psi| O |\psi\rangle|^2$. Equation (4.9) describes the effect of a perturbation to the Kraus operators on the dynamics of states in a DFS. The entire procedure above can be straightforwardly extended to higher orders in ε.

4.4 Susceptibility

We now consider the short-time expansion of $F^{(2)}$. The first non-vanishing term is proportional to t^2. We define the proportionality constant χ (with an extra minus sign) as *the dynamical fidelity susceptibility of DFSs*. That is, $\chi = -\frac{1}{4}\frac{\partial^2}{\partial\varepsilon^2}\frac{\partial^2 F}{\partial t^2}|_{\varepsilon,t=0}$, so that

$$F = 1 - \chi\,\varepsilon^2 t^2 + O(\varepsilon^2 t^4). \tag{4.10}$$

This is not yet a computation but only a definition. To obtain an expression for χ involving H, note that, in general, the perturbing Hamiltonian can be written as $V = \sum_\alpha S_\alpha \otimes B_\alpha$.[2] We substitute $A_i^{(1)}(t) = \langle\varphi_i| - itV\,|\varphi_0\rangle + O(t^2)$ into Eq. (4.9) and collect terms proportional to $\varepsilon^2 t^2$. Using the (connected) system correlation function $\mathbf{S}$ with matrix elements $\mathbf{S}_{\alpha\beta} = \langle\psi|\,S_\alpha^\dagger S_\beta\,|\psi\rangle - \langle\psi|\,S_\alpha^\dagger\,|\psi\rangle\,\langle\psi|\,S_\beta\,|\psi\rangle$ and the bath correlation function $\mathbf{B}_{\alpha\beta} = \langle\varphi_0|\,B_\alpha^\dagger B_\beta\,|\varphi_0\rangle$, the result can be written as

$$\chi = \mathrm{tr}(\mathbf{B}\mathbf{S}^T). \tag{4.11}$$

Here, the trace is not over $\mathcal{H}_S$ or $\mathcal{H}_B$ but over the indices of the correlation functions. When V is a simple tensor product, $V = S \otimes B$, this reduces to $\chi = \langle\varphi_0|\,B^2\,|\varphi_0\rangle\,\sigma_\psi^2[S]$.

Equation (4.11) assumes the initial system state to be in a DFS, but does not depend directly on H_{SB}. So in particular, it holds for $H_{SB} = 0$, in which case the DFS is all of $\mathcal{H}_S$. Thus Eq. (4.11) can be used outside of the context of DFSs to study the effects of perturbative system-bath coupling as long as there is no initial system-bath coupling.

Mathematically, the only restriction on V is its Hermiticity. For S a qubit register with n qubits, any V may be written as $V = \sum_\alpha c_\alpha \mathcal{P}_\alpha \otimes B_\alpha$, with c^α real, $\mathcal{P}^\alpha$ elements of the Pauli group $\{\mathbb{1}, \sigma_x, \sigma_y, \sigma_z\}^{\otimes n}$ (see Sec. 1.4.4), and B_α bath operators. In this form there are at most $4^n = 2^{2n}$ linearly independent terms. Under the assumption that adding a qubit does not change how the former qubits couple to the bath, we have that c_α and B_α do not depend on n. It then follows from Eq. (4.11) that $\chi = O(2^{4n})$. Now consider the physical restriction that V acts k-locally on the system, which means that every S_α acts on no

[2] Any operator on $\mathcal{H}_{SB}$ can be written as $V = \sum_{ij} v_{ij} F_i \otimes G_j$, with F_i and G_j operator bases for $\mathcal{H}_S$ and $\mathcal{H}_B$, respectively. If we write out the sum in an arbitrary but specific order, we can label these terms with integers α. Absorbing v_{ij} into the system operator in every term (we may as well absorb it into the bath operator), writing the system operator in that same term α as S_α, the bath operator in term B_α, we may write $V = \sum_\alpha S_\alpha \otimes B_\alpha$.

more than k qubits, with k independent of n. Then V contains $O(n^k)$ terms. By Eq. (4.11) it thus follows that $\chi = O(n^{2k})$.

4.5 Three examples

Here we calculate χ explicitly in three examples. Although χ does not depend on the unperturbed Hamiltonian, we describe possible unperturbed Hamiltonians to give physical context.

4.5.1 Long wavelength dephasing

For the first example, consider the DFS that is currently used in ion-trap quantum computers [86, 85]. The register-environment model is that of collinear single-reservoir collective dephasing (Chapter 3) in the long wavelength limit, which is the main source of decoherence for unencoded quantum states in this setup [104]. The system-bath interaction term of the model is given by [cf. Eq. (3.6)]

$$H_{SB} = J^z_{\text{tot}} \otimes \sum_k (g_k a_k + g_k^* a_k^\dagger),$$

with $J^z_{\text{tot}} = \sum_{i=1}^n \sigma_i^z/2$ the z-component of the total spin operator, where σ_i^z is the the Pauli z-operator that only acts on qubit i, g_k the register-environment coupling strength, a_k ($a_k^\dagger$) the annihilation (creation) operator of a collinear an electromagnetic mode with wavenumber k and polarization along the z-axis, and n the number of physical qubits.

Using two physical qubits ($n = 2$), one logical qubit is protected from the decohering influence of H_{SB} by encoding it in the DFS spanned by the logical states $|\bar{0}\rangle = |01\rangle$ and $|\bar{1}\rangle = |10\rangle$. For $n > 2$ even, the qubits are paired, and each pair encodes one logical qubit. The GHZ state is highly non-classical and known to be highly sensitive to the environment, which is why it is used in quantum metrology [57] and as a probe for the preservation of coherence [104]. It can be protected by encoding it as $|\psi\rangle = (|\bar{0}\rangle^{n/2} + |\bar{1}\rangle^{n/2})/\sqrt{2}$.

We perturb the model by adding a bosonic mode that couples to the staggered magnetic moment of the system. This corresponds to an electromagnetic mode with wavelength π/d (in units where $c = 1$) coupling locally to the individual spin operators,

$$\varepsilon V = \varepsilon J^z_{\text{stag}} \otimes (a_{\pi/d} + a^\dagger_{\pi/d}), \tag{4.12}$$

where $J^z_{\text{stag}} = \sum_{i=1}^{n}(-1)^i\sigma_i^z/2$. We take the state of the perturbing mode to be the vacuum, that is, the state $|\varphi_0\rangle$ such that $a_{\pi/d}\,|\varphi_0\rangle = 0$. [The state of the other modes is irrelevant, see Eq. (4.11).] This state is chosen because it forms a best-case scenario; the thermal bath can at best be at zero temperature. The computation is not more involved when the thermal or number state is assumed. With all definitions in place, we can directly apply Eq. (4.11), to find

$$\chi = \frac{1}{4}n^2.$$

This example saturates the bound on the system size scaling for a completely local noise model.

4.5.2 Long wavelength dephasing, absorption and emission

For our second example, we consider a DFS that, next to dephasing, includes protection against collective absorption and emission of radiation [147, 97]. To the best of our knowledge, at the moment this DFS is not used in quantum computers. The coupling term in the unperturbed Hamiltonian reads

$$H_{SB} = \sum_k [f_k J^+ a_k + g_k J^- a_k^\dagger + J^z_{\text{tot}}(h_k a_k + h_k^* a_k^\dagger)]$$

(with tensor products omitted). Here, $J^\pm = \sum_{i=1}^{n}\sigma_i^\pm/2$ excites (relaxes) the system collectively, with $\sigma_i^\pm = \sigma_i^x \pm i\sigma_i^y$ a combination of Pauli operators, and with coupling constants f_k, g_k and h_k. Other symbols are defined as before. For four qubits, two logical states that span a DFS that protects against H_{SB} are

$$\begin{aligned}|\bar{0}\rangle &= |s\rangle \otimes |s\rangle\,,\\ |\bar{1}\rangle &= (|t_1 t_{-1}\rangle + |t_{-1}t_1\rangle - |t_0 t_0\rangle)/\sqrt{3},\end{aligned}$$

with $|s\rangle$ and $|t_i\rangle$ the singlet and the triplet,

$$|s\rangle = (|01\rangle - |10\rangle)/\sqrt{2}, \qquad \begin{cases} |t_{-1}\rangle = |11\rangle \\ |t_0\rangle = (|01\rangle + |10\rangle)/\sqrt{2} \\ |t_1\rangle = |00\rangle\,. \end{cases}$$

The system state we consider here is similar to that in the first example, $|\psi\rangle = (|\bar{0}\rangle^{n/4} + |\bar{1}\rangle^{n/4})/\sqrt{2}$. It is in the DFS of H_{SB} for $n \geq 4$ a multiple of 4. It is an encoded GHZ state when the larger DFS is constructed by

simple concatenation of single logical qubit DFSs, like in the previous example, but other methods exist [147, 97].

As the perturbation, we again consider a staggered field, with εV as in the previous example [Eq. (4.12)]. Also, we assume the perturbing mode to be in the vacuum state. Using Eq. (4.11), a computation shows that

$$\chi = \frac{1}{3}n,$$

for $n > 4$ a multiple of 4. (For $n = 4$ the prefactor is different.)

4.5.3 Discussion

In both of the examples discussed so far, V acts on the system 1-locally, but only in the first example the bound on χ for 1-local perturbations is saturated. Even though χ scales polynomially with n in both examples, the different powers can be an important distinction in practice. The difference can be traced back to the fact that, in the first example, both branches of the superposition that make up the encoded GHZ state are eigenstates of σ_i^z. That is, $\sigma_i^z \left|\bar{0}\right\rangle^{n/2} = \pm \left|\bar{0}\right\rangle^{n/2}$ and similarly for $\left|\bar{1}\right\rangle^{n/2}$. This results in non-zero 'inter-block cross terms' such as $\left\langle\bar{0}\right|^{n/2} \sigma_i^z \sigma_j^z \left|\bar{0}\right\rangle^{n/2}$, for i, j belonging to a different pair of qubits. There are $\sim n^2$ of those terms, and thus χ scales with n^2. In contrast, in the second example, the states $\left|\bar{0}\right\rangle^{n/4}$ and $\left|\bar{1}\right\rangle^{n/4}$ are not eigenstates of σ_i^z. This leads to vanishing 'inter-block cross terms', such as $\left\langle\bar{0}\right|^{n/4} \sigma_i^z \sigma_j^z \left|\bar{0}\right\rangle^{n/4}$ where i, j belong to different groups of four qubits. When $i = j$, $\sigma_i^z \sigma_j^z = \mathbb{1}$. There are $\sim n$ of such terms, and hence χ scales as n.

4.5.4 Full dephasing

For our third example, we take the $H_{SB} = 0$. In that case, the DFS spans the entire system Hilbert space. As the perturbation, we consider the interaction term of the complete single-reservoir dephasing model of the previous chapter [Eq. (3.6)]. We assume the reservoir is in some product state of number states. We consider any system state that is of the form $\left|\psi\right\rangle = (\left|\mathbf{i}\right\rangle + \left|\mathbf{j}\right\rangle)/\sqrt{2}$. After substituting $g_{\mathbf{k}} \to \varepsilon g_{\mathbf{k}}$, the Hamiltonian of the single-reservoir dephasing model [Eq. (3.6)] is of the form of Eq. (4.3), with $H_{SB} = 0$, $\varepsilon V = \varepsilon \sum_\ell S_\ell \otimes B_\ell$, where

$$S_\ell = J_\ell^z, \qquad B_\ell = \sum_{\mathbf{k}} (g_{\mathbf{k}\ell}^* a_{\mathbf{k}} + g_{\mathbf{k}\ell} a_{\mathbf{k}}^\dagger).$$

For system states of the form $|\psi\rangle = (|\mathbf{i}\rangle + |\mathbf{j}\rangle)/\sqrt{2}$, we find

$$\chi = \frac{1}{4}\sum_{\ell m \mathbf{k}\mathbf{k}'} \mathbf{d}_\ell \mathbf{d}_m \left[g_{\mathbf{k}\ell} g^*_{\mathbf{k}'m} (\delta_{\mathbf{k}\mathbf{k}'} + 2\langle a^\dagger_{\mathbf{k}} a_{\mathbf{k}'}\rangle_\varphi) + g_{\mathbf{k}\ell} g_{\mathbf{k}'m} \langle a^\dagger_{\mathbf{k}} a^\dagger_{\mathbf{k}'}\rangle_\varphi + c.c. \right],$$

with $\mathbf{d} = \mathbf{i} - \mathbf{j}$, and where *c.c.* stands for the complex conjugate of the preceding term only. Using that $|\varphi\rangle$ is a product of number states, we have

$$\chi = \frac{1}{4}\sum_{\ell m \mathbf{k}} \mathbf{d}_\ell \mathbf{d}_m g_{\mathbf{k}\ell} g^*_{\mathbf{k}m} (1 + 2\langle N_{\mathbf{k}}\rangle_\varphi).$$

Using plane waves, $g_{\mathbf{k}\ell} = g_{\mathbf{k}}, e^{i\mathbf{k}\cdot\mathbf{r}_\ell}$ and introducing the dephasing susceptibility $\gamma_{\mathbf{d}}(\mathbf{k})$ as the spectral density of $\mathbf{d}$ (see Sec. 3.3), we obtain

$$\chi = \frac{1}{4}\sum_{\mathbf{k}} |g_{\mathbf{k}}|^2 \gamma_{\mathbf{d}}(\mathbf{k})(1 + 2\langle N_{\mathbf{k}}\rangle_\varphi). \tag{4.13}$$

This says that, per momentum $\mathbf{k}$, the leading order effect of turning on a system-bath coupling between a quantum register and a single dephasing reservoir is essentially the dephasing susceptibility $\gamma_{\mathbf{d}}(\mathbf{k})$ multiplied by the occupation of that mode, $(1 + 2\langle N_{\mathbf{k}}\rangle_\varphi)$, where the addition of unity accounts for the vacuum effects. This supports our interpretation of the dephasing susceptibility as an important physical quantity in the study of the dephasing of quantum registers.

Note that here we have obtained χ without ever solving for the reduced time evolution of the system state, showing the potential of Eq. (4.11). In fact, with Eq. (4.13) we have already obtained a result that could not be obtained by using the solution of the full time evolution of the spin-boson single-reservoir dephasing model, because the latter relies on the assumption that the initial reservoir state is a displaced thermal state. Equation (4.13) holds for a product of number states, some of which cannot be described as a displaced thermal state. We can take the continuum limit of Eq. (4.13), just as we have done Chapter 3, and show, in exactly the same way, that $\chi = O(L)$ in bounded reservoirs. This extends the results of Chapter 3 to include reservoir states that are products of number states, albeit only for the leading order in time.

4.6 Generalization to all orders in time

Here, we derive an expression for $F^{(2)}$ [Eq. (4.9)] that includes all orders in time, as opposed to Eq. (4.11). To do so, we go to the interaction picture, denoted by the superscript I. (If there is no

superscript denoting the picture the Schrödinger picture is assumed here.) See Secs. 1.4.5.3 and 1.4.6.1 for a detailed introduction to the interaction picture in open quantum systems. To summarize, in the interaction picture, the initial SB state at $t = 0$, which is equal in any picture, evolves as $\rho^I_{SB}(\varepsilon, t) = U^I(t)\rho_{SB,\text{init}}U^{I\dagger}(t)$, with $U^I(t) = e^{itH_0}e^{-itH} = Te^{-i\varepsilon\int_0^t dt' H^I(t')}$. The operator $U^I(t)$ depends also on ε but this notation is suppressed in $U^I(t)$ and its dependencies. Here, T is the time-ordering operator and $H^I(t)$ is the interaction picture Hamiltonian $\varepsilon H^I(t) = e^{itH_0}\varepsilon V e^{-itH_0}$. As before, the Schrödinger picture operator H_0 contains the system and bath Hamiltonians, and the original coupling H_{SB}, against which the system state is protected by the DFS. The perturbed Hamiltonian H contains an extra perturbation εV which causes the system state to decohere.

Assuming, as before, that $\rho_{SB,\text{init}} = |\psi\rangle\langle\psi| \otimes |\varphi_0\rangle\langle\varphi_0|$, and that $|\psi\rangle$ is in a DFS, we find the dynamical fidelity equals

$$F = \langle\psi|\, \rho^I_S(\varepsilon, t)\, |\psi\rangle\,, \tag{4.14}$$

with $\rho^I_S(\varepsilon, t) \equiv \text{tr}_B[\rho^I_S(\varepsilon, t)]$ the interaction picture system state. Note that, like the expectation value of operators, the fidelity is invariant under change of picture even though states and operators are not.

The state $\rho^I_S(\varepsilon, t)$ can be expressed as

$$\rho^I_S(\varepsilon, t) = \sum_i A^I_i(\varepsilon, t)\, |\psi\rangle\langle\psi|\, A^{I\dagger}_i(\varepsilon, t),$$

where we define the *interaction picture Kraus operators*,

$$A^I_i(\varepsilon, t) = \langle\varphi_i|\, U^I(t)\, |\varphi_0\rangle\,.$$

Using the Dyson series (Sec. 1.4.5.1), we can expand the interaction picture Kraus operators as

$$A^I_i(\varepsilon, t) = A^{I(0)}_i(t) + \varepsilon A^{I(1)}_i(t) + \varepsilon^2 A^{I(2)}_i(t) + \ldots,$$

where now $A^{I(0)}_i(t) = A^{I(0)}_i = \langle\varphi_i|\varphi_0\rangle$, and

$$A^{I(1)}_i(t) = -i\int_0^t dt'\ \langle\varphi_i|\, H^I(t')\, |\varphi_0\rangle\,. \tag{4.15}$$

A similar expression holds for $A^{I(2)}_i(t)$, but it is of no interest here because it is eliminated by using the normalization conditions in Eqs. (4.5) and (4.6) in their interaction form, which amounts to putting a superscript I everywhere.

Comparing the expression for F in the Schrödinger picture [Eq. (4.7)] to that in the interaction picture [Eq. (4.14)], we see they are essentially equal. The difference is that, in the interaction picture, the extra factor $U(t)$ is absent, and that the state is not $\rho_S(\varepsilon, t)$ but $\rho_S^I(\varepsilon, t)$. Since we have similar expressions for these states in terms of the (interaction picture) Kraus operators, it is straightforward to show that

$$F^{(2)} = -\sum_i \sigma_\psi^2[A_i^{I(1)}(t)], \tag{4.16}$$

with σ_ψ^2 defined as before. Of course $F^{(2)}$ itself is invariant under change of picture, it is just the expression that changes form. Also note the absence of $A_i^{I(2)}(t)$ and thus any time ordering. This absence is due to the normalization conditions Eqs. (4.5) and (4.6) in their interaction form. Equation (4.16) says that the change of fidelity in a DFS, due to an extra system-bath coupling εV, is proportional to the sum of the auto-correlation functions of the interaction picture Kraus operators.

We can gain further insight into the change of fidelity by studying how the $A_i^{I(1)}(t)$ depend on the specific system and bath operators appearing in $V = \sum_\alpha S_\alpha \otimes B_\alpha$. To do so we *define* $S_\alpha^I(t)$ and $B_\alpha^I(t)$ by

$$H^I(t) = \sum_\alpha S_\alpha^I(t) \otimes B_\alpha^I(t). \tag{4.17}$$

Given any $H^I(t)$ (or equivalently any V), such $S_\alpha^I(t)$ and $B_\alpha^I(t)$ can always be found. Note that only in the case $H_{SB} = 0$, from which it follows that $e^{\mathrm{i}tH_0} = e^{\mathrm{i}tH_S} e^{\mathrm{i}tH_B}$, we may choose $S_\alpha^I(t) = e^{\mathrm{i}tH_S} S_\alpha e^{-\mathrm{i}tH_S}$ and $B_\alpha^I(t) = e^{\mathrm{i}tH_B} B_\alpha e^{-\mathrm{i}tH_B}$.

Plugging Eq. (4.17) into Eq. (4.15), and the result into Eq. (4.16), we find the generalization of Eqs. (4.10) and (4.11),

$$F = 1 - \varepsilon^2 \int_0^t \mathrm{d}t' \mathrm{d}t'' \, \mathrm{tr}[\mathbf{B}(t', t'')\mathbf{S}^T(t', t'')] + O(\varepsilon^3), \tag{4.18}$$

with correlation functions

$$\mathbf{B}_{\alpha\beta}(t', t'') = \langle \varphi_0 | \, B_\alpha^{I\dagger}(t') B_\beta^I(t'') \, | \varphi_0 \rangle \,,$$
$$\mathbf{S}_{\alpha\beta}(t', t'') = \langle \psi | \, S_\alpha^{I\dagger}(t') S_\beta^I(t'') \, | \psi \rangle - \langle \psi | \, S_\alpha^{I\dagger}(t') \, | \psi \rangle \, \langle \psi | \, S_\beta^I(t'') \, | \psi \rangle \,.$$

4.7 Conclusion

Using the dynamical fidelity, we quantified the behaviour of DFSs under perturbations of the system-bath interaction. The response to perturbations is of second order. We defined the strength of this second

order as the dynamical fidelity susceptibility. It does not depend on the unperturbed system-bath interaction, so to leading order, states in a DFS respond to perturbations as if there were no unperturbed coupling. Our expressions are applicable outside the context of DFSs whenever the perturbation is the only system-bath interaction.

Instead of the robustness or stability of DFSs, we put forward the scaling of the susceptibility with the system size to assess the value of DFSs. For general perturbations, the susceptibility is upper bounded by an exponential in the system size. However, under the restriction of k-locality of the system operators appearing in the perturbation, the upper bound is polynomial. Therefore, DFSs can be considered scalable in theory. It remains to be shown that perturbations can be made sufficiently weak and uncorrelated to allow practical use of DFSs in large-scale quantum computers.

By identifying the 'good' DFSs, the susceptibility is a tool to increase coherence times. Our quantitative results could be generalized to arbitrary system states, and to more general forms of passive error correcting, such as noiseless subsystems. They could also be adjusted to yield the average-case susceptibility or the worst-case susceptibility.

Appendix

4.A Analyticity of the Fidelity

Here we prove a lemma concerning the fidelity

$$F(\rho,\sigma) = \left[\mathrm{tr}\sqrt{\sqrt{\rho}\sigma\sqrt{\rho}}\right]^2 .$$

Note that in the following, we do not assume ρ or σ to be in a DFS.

Lemma 4.A.1. *Let $\{\sigma(\varepsilon)\}$ be a family of finite-dimensional density matrices that is analytic at $\varepsilon = 0$. Then the fidelity $F[\sigma(0),\sigma(\varepsilon)]$ is analytic at $\varepsilon = 0$.*

Proof. Since $\sigma(\varepsilon)$ is analytic we may expand it as a power series, $\sigma(\varepsilon) = \sigma^{(0)}+\varepsilon\sigma^{(1)}+\varepsilon^2\sigma^{(2)}+\ldots$, where the $\sigma^{(i)}$ are constant and finite. Suppose $\sigma^{(0)}$ is given as an $N\times N$ matrix, and let $\{p_1,\ldots p_m\}$, with $1\leq m\leq N$, be its (not necessarily distinct) non-zero eigenvalues. There exists a basis in which $\sigma^{(0)} = \mathrm{diag}(p_1,\ldots,p_m,0,\ldots,0)$. Naturally, in this basis, $\sqrt{\sigma^{(0)}} = \mathrm{diag}(\sqrt{p_1},\ldots,\sqrt{p_m},0,\ldots,0)$. Note that this is a projector

onto the non-zero eigenspace of $\sigma^{(0)}$. Thus

$$F[\sigma(0), \sigma(\varepsilon)] = \left[\mathrm{tr}\sqrt{(\sigma^{(0)})^2 + \varepsilon\sqrt{\sigma^{(0)}}\sigma^{(1)}\sqrt{\sigma^{(0)}} + \ldots}\right]^2$$
$$\equiv \left[\mathrm{tr}\sqrt{M(\varepsilon)}\right]^2,$$

where $M(\varepsilon) = M^{(0)} + \varepsilon M^{(1)} + \ldots$, with $M^{(0)} = \mathrm{diag}[(p_1)^2, \ldots, (p_m)^2]$. Here we have used the fact that all matrices in the expansion of $\sigma(\varepsilon)$ are projected onto the zero-eigenspace of $\sigma^{(0)}$ so that we can reduce the dimension of the matrix under the square root. Thus, the $M^{(i)}$ are constant matrices of dimension $m \times m$ (as opposed to $N \times N$), and $M(\varepsilon)$ is Hermitian and analytic. Denote the set of eigenvalues of $M(\varepsilon)$ by $\{a_i(\varepsilon)\}_{i=1}^m$. It follows from Theorem 6.1 in Kato (1966) [75] that the $a_i(\varepsilon)$ are analytic. Since, furthermore, $a_i(0) > 0$, there exist a $\delta > 0$ such that $a_i(\varepsilon) > 0$ for all ε in the domain $D = (-\delta, \delta)$. In other words, $M(\varepsilon)$ is positive definite and analytic on the domain D. Thus the eigenvalues of $\sqrt{M(\varepsilon)}$ are given by $\{\sqrt{a_i(\varepsilon)}\}_{i=1}^m$, which are again all analytic on D. Therefore

$$F[\sigma(0), \sigma(\varepsilon)] = \left[\sum_{i=1}^{m} \sqrt{a_i(\varepsilon)}\right]^2 \tag{4.19}$$

is analytic around $\varepsilon = 0$. □

4.B Alternative derivation of $F^{(1)} = 0$

Here, we give an alternative proof to the theorem in the main text in the case that the analytic family under consideration is obtained by a perturbation. Strictly speaking this proof is redundant because a proof was already given in the main text. Nevertheless, the proof here is much more instructive. This is because it shows explicitly how the normalization conditions play a crucial role. Furthermore, it may act as a stepping stone for a more general result; in order to calculate $F^{(2)}$ for general $|\psi\rangle \in \mathcal{H}_S$, thus obtaining a generalization valid also for states outside a DFS, essentially the same steps need to be followed as in the following derivation.

To calculate $F^{(1)}$ explicitly, we adopt the notation from the proof of Lemma 4.A.1 and continue from Eq. (4.19). We consider the time $t \geq 0$ here as fixed, and will drop the notation of t. The first order correction to the eigenvalues $a_i(0)$ can be found using standard perturbation theory. Note, however, that in the standard setting one is

interested in the corrections to the eigenvalues of a Hamiltonian. Here we are interested in corrections to the eigenvalues of $M^{(0)}$, which is, like a Hamiltonian, a Hermitian linear operator. Note that, in connection to the notation in the proof of Lemma 4.A.1, we are now using the explicit states $\sigma(0) = \rho_S(0,t) = \rho_S(0)$ and $\sigma(\varepsilon) = \rho_S(\varepsilon,t) = \rho_S(\varepsilon)$. Thus, by standard perturbation theory,

$$\begin{aligned} a_i(\varepsilon) &= a_i(0) + \varepsilon \langle i| \sqrt{\rho_S^{(0)}} \rho_S^{(1)} \sqrt{\rho_S^{(0)}} |i\rangle + \dots \\ &= a_i(0) + \varepsilon\, p_i \langle i| \rho_S^{(1)} |i\rangle + \dots, \end{aligned}$$

where

$$\rho_S^{(1)} = \sum_j \left(A_j^{(0)} \rho_{S,\text{init}} A_j^{(1)\dagger} + A_j^{(1)} \rho_{S,\text{init}} A_j^{(0)\dagger} \right),$$

with $\rho_{S,\text{init}}$ the initial system state and, as before [but now using the specific density operator $\rho_S(\varepsilon)$], $\rho_S(\varepsilon) = \rho_S^{(0)} + \varepsilon\rho^{(1)} + \dots$. The system states $\{|i\rangle\}$ are the non-zero eigenvectors of $\rho_S(0)$ and are thus *all* eigenvectors of $M^{(0)}$. From the equations above, it follows that

$$\begin{aligned} F[\rho_S(0), \rho_S(\varepsilon)] &= \left[\sum_{i=1}^m \sqrt{a_i(0) + \varepsilon\, p_i \langle i| \rho_S^{(1)} |i\rangle + \dots} \right]^2 \\ &= \left[\sum_{i=1}^m \left(p_i + \frac{\varepsilon}{2} \langle i| \rho_S^{(1)} |i\rangle + \dots \right) \right]^2 . \end{aligned} \tag{4.20}$$

Again, it seems that $F^{(1)} \neq 0$. Now either $\rho_S(0)$ is full rank or it is not full rank. Let us first assume it is full rank, that is, assume $m = N$ with $N = \dim(\mathcal{H}_S)$. Then by the normalization conditions in the main text, $\sum_{i=1}^m \langle i| \rho_S^{(1)} |i\rangle = \operatorname{tr} \rho_S^{(1)} = 0$. Therefore, in this case, $F^{(1)} = 0$. Now assume that $\rho_S(0) = \sum_j A_j^{(0)} \rho_{S,\text{init}} A_j^{(0)\dagger}$ is not full rank. We may write $\rho_S(0) = \sum_{k=1}^m \mathfrak{p}_k |k\rangle\langle k|$, where $m < N$. We can expand the basis $\{|i\rangle\}$ to span all of $\mathcal{H}_S$ (in practice this could be done by a Gram-Schmidt

process), and write

$$\begin{aligned}\sum_{i=1}^{m} \langle i|\, \rho_S^{(1)}\, |i\rangle &= \sum_{i=1}^{N} \langle i|\, \rho_S^{(1)}\, |i\rangle - \sum_{i=m+1}^{N} \langle i|\, \rho_S^{(1)}\, |i\rangle \\ &= -\sum_{i=m+1}^{N} \langle i|\, \rho_S^{(1)}\, |i\rangle \\ &= -\sum_{i=m+1}^{N} \sum_j (\langle i|\, A_j^{(0)} \rho_S(0) A_j^{(1)\dagger}\, |i\rangle + c.c.) \\ &= -\sum_{i=m+1}^{N} \sum_{j,k} \mathfrak{p}_k (\langle i|\, A_j^{(0)}\, |k\rangle\langle k|\, A_j^{(1)\dagger}\, |i\rangle + c.c.).\end{aligned}$$

Here *c.c.* stands for the complex conjugate of the preceding term. For all $m+1 \leq i \leq N$, we have by definition that $\langle i|\, \rho_S^{(0)}\, |i\rangle = 0$. Hence, for these i,

$$\begin{aligned}\langle i|\sum_j A_j^{(0)} \rho_S(0) A_j^{(0)\dagger}\, |i\rangle &= \sum_{j,k} \mathfrak{p}_k\, \langle i|\, A_j^{(0)}\, |k\rangle\langle k|\, A_j^{(0)\dagger}\, |i\rangle \\ &= \sum_{j,k} \mathfrak{p}_k\, |\, \langle i|\, A_j^{(0)}\, |k\rangle\, |^2 = 0.\end{aligned}$$

It follows that

$$\langle i|\, A_j^{(0)}\, |k\rangle = 0$$

for all $m+1 \leq i < N$ and all $1 \leq k \leq m$. Thus, combining the two cases (i.e. $\rho_S(0)$ full rank, $\rho_S(0)$ not full rank), we have

$$\sum_{i=1}^{m} \langle i|\, \rho_S^{(1)}\, |i\rangle = 0$$

for all $1 \leq m \leq N$. Therefore, by Eq. (4.20), $F^{(1)} = 0$ for any t and any perturbation to a quantum channel as defined in the main text, including perturbations obtained by perturbing the overall Hamiltonian.

4.C Relation between χ and the Bures metric

The fidelity can be used to define a distance on the space of $N \times N$ density operators. This is the Bures distance [67, 116]

$$d_B^2(\rho, \sigma) = 2(1 - \sqrt{F(\rho, \sigma)}).$$

In the main text of this chapter we have expanded $F = F[\rho_S(0,t), \rho_S(\varepsilon,t)]$, which gives

$$\begin{aligned} d_B^2[\rho_S(0,t), \rho_S(\varepsilon,t)] &= F^{(2)}(t)\,\varepsilon^2 + O(\varepsilon^3) \\ &= [\chi t^2 + O(t^3)]\varepsilon^2 + O(\varepsilon^3). \end{aligned}$$

Thus $F^{(2)}(t)$ can be interpreted as (the only entry of) the pullback of the Bures metric tensor on the submanifold $\{\rho(\varepsilon,t)\}_\varepsilon$ at $\varepsilon = 0$,

$$\mathrm{d}_B^2(\rho_S(\epsilon,t), \rho(\epsilon + d\epsilon, t))|_{\epsilon=0} = F_2(t)\,\mathrm{d}\epsilon^2 = (\chi t^2 + \ldots)\mathrm{d}\epsilon^2.$$

Here, we have identified ε as $d\epsilon$. (We use 'd' for infinitesimals and 'd' for one-forms. Denoting the metric tensor by $\mathrm{d}_B^2[\rho(\epsilon), \rho(\epsilon + d\epsilon)]$, which is not the square of a one-form, is a common abuse of notation.) Note that the expression above defines a family of metric tensors, one for every t.

In this geometrical picture, t itself is not a coordinate, like ϵ, because we are never comparing $\rho(0,t)$ and $\rho(\varepsilon,t)$ at different times. The Bures metric tensor being a metric tensor, it may seem obvious that there is no first order dependence of F on $\varepsilon = d\epsilon$. This is ultimately a consequence of the fact that the set of all $N \times N$ density matrices is a Riemannian manifold. However, such an argument requires the machinery of differentiable manifolds. Theorem 4.3.1 gives a elementary proof that can be understood without the need of introducing differentiable manifolds. To the best of our knowledge, the connection between the pullback of the Bures metric and the 'robustness' (i.e. the absence of a term proportional to ε in F) of DFSs, which is the important issue here, had in any case not been noticed before.

***

Bibliography

[1] C. Addis et al. *Coherence trapping and information backflow in dephasing qubits*. Physical Review A **89**, 2 (2014), p. 024101. DOI: 10.1103/PhysRevA.89.024101.

[2] G. Adesso, S. Ragy, and A. R. Lee. *Continuous variable quantum information: Gaussian states and beyond*. Open Systems & Information Dynamics **21**, 01n02 (2014), p. 1440001. DOI: 10.1142/s1230161214400010.

[3] D. Aharonov and T. Naveh. *Quantum NP-a survey*. 2002. arXiv: quant-ph/0210077 [quant-ph].

[4] G. Alagic et al. *Status report on the first round of the NIST post-quantum cryptography standardization process*. Tech. rep. 2019. DOI: 10.6028/nist.ir.8240.

[5] V. V. Albert et al. *Geometry and Response of Lindbladians*. Physical Review X **6**, 4 (2016), p. 041031. DOI: 10.1103/PhysRevX.6.041031.

[6] J. B. Altepeter et al. *Experimental Investigation of a Two-Qubit Decoherence-Free Subspace*. Physical Review Letters **92**, 14 (2004), p. 147901. DOI: 10.1103/PhysRevLett.92.147901.

[7] F. B. Anders, R. Bulla, and M. Vojta. *Equilibrium and Nonequilibrium Dynamics of the Sub-Ohmic Spin-Boson Model*. Physical Review Letters **98**, 21 (2007), p. 210402. DOI: 10.1103/PhysRevLett.98.210402.

[8] C. K. Andersen et al. *Repeated quantum error detection in a surface code*. Nature Physics **16**, 8 (2020), pp. 875–880. DOI: 10.1038/s41567-020-0920-y.

[9] P. W. Anderson. *Resonating valence bonds: A new kind of insulator?* Materials Research Bulletin **8**, 2 (1973), pp. 153–160. DOI: 10.1016/0025-5408(73)90167-0.

[10] S. M. Anton et al. *Pure dephasing in flux qubits due to flux noise with spectral density scaling as* $1/f^{\alpha}$. Physical Review B **85**, 22 (2012), p. 224505. DOI: 10.1103/PhysRevB.85.224505.

[11] F. Arute et al. *Quantum supremacy using a programmable superconducting processor*. Nature **574**, 7779 (2019), pp. 505–510. DOI: 10.1038/s41586-019-1666-5.

[12] F. Arute et al. *Observation of separated dynamics of charge and spin in the Fermi-Hubbard model*. 2020. arXiv: 2010.07965 [quant-ph].

[13] D. Bacon, D. A. Lidar, and K. B. Whaley. *Robustness of decoherence-free subspaces for quantum computation*. Physical Review A **60**, 3 (1999), pp. 1944–1955. DOI: 10.1103/PhysRevA.60.1944.

[14] C. A. Balanis. *Antenna theory: analysis and design*. John Wiley & Sons, 2016. ISBN: 978-1-118-64206-1.

[15] P. Barthelemy and L. M. K. Vandersypen. *Quantum dot systems: a versatile platform for quantum simulations*. Annalen der Physik **525**, 10-11 (2013), pp. 808–826. DOI: 10.1002/andp.201300124.

[16] M. J. S. Beach et al. *Making trotters sprint: A variational imaginary time ansatz for quantum many-body systems*. Physical Review B **100**, 9 (2019), p. 094434. DOI: 10.1103/PhysRevB.100.094434.

[17] C. Benedetti and M. G. Paris. *Effective dephasing for a qubit interacting with a transverse classical field*. International Journal of Quantum Information **12**, 02 (2014), p. 1461004. DOI: 10.1142/S0219749914610048.

[18] C. Benedetti et al. *Quantum probes for the cutoff frequency of Ohmic environments*. Physical Review A **97**, 1 (2018), p. 012126. DOI: 10.1103/PhysRevA.97.012126.

[19] P. Benioff. *The computer as a physical system: A microscopic quantum mechanical Hamiltonian model of computers as represented by Turing machines*. Journal of statistical physics **22**, 5 (1980), pp. 563–591. DOI: 10.1007/bf01011339.

[20] G. P. Berman, D. I. Kamenev, and V. I. Tsifrinovich. *Collective decoherence of the superpositional entangled states in the quantum Shor algorithm*. Physical Review A **71**, 3 (2005), p. 032346. DOI: 10.1103/PhysRevA.71.032346.

[21] E. Bernstein and U. Vazirani. *Quantum complexity theory*. SIAM Journal on computing **26**, 5 (1997), pp. 1411–1473. DOI: 10.1137/s0097539796300921.

[22] H. Bethe. *Zur theorie der metalle*. Zeitschrift für Physik **71**, 3-4 (1931), pp. 205–226. DOI: 10.1007/bf01341708.

[23] A. Blais et al. *Cavity quantum electrodynamics for superconducting electrical circuits: An architecture for quantum computation*. Physical Review A **69**, 6 (2004), p. 062320. DOI: 10.1103/PhysRevA.69.062320.

[24] R. Blume-Kohout et al. *Information-preserving structures: A general framework for quantum zero-error information*. Physical Review A **82**, 6 (2010), p. 062306. DOI: 10.1103/PhysRevA.82.062306.

[25] S. B. Bravyi and A. Y. Kitaev. *Fermionic quantum computation*. Annals of Physics **298**, 1 (2002), pp. 210–226. DOI: 10.1006/aphy.2002.6254.

[26] H.-P. Breuer and F. Petruccione. *The theory of open quantum systems*. Oxford University Press, 2010. DOI: 0.1093/acprof:oso/9780199213900.001.0001.

[27] R. Bulla, N. Tong, and M. Vojta. *Numerical renormalization group for bosonic systems and application to the sub-ohmic spin-boson model*. Physical Review Letters **91**, 17 (2003). DOI: 10.1103/PhysRevLett.91.170601.

[28] C. Cade et al. *Strategies for solving the Fermi-Hubbard model on near-term quantum computers*. Physical Review B **102**, 23 (2020), p. 235122. DOI: 10.1103/physrevb.102.235122.

[29] J.-S. Caux. *Correlation functions of integrable models: A description of the ABACUS algorithm*. Journal of Mathematical Physics **50**, 9 (2009), p. 095214. DOI: 10.1063/1.3216474.

[30] A. M. Childs et al. *Theory of Trotter Error with Commutator Scaling*. Physical Review X **11**, 1 (2021), p. 011020. DOI: 10.1103/PhysRevX.11.011020.

[31] M. A. Cirone et al. *Collective decoherence of cold atoms coupled to a Bose–Einstein condensate*. New Journal of Physics **11**, 10 (2009), p. 103055. DOI: 10.1088/1367-2630/11/10/103055.

[32] T. H. Cormen et al. *Introduction to algorithms*. MIT press, 2009.

[33] B. J. Dalton. *Scaling of decoherence effects in quantum computers*. Journal of Modern Optics **50**, 6-7 (2003), pp. 951–966. DOI: 10.1080/09500340308234544.

[34] R. De Wolf. *Quantum computing: Lecture notes*. 2019. arXiv: 1907.09415 [quant-ph].

[35] C. van Diepen et al. *Quantum simulation of antiferromagnetic Heisenberg chain with gate-defined quantum dots*. 2021. arXiv: 2103.08238 [cond-mat].

[36] P. A. M. Dirac. *The principles of quantum mechanics*. 27. Oxford university press, 1981.

[37] R. Doll. *Decoherence of spatially separated quantum bits*. Universität Augsburg PhD thesis, https://opus.bibliothek.uni-augsburg.de/opus4/frontdoor/deliver/index/docId/673/file/doll_diss.pdf. 2008.

[38] R. Doll et al. *Incomplete pure dephasing of N-qubit entangled W states*. Physical Review B **76**, 4 (2007), p. 045317. DOI: 10.1103/PhysRevB.76.045317.

[39] R. Doll et al. *Limitation of entanglement due to spatial qubit separation*. Europhysics Letters **76**, 4 (2006), p. 547. DOI: 10.1209/epl/i2006-10326-y.

[40] L.-M. Duan and G.-C. Guo. *Preserving Coherence in Quantum Computation by Pairing Quantum Bits*. Physical Review Letters **79**, 10 (1997), pp. 1953–1956. DOI: 10.1103/PhysRevLett.79.1953.

[41] L.-M. Duan and G.-C. Guo. *Reducing decoherence in quantum-computer memory with all quantum bits coupling to the same environment*. Physical Review A **57**, 2 (1998), pp. 737–741. DOI: 10.1103/PhysRevA.57.737.

[42] G. Evenbly and G. Vidal. *Frustrated antiferromagnets with entanglement renormalization: Ground state of the spin-1 2 heisenberg model on a kagome lattice*. Physical Review Letters **104**, 18 (2010), p. 187203. DOI: 10.1103/physrevlett.104.187203.

[43] A. Ferraro, S. Olivares, and M. G. A. Paris. *Gaussian states in continuous variable quantum information*. Mar. 2005. arXiv: quant-ph/0503237 [quant-ph].

[44] R. Feynman. *The Character of Physical Law*. The MIT Press, 2017. DOI: 10.7551/mitpress/11068.001.0001.

[45] R. P. Feynman. *Simulating physics with computers*. International Journal of Theoretical Physics **21**, 6-7 (1982), pp. 467–488. DOI: 10.1007/bf02650179.

[46] P. S. Foundation. *Python Language Reference, version 2.8*. 2019. URL: https://docs.python.org/3.8/.

[47] A. G. Fowler et al. *Surface codes: Towards practical large-scale quantum computation*. Physical Review A **86**, 3 (2012), p. 032324. DOI: 10.1103/PhysRevA.86.032324.

[48] B. Foxen et al. *Demonstrating a continuous set of two-qubit gates for near-term quantum algorithms*. Physical Review Letters **125**, 12 (2020), p. 120504. DOI: 10.1103/PhysRevLett.125.120504.

[49] D. S. Franca and R. Garcia-Patron. *Limitations of optimization algorithms on noisy quantum devices*. 2020. arXiv: 2009.05532 [quant-ph].

[50] F. Franchini. *An Introduction to Integrable Techniques for One-Dimensional Quantum Systems*. Springer International Publishing, 2017. DOI: 10.1007/978-3-319-48487-7.

[51] F. Galve et al. *Microscopic description for the emergence of collective dissipation in extended quantum systems*. Scientific Reports **7**, 1 (2017). DOI: 10.1038/srep42050.

[52] J. D. Giorgini and JPL Solar System Dynamics Group. *On-Line Ephemeris System*. 2021. URL: https://ssd.jpl.nasa.gov/?horizons.

[53] J. Giorgini, P. Chodas, and D. Yeomans. *Orbit uncertainty and close-approach analysis capabilities of the horizons on-line ephemeris system*. AAS/Division for Planetary Sciences Meeting Abstracts. Vol. 33. 2001, pp. 58–13.

[54] J. Giorgini and D. Yeomans. *On-line system provides accurate ephemeris and related data*. NASA Tech Briefs, NPO-20416 **48** (1999).

[55] J. D. Giorgini. *Status of the JPL Horizons Ephemeris System*. IAU General Assembly. Vol. 29. 2015, p. 2256293.

[56] V. Giovannetti, S. Lloyd, and L. Maccone. *Quantum Metrology*. Physical Review Letters **96**, 1 (2006). DOI: 10.1103/physrevlett.96.010401.

[57] V. Giovannetti, S. Lloyd, and L. Maccone. *Quantum-Enhanced Measurements: Beating the Standard Quantum Limit*. Science **306**, 5700 (2004), pp. 1330–1336. DOI: 10.1126/science.1104149.

[58] T. Gorin et al. *Dynamics of Loschmidt echoes and fidelity decay*. Phys. Rep. **435**, 2-5 (2006), pp. 33–156. DOI: 10.1016/j.physrep.2006.09.003.

[59] D. Gottesman. *Stabilizer codes and quantum error correction*. Jan. 1997. arXiv: quant-ph/9705052 [quant-ph].

[60] H. R. Grimsley et al. *An adaptive variational algorithm for exact molecular simulations on a quantum computer*. Nature communications **10**, 1 (2019), pp. 1–9. DOI: 10.1038/s41467-019-10988-2.

[61] S.-J. Gu. *Fidelity approach to quantum phase transitions*. International Journal of Modern Physics B **24**, 23 (2010), p. 4371. DOI: 10.1142/S0217979210056335.

[62] C. R. Harris et al. *Array programming with NumPy*. Nature **585**, 7825 (2020), pp. 357–362. DOI: 10.1038/s41586-020-2649-2.

[63] N. W. Hendrickx et al. *A four-qubit germanium quantum processor*. Nature **591**, 7851 (2021), pp. 580–585. DOI: 10.1038/s41586-021-03332-6.

[64] C. D. Hill et al. *A surface code quantum computer in silicon*. Science advances **1**, 9 (2015), e1500707. DOI: 10.1126/sciadv.1500707.

[65] W. W. Ho and T. H. Hsieh. *Efficient variational simulation of non-trivial quantum states*. SciPost Phys. **6**, 3 (2019), p. 29. DOI: 10.21468/SciPostPhys.6.3.029.

[66] H.-Y. Huang, R. Kueng, and J. Preskill. *Efficient estimation of Pauli observables by derandomization*. 2021. arXiv: 2103.07510 [quant-ph].

[67] M. Hübner. *Explicit computation of the Bures distance for density matrices*. Physics Letters A **163**, 4 (1992), pp. 239–242. DOI: 10.1016/0375-9601(92)91004-B.

[68] B. Ischi, M. Hilke, and M. Dubé. *Decoherence in a N-qubit solid-state quantum register*. Physical Review B **71**, 19 (2005), p. 195325. DOI: 10.1103/PhysRevB.71.195325.

[69] H.-C. Jiang, Z.-Y. Weng, and D. N. Sheng. *Density matrix renormalization group numerical study of the kagome antiferromagnet*. Physical Review Letters **101**, 11 (2008), p. 117203. DOI: 10.1103/PhysRevLett.101.117203.

[70] Z. Jiang et al. *Optimal fermion-to-qubit mapping via ternary trees with applications to reduced quantum states learning*. Quantum **4** (2020), p. 276. DOI: 10.22331/q-2020-06-04-276.

[71] R. Jozsa. *Fidelity for Mixed Quantum States*. Journal of Modern Optics **41**, 12 (1994), pp. 2315–2323. DOI: 10.1080/09500349414552171.

[72] G. Kalai. *How Quantum Computers Fail: Quantum Codes, Correlations in Physical Systems, and Noise Accumulation*. arXiv: 1106.0485 [quant-ph].

[73] G. Kalai. *The quantum computer puzzle*. Notices of the AMS **63**, 5 (2016), pp. 508–516. DOI: 10.1090/noti1380.

[74] A. Kandala et al. *Hardware-efficient variational quantum eigensolver for small molecules and quantum magnets*. Nature **549**, 7671 (2017), pp. 242–246. DOI: 10.1038/nature23879.

[75] T. Kato. *Perturbation theory for linear operators*. Springer-Verlag, Berlin, 1966.

[76] J. J. Kattemölle. *HeisenbergVQE*. 2020. URL: https://github.com/barbireau/HVQE.

[77] J. J. Kattemölle. *Quantumcomputers*. 2017. URL: https://www.quantumuniverse.nl/quantumcomputers-1-makkelijk-of-moeilijk.

[78] J. J. Kattemölle. *Short introduction to Quantum Computing*. 2017. URL: http://www.kattemolle.com/KattemolleShortIntroToQC.pdf.

[79] J. J. Kattemölle and B. Freivogel. *Entangled wavepackets in the vacuum*. Journal of High Energy Physics **2017**, 10 (2017), p. 32. DOI: 10.1007/JHEP10(2017)092.

[80] J. J. Kattemölle and J. van Wezel. *Conditions for superdecoherence*. Quantum **4** (2020), p. 265. DOI: 10.22331/q-2020-05-14-265.

[81] J. J. Kattemölle and J. van Wezel. *Dynamical fidelity susceptibility of decoherence-free subspaces*. Physical Review A **99**, 6 (2019), p. 062340. DOI: 10.1103/PhysRevA.99.062340.

[82] S. K. Kehrein and A. Mielke. *On the spin-boson model with a sub-ohmic bath*. Physics Letters A **219**, 5-6 (1996), pp. 313–318. DOI: 10.1016/0375-9601(96)00475-6.

[83] J. Kempe et al. *Theory of decoherence-free fault-tolerant universal quantum computation*. Physical Review A **63**, 4 (2001), p. 042307. DOI: 10.1103/PhysRevA.63.042307.

[84] J. Kempe, A. Kitaev, and O. Regev. *The complexity of the local Hamiltonian problem*. SIAM Journal on Computing **35**, 5 (2006), pp. 1070–1097. DOI: 10.1137/s0097539704445226.

[85] D. Kielpinski, C. Monroe, and D. J. Wineland. *Architecture for a large-scale ion-trap quantum computer*. Nature **417**, 6890 (2002), p. 709. DOI: 10.1038/nature00784.

[86] D. Kielpinski et al. *A decoherence-free quantum memory using trapped ions*. Science **291**, 5506 (2001), pp. 1013–1015. DOI: 10.1126/science.1057357.

[87] D. Kribs, R. Laflamme, and D. Poulin. *Unified and Generalized Approach to Quantum Error Correction*. Physical Review Letters **94**, 18 (2005), p. 180501. DOI: 10.1103/PhysRevLett.94.180501.

[88] J. Latorre, E. Rico, and G. Vidal. *Ground state entanglement in quantum spin chains*. Quantum Information and Computation **4**, 1 (2004), pp. 48–92. DOI: 10.26421/qic4.1-4.

[89] A. M. Läuchli, J. Sudan, and R. Moessner. *S=1/2 kagome Heisenberg antiferromagnet revisited*. Physical Review B **100**, 15 (2019), p. 155142. DOI: 10.1103/PhysRevB.100.155142.

[90] A. J. Leggett et al. *Dynamics of the dissipative two-state system*. Reviews of Modern Physics **59**, 1 (1987), pp. 1–85. DOI: 10.1103/RevModPhys.59.1.

[91] R. B. Lehoucq, D. C. Sorensen, and C. Yang. *ARPACK users' guide: solution of large-scale eigenvalue problems with implicitly restarted Arnoldi methods*. SIAM, 1998. DOI: 10.1137/1.9780898719628.

[92] R. Li et al. *A crossbar network for silicon quantum dot qubits*. Science advances **4**, 7 (2018), eaar3960. DOI: 10.1126/sciadv.aar3960.

[93] I. Liberal, I. Ederra, and R. W. Ziolkowski. *Quantum antenna arrays: The role of quantum interference on direction-dependent photon statistics*. Physical Review A **97**, 5 (2018), p. 053847. DOI: 10.1103/PhysRevA.97.053847.

[94] D. A. Lidar, D. Bacon, and K. B. Whaley. *Concatenating Decoherence-Free Subspaces with Quantum Error Correcting Codes*. Physical Review Letters **82**, 22 (1999), pp. 4556–4559. DOI: 10.1103/PhysRevLett.82.4556.

[95] D. A. Lidar, I. L. Chuang, and K. B. Whaley. *Decoherence-Free Subspaces for Quantum Computation*. Physical Review Letters **81**, 12 (1998), pp. 2594–2597. DOI: 10.1103/PhysRevLett.81.2594.

[96] D. A. Lidar and T. A. Brun. *Quantum error correction*. Cambridge University Press, 2013.

[97] D. A. Lidar and K. B. Whaley. *Decoherence-free subspaces and subsystems. Irreversible quantum dynamics*. Springer, 2003, pp. 83–120. DOI: 10.1007/3-540-44874-8_5.

[98] S. Lloyd. *Universal quantum simulators*. Science (1996), pp. 1073–1078. DOI: 10.1126/science.279.5354.1113h.

[99] D. Loss and D. P. DiVincenzo. *Quantum computation with quantum dots*. Physical Review A **57**, 1 (1998), p. 120. DOI: 10.1103/physreva.57.120.

[100] J. Marston and C. Zeng. *Spin-Peierls and spin-liquid phases of Kagomé quantum antiferromagnets*. Journal of Applied Physics **69**, 8 (1991), pp. 5962–5964. DOI: 10.1063/1.347830.

[101] J. R. McClean et al. *Barren plateaus in quantum neural network training landscapes*. Nature communications **9**, 1 (2018), pp. 1–6. DOI: 10.1038/s41467-018-07090-4.

[102] J. R. McClean et al. *The theory of variational hybrid quantum-classical algorithms*. New Journal of Physics **18**, 2 (2016), p. 023023. DOI: 10.1088/1367-2630/18/2/023023.

[103] B. Mera et al. *Dynamical phase transitions at finite temperature from fidelity and interferometric Loschmidt echo induced metrics*. Physical Review B **97**, 9 (2018), p. 094110. DOI: 10.1103/PhysRevB.97.094110.

[104] T. Monz et al. *14-Qubit Entanglement: Creation and Coherence*. Physical Review Letters **106**, 13 (2011), p. 130506. DOI: 10.1103/PhysRevLett.106.130506.

[105] D. Morgan. *Surface acoustic wave filters: With applications to electronic communications and signal processing*. Academic Press, 2010. DOI: 10.1016/B978-0-12-372537-0.X5000-6.

[106] M. A. Nielsen. *Neural networks and deep learning*. Vol. 25. Determination press, 2015.

[107] M. A. Nielsen et al. *The Fermionic canonical commutation relations and the Jordan-Wigner transform*. School of Physical Sciences, The University of Queensland **59** (2005).

[108] M. A. Nielsen and I. L. Chuang. *Quantum Computation and Quantum Information: 10th Anniversary Edition*. Cambridge University Press, 2010. DOI: 10.1017/CBO9780511976667.

[109] P. Nikolic and T. Senthil. *Physics of low-energy singlet states of the Kagome lattice quantum Heisenberg antiferromagnet*. Physical Review B **68**, 21 (2003), p. 214415. DOI: 10.1103/physrevb.68.214415.

[110] R. Nishino and S. H. C. Loomis. *CuPy: A NumPy-compatible library for NVIDIA GPU calculations*. 31st confernce on neural information processing systems (2017), p. 151.

[111] M. Norman. *Colloquium : Herbertsmithite and the search for the quantum spin liquid*. Reviews of Modern Physics **88**, 4 (2016). DOI: 10.1103/revmodphys.88.041002.

[112] J. Nørskov et al. *Sustainable Ammonia Synthesis–Exploring the scientific challenges associated with discovering alternative, sustainable processes for ammonia production*. Tech. rep. US DOE Office of Science, 2016. DOI: 10.2172/1283146.

[113] P. J. O'Malley et al. *Scalable quantum simulation of molecular energies*. Physical Review X **6**, 3 (2016), p. 031007. DOI: 10.1103/PhysRevX.6.031007.

[114] T. Palm and P. Nalbach. *Nonperturbative environmental influence on dephasing*. Physical Review A **96**, 3 (2017), p. 032105. DOI: 10.1103/PhysRevA.96.032105.

[115] G. M. Palma, K.-A. Suominen, and A. K. Ekert. *Quantum computers and dissipation*. Proc. R. Soc. Lond. A **452**, 1946 (1996), pp. 567–584. DOI: 10.1098/rspa.1996.0029.

[116] M. G. Paris. *Quantum estimation for quantum technology*. International Journal of Quantum Information **7**, supp01 (2009), pp. 125–137. DOI: 10.1142/S0219749909004839.

[117] A. Peruzzo et al. *A variational eigenvalue solver on a photonic quantum processor*. Nature communications **5**, 1 (2014), pp. 1–7. DOI: 10.1038/ncomms5213.

[118] S. Piddock and A. Montanaro. *The complexity of antiferromagnetic interactions and 2D lattices*. Quantum Information and Computation **17**, 7&8 (2017), pp. 636–672. DOI: 10.26421/qic17.7-8-6.

[119] J. Preskill. *Lecture notes for physics 229: Quantum information and computation*. http://www.theory.caltech.edu/people/preskill/ph229/notes/chap7.pdf. 1998.

[120] J. Preskill. *Quantum Computing in the NISQ era and beyond*. Quantum **2** (2018), p. 79. DOI: 10.22331/q-2018-08-06-79.

[121] J. Preskill. *Sufficient condition on noise correlations for scalable quantum computing*. Quantum Information & Computation **13**, 3-4 (2013), pp. 181–194. DOI: 10.26421/qic13.3-4-1.

[122] J. H. Reif and S. R. Tate. *The complexity of N-body simulation*. Springer, 1993. DOI: 10.1007/3-540-56939-1_70.

[123] M. Reiher et al. *Elucidating reaction mechanisms on quantum computers*. Proceedings of the National Academy of Sciences **114**, 29 (2017), pp. 7555–7560. DOI: 10.1073/pnas.1619152114.

[124] J. H. Reina, L. Quiroga, and N. F. Johnson. *Decoherence of quantum registers*. Physical Review A **65**, 3 (2002), p. 032326. DOI: 10.1103/PhysRevA.65.032326.

[125] J.-M. Reiner et al. *Finding the ground state of the Hubbard model by variational methods on a quantum computer with gate errors*. Quantum Science and Technology **4**, 3 (2019), p. 035005. DOI: 10.1088/2058-9565/ab1e85.

[126] D. Reinsel, J. Gantz, and J. Rydning. *The digitization of the world from edge to core*. Framingham: International Data Corporation (2018).

[127] J. J. Sakurai and J. Napolitano. *Modern Quantum Mechanics*. Cambridge University Press, 2020. DOI: 10.1017/9781108587280.

[128] M. Schlosshauer. *The quantum-to-classical transition and decoherence*. 2014. arXiv: 1404.2635 [quant-ph].

[129] M. A. Schlosshauer. *Decoherence and the quantum-to-classical transition*. Springer-Verlag Berlin Heidelberg, 2007. DOI: 10.1007/978-3-540-35775-9.

[130] P. W. Shor. *Algorithms for quantum computation: discrete logarithms and factoring*. Proceedings 35th annual symposium on foundations of computer science. Ieee. 1994, pp. 124–134. DOI: 10.1109/sfcs.1994.365700.

[131] P. W. Shor. *Fault-tolerant quantum computation*. Foundations of Computer Science. IEEE. 1996, pp. 56–65. DOI: 10.1109/SFCS.1996.548464.

[132] P. W. Shor. *Polynomial-time algorithms for prime factorization and discrete logarithms on a quantum computer*. SIAM review **41**, 2 (1999), pp. 303–332. DOI: 10.1137/s0036144598347011.

[133] R. R. Singh and D. A. Huse. *Ground state of the spin-1/2 kagome-lattice Heisenberg antiferromagnet*. Physical Review B **76**, 18 (2007), p. 180407. DOI: 10.1103/PhysRevB.76.180407.

[134] R. R. Singh and D. A. Huse. *Triplet and singlet excitations in the valence bond crystal phase of the kagome lattice Heisenberg model*. Physical Review B **77**, 14 (2008), p. 144415. DOI: 10.1103/PhysRevB.77.144415.

[135] J. T. Stockburger. *Superdecoherence through gate control noise*. Jan. 2007. arXiv: quant-ph/0701062 [quant-ph].

[136] A. Szabo and N. S. Ostlund. *Modern quantum chemistry: introduction to advanced electronic structure theory*. Courier Corporation, 2012.

[137] S. Tokui et al. *Chainer: a next-generation open source framework for deep learning*. Proceedings of workshop on machine learning systems (LearningSys) in the twenty-ninth annual conference on neural information processing systems (NIPS). Vol. 5. 2015, pp. 1–6.

[138] W. G. Unruh. *Maintaining coherence in quantum computers*. Physical Review A **51**, 2 (1995), pp. 992–997. DOI: 10.1103/PhysRevA.51.992.

[139] R. Versluis et al. *Scalable Quantum Circuit and Control for a Superconducting Surface Code*. Physical Review Applied **8**, 3 (2017). DOI: 10.1103/physrevapplied.8.034021.

[140] P. Virtanen et al. *SciPy 1.0: Fundamental Algorithms for Scientific Computing in Python*. Nature Methods **17** (2020), pp. 261–272. DOI: 10.1038/s41592-019-0686-2.

[141] M. Vojta, N. Tong, and R. Bulla. *Quantum phase transitions in the sub-Ohmic spin-boson model: Failure of the quantum-classical mapping*. Physical Review Letters **94**, 7 (2005). DOI: 10.1103/PhysRevLett.94.070604.

[142] D. Wecker, M. B. Hastings, and M. Troyer. *Progress towards practical quantum variational algorithms*. Physical Review A **92**, 4 (2015), p. 042303. DOI: 10.1103/physreva.92.042303.

[143] R. Wiersema et al. *Exploring entanglement and optimization within the Hamiltonian Variational Ansatz*. PRX Quantum **1**, 2 (2020), p. 020319. DOI: 10.1103/prxquantum.1.020319.

[144] R. de Wolf. *The potential impact of quantum computers on society*. Ethics and Information Technology **19**, 4 (2017), pp. 271–276. DOI: 10.1007/s10676-017-9439-z.

[145] S. Yan, D. A. Huse, and S. R. White. *Spin-liquid ground state of the S=1/2 kagome Heisenberg antiferromagnet*. Science **332**, 6034 (2011), pp. 1173–1176. DOI: 10.1126/science.1201080.

[146] W.-L. You, Y.-W. Li, and S.-J. Gu. *Fidelity, dynamic structure factor, and susceptibility in critical phenomena*. Physical Review E **76**, 2 (2007), p. 022101. DOI: 10.1103/PhysRevE.76.022101.

[147] P. Zanardi and M. Rasetti. *Noiseless Quantum Codes*. Physical Review Letters **79**, 17 (1997), pp. 3306–3309. DOI: 10.1103/PhysRevLett.79.3306.

[148] P. Zanardi. *Dissipation and decoherence in a quantum register*. Physical Review A **57**, 5 (1998), pp. 3276–3284. DOI: 10.1103/PhysRevA.57.3276.

[149] P. Zanardi and L. Campos Venuti. *Geometry, robustness, and emerging unitarity in dissipation-projected dynamics*. Physical Review A **91**, 5 (2015), p. 052324. DOI: 10.1103/PhysRevA.91.052324.

[150] P. Zanardi, P. Giorda, and M. Cozzini. *Information-Theoretic Differential Geometry of Quantum Phase Transitions*. Physical Review Letters **99**, 10 (2007), p. 100603. DOI: 10.1103/PhysRevLett.99.100603.

[151] P. Zanardi and M. Rasetti. *Error Avoiding Quantum Codes*. Modern Physics Letters B **11**, 25 (1997), pp. 1085–1093. DOI: 10.1142/S0217984997001304.

[152] J. Zhang et al. *Observation of a many-body dynamical phase transition with a 53-qubit quantum simulator*. Nature **551**, 7682 (2017), p. 601. DOI: 10.1038/nature24654.

[153] H.-S. Zhong et al. *Quantum computational advantage using photons*. Science **370**, 6523 (2020), pp. 1460–1463. DOI: 10.1126/science.abe8770.

[154] Z.-W. Zhou et al. *Scalable Fault-Tolerant Quantum Computation in Decoherence-Free Subspaces*. Physical Review Letters **93**, 1 (2004), p. 010501. DOI: 10.1103/PhysRevLett.93.010501.

Acknowledgements

First of all, I would like to thank you, the reader of this thesis, for showing an interest in my work. Without you, this thesis would only be half as valuable.

Throughout my time at QuSoft, I enjoyed the luxury of having two 'homes': the UvA and the CWI. I am grateful to have had such a rich and diverse scientific environment. My time here started after I received an email from Jasper, saying that he had a position available and asking whether I was interested. I was travelling at the time, but fortunately we managed to arrange a meeting during a transfer in Amsterdam. Still wearing my hiking boots, I set foot to Jasper's office, where we had an interesting discussion. Jasper said he would reach a conclusion in a couple of days. The coming couple of days, however, I was high up in the Alps. I was trying to refresh my inbox with every trace of reception I could find. Finally, a few days after it was sent, I received word that I was offered the position. The difficulty of receiving the message made its content all the more exciting.

Jasper, thank your for being my supervisor for the past years. The freedom you gave me, with - seemingly paradoxically - at the same time plenty of time and support, made my PhD a success. Your broad enthusiasm for physics surely kept that of my own alive. This forms a major factor in my continuation in academics. Thank you also for your empathy and patience in times of difficulty. Maybe the best compliment I can give you is to reiterate what Corentin once said when advising your master students about PhD positions: 'one thing to keep in mind is that most supervisors are not as nice as Jasper'. It is admirable how you have brought together such a nice group, and how you managed to keep it together during the pandemic. Ananya, Corentin, Ana, Jorrit, Mariya, Jans and Lotte, and master students Jonas, Matthijs, Niels, Alonso, Antara, Lars, Srinivas, Rosa and Jelle, thank you for the discussions and everything you taught me. I thank Jasper, together with Ben, Kareljan and Philippe, for your support in my search for a postdoc position. Jasper, Marcel, and Ralph, I thank you for your trust in me as a teacher of 'quantumfysica'. I thank Joost for his empathic leadership in times of difficulty. This made me feel acknowledged and valued.

Ben, you have been a mentor to me ever since your supervision of my master's project. Your attitude towards physics will stay with me forever. Allowing me to give a yearly guest lecture in your Advanced Quantum Physics course gave me the opportunity to build experience as a lecturer.

During my master's and PhD, I witnessed the first years of QuSoft. It was wonderful to be in an environment that has been expanding and is filled with youthful enthusiasm. I thank Harry, Kareljan and all support staff for creating this environment, and the PIs, Harry, Kareljan, Ronald, Māris, Michael, Chris and Stacey for being so approachable and helpful. A special word of thanks to Ronald and Māris for organising the Quantum Chemistry reading group. It is this group that sparked my work on Chapter 2 of this thesis.

I thank all the office mates I had over the years for their company and knowledge, Jonas, Sebastiaan and Srini for your humour, Koen for your deceivingly simple explanations of difficult concepts, Tom for sharing with me your knowledge on analysis, (classical) computing and (computer) chess, and Freek for being my mathematical oracle and paranymph. Doutzen and Susanne, thank you for the warm atmosphere and for organizing the QuTeas and the CWI Choir next to all your other organisational efforts. I thank my fellow QuSoft PhD students and postdocs that I have not mentioned so far, Ralph, Jeroen, András, Mathys, Alex, Yinan, Sander, Joran, Farrokh, Jan, Jelle, Chris C., Chris M., Ido, Subha, Alvaro, Yfke, Arjan, Harold, Jana, Rene, Bas, Florian, Marten, Jordi, Dion, Mehrdad and Yanlin for the good times and for being such knowledgable and kind peers.

Harmen, Mehran, Onno, Laurent, Djoeke and Manon, without you my master's would not have been half as fun and instructive. I learned from you just as much as I have from professors and T.As. Harmen, it is an honour and a pleasure to have had such a good friend and gifted scientist at my side, from the first year of our bachelor's in Utrecht to the last year of our PhDs in Amsterdam. For the first time in 11 years, our paths will diverge, but of course you are always welcome to visit us in Konstanz. I wish you all the best with Audrey and your new job.

I thank Paco, Floris, Kaustav and Stanley for trusting somebody as junior as me to be your bachelor's thesis supervisor. Supervising your projects has been a pleasure. I hope you learned at least as much from your projects as I did. I thank Rosa, Lieke, Liselot, Maarten and Hans for their valuable input on Chapter 1 of this thesis, and Anneloes for valuable input on the cover of this thesis.

I am equally indebted to my family and friends outside of academia. I tank my parents, and Annerieke, Liselot, Anneloes, Eric, Geertje and my grandmothers for their support in my studies and life in general. Leny, you once said you would probably not get the chance to see your grandson become a doctor. I am proud to say that, in fact, you can! Maarten, Welmoed, Reinout, Timothé, Janske, Lonneke, Bianca, Dafne and Ko, thank your so much for your friendship.

Last, but foremost, I thank Lieke and Julius. Lieke, your extra support and patience in the last months were more than anyone could ask for. Without you, this thesis would not be here in its current form, so you can practically consider yourself a co-author. Now that we have entered the post-thesis-writing era, we can finally catch up on some well-deserved quality time. It is truly humbling that your decision to follow me to Konstanz was a matter of course to you. I am very grateful for this.

Julius, you make me so happy and proud of all the things you can already do. Your challenges and accomplishments in the past 1.5 years put those of myself in perspective. You enjoy carrying this thesis around the house, and can already turn the pages remarkably carefully while admiring the pretty figures and symbols. With the help of our generous family, friends and colleagues, your have already acquired a modest library, containing authoritative underundergraduate textbooks such as 'quantum physics for babies'. So, you are well prepared to read this thesis someday.